


1997

Physicochemical properties of the anion-modified surfaces of silver nanostructures

Morgan Scot Sibbald
Iowa State University

Follow this and additional works at: <https://lib.dr.iastate.edu/rtd>

 Part of the [Analytical Chemistry Commons](#), [Condensed Matter Physics Commons](#), and the [Physical Chemistry Commons](#)

Recommended Citation

Sibbald, Morgan Scot, "Physicochemical properties of the anion-modified surfaces of silver nanostructures " (1997). *Retrospective Theses and Dissertations*. 12245.
<https://lib.dr.iastate.edu/rtd/12245>

This Dissertation is brought to you for free and open access by the Iowa State University Capstones, Theses and Dissertations at Iowa State University Digital Repository. It has been accepted for inclusion in Retrospective Theses and Dissertations by an authorized administrator of Iowa State University Digital Repository. For more information, please contact digirep@iastate.edu.

INFORMATION TO USERS

This manuscript has been reproduced from the microfilm master. UMI films the text directly from the original or copy submitted. Thus, some thesis and dissertation copies are in typewriter face, while others may be from any type of computer printer.

The quality of this reproduction is dependent upon the quality of the copy submitted. Broken or indistinct print, colored or poor quality illustrations and photographs, print bleedthrough, substandard margins, and improper alignment can adversely affect reproduction.

In the unlikely event that the author did not send UMI a complete manuscript and there are missing pages, these will be noted. Also, if unauthorized copyright material had to be removed, a note will indicate the deletion.

Oversize materials (e.g., maps, drawings, charts) are reproduced by sectioning the original, beginning at the upper left-hand corner and continuing from left to right in equal sections with small overlaps. Each original is also photographed in one exposure and is included in reduced form at the back of the book.

Photographs included in the original manuscript have been reproduced xerographically in this copy. Higher quality 6" x 9" black and white photographic prints are available for any photographs or illustrations appearing in this copy for an additional charge. Contact UMI directly to order.

UMI

A Bell & Howell Information Company
300 North Zeeb Road, Ann Arbor MI 48106-1346 USA
313/761-4700 800/521-0600

Physicochemical properties of the anion-modified surfaces of
silver nanostructures

by

Morgan Scot Sibbald

A dissertation submitted to the graduate faculty
in partial fulfillment of the requirements for the degree of
DOCTOR OF PHILOSOPHY

Major: Analytical Chemistry

Major Professor: Therese M. Cotton

Iowa State University

Ames, Iowa

1997

UMI Number: 9737758

UMI Microform 9737758
Copyright 1997, by UMI Company. All rights reserved.

**This microform edition is protected against unauthorized
copying under Title 17, United States Code.**

UMI
300 North Zeeb Road
Ann Arbor, MI 48103

**Graduate College
Iowa State University**

This is to certify that the Doctoral dissertation of

Morgan Scot Sibbald

has met the dissertation requirements of Iowa State University

Signature was redacted for privacy.

Major Professor

Signature was redacted for privacy.

For the Major Program

Signature was redacted for privacy.

For the Graduate College

*To my wife JeNell and my family
whose love and encouragement were an integral part
of composing this dissertation.*

TABLE OF CONTENTS

CHAPTER 1. GENERAL INTRODUCTION.....	1
Dissertation Organization.....	1
Nanostructured Materials.....	3
Optical Properties of Metal Nanostructures.....	3
Surface-Enhanced Spectroscopies at Nanostructured Metals.....	14
Surface-Enhanced Raman Spectroscopy.....	18
Theoretical Considerations.....	19
Analytical Applications of SERS.....	25
Single Molecule Detection.....	27
References.....	30
CHAPTER 2. THE SHAPE AND STRUCTURE OF SERS ACTIVE SILVER NANOSTRUCTURES.....	34
Abstract.....	34
Introduction.....	34
Experimental Methods.....	36
Results and Discussion.....	37
Conclusions.....	45
Acknowledgment.....	45
References.....	46
CHAPTER 3. REDUCTION OF CYTOCHROME C BY HALIDE-MODIFIED, LASER-ABLATED SILVER COLLOIDS.....	47
Abstract.....	47
Introduction.....	47
Experimental Section.....	51
Chemicals and Materials.....	51
Colloid Preparation.....	51
Colloidal Metal Film (CMF) Preparation.....	52
Raman Spectroscopy.....	52
Electronic Absorption Spectroscopy.....	54
Results.....	54
Cytochrome <i>c</i> Reduction in Modified Ag Colloid.....	54
Cytochrome <i>c</i> Reduction on Modified CMFs.....	59
Iodide Adsorption on Silver.....	61
Discussion.....	67
Conclusions.....	74
Acknowledgment.....	74
References and Notes.....	74
CHAPTER 4. REDUCTIVE PROPERTIES OF IODIDE-MODIFIED SILVER NANOPARTICLES.....	77
Abstract.....	77

Introduction.....	77
Experimental Methods.....	79
Reagents.....	79
Colloidal Metal Film (CMF) Preparation.....	80
Electronic Absorption Spectroscopy.....	80
Raman Spectroscopy.....	81
Electrochemical Measurements.....	81
Results and Discussion.....	81
Conclusions.....	99
Acknowledgments.....	100
References.....	100
CHAPTER 5. MULTIPLE OVERTONE RESONANCE RAMAN SCATTERING AND RESONANCE FLUORESCENCE FROM IODIDE ADSORBED ON SILVER SURFACES.....	102
Abstract.....	102
Introduction.....	102
Experimental Methods.....	105
Modification of Silver Surfaces.....	105
Temperature Control.....	106
Raman Spectroscopy.....	106
Results and Discussion.....	107
Conclusions.....	121
Acknowledgments.....	124
References.....	125
CHAPTER 6. GENERAL CONCLUSIONS.....	127
Recommendations for Future Research.....	129
ACKNOWLEDGMENTS.....	130

CHAPTER 1. GENERAL INTRODUCTION

Nanostructured materials are an emerging field for modern technology because their physical and chemical properties can be significantly different than those of bulk materials.¹⁻³ A fundamental problem in this area is concerned with properties of the material/medium interface, especially in view of the extremely high surface-to-volume ratio of the nanostructure. Understanding how the adsorption of different molecules and ions on the surface modifies the interfacial behavior is important for many practical applications including microelectronics, non-linear optics, catalysis, and sensor design.^{1,4}

The specific research objectives of this dissertation were fourfold: to prepare and characterize nanostructures of silver, to chemically modify the surfaces of the structures, to study the adsorption state and reactivity of the modifiers, and especially to monitor the optical properties of the surface-modified metal.

Dissertation Organization

The remainder of this chapter includes background and literature reviews for two important areas related to the dissertation research. First, the unique optical properties of nanostructured metals are described, including the possible influences of surface modification. Second, surface-enhanced Raman spectroscopy (SERS), a laser-based analytical method extensively used in the current work, is described in a brief theoretical treatment. A review of recent practical applications of SERS as well as advances in single nanostructure and single molecule detection is also provided.

Chapters 2 through 5 of this dissertation include papers that have been written for peer-reviewed journals. Chapter 2, a paper to be submitted to the *Journal of Solid State Chemistry*, was an analysis of chemically-prepared, nanostructures of silver by transmission electron microscopy. Both imaging and diffraction modes of the electron microscope were employed to characterize the two- and three-dimensional shape and crystal structure of the metal. Chapter 3, a paper published in the *Journal of Physical Chemistry*, Volume 100 (1996), Page 4672, was both a phenomenological report and a fundamental study describing the reduction of the protein cytochrome *c* at halide-modified surfaces of silver nanostructures. The optical properties of the modified metal as well as the chemical interactions of the protein and halide modifiers with the metal surface were of particular interest.

Chapter 4, a paper accepted for publication in the *Journal of Electroanalytical Chemistry*, manuscript number 5131, was a continued study of the reductive properties of halide-modified silver nanoparticles. More quantitative measurements using a redox active dye molecule were performed in order to elucidate the mechanism of the reduction process. Chapter 5, a paper submitted to the *Journal of Chemical Physics*, was a detailed spectroscopic study on the photophysics of iodide adsorbed on silver surfaces. Under appropriate conditions, an extraordinary emission spectrum was observed from the modified-silver surface which contained contributions from resonance Raman and resonance and relaxed fluorescence.

The dissertation concludes with a general summary of research achievements and possible directions for future work.

Nanostructured Materials

The intense purple and gold colors of 4th century Roman glasses, the ruby red and yellow brilliance of 12th century stained glass cathedral windows, and the pink tones of 18th century Chinese K'ang Hsi porcelain were all crafted by embedding nanostructured gold, silver, and copper metals into the bulk materials.⁵ These nanostructured metals fall into the size range of ca. 20 Å (around 250 atoms) up to ca. 100 nm (over 10^6 atoms) which places them in the “intermediate region of matter” between classical atomic and cluster theories for discrete molecular orbitals and solid state physics descriptions of the band structure in bulk materials. In the following sub-section, the theoretical treatments used to explain the unique optical properties of metal nanostructures are discussed.

Optical Properties of Metal Nanostructures

Metal structures derive their optical properties (reflection, absorption, etc.) from the behavior of the “free” conduction band electrons.⁶ These electrons are free to move throughout the volume of the metal, defined by a fixed background of positive ion cores. From a modern physics point of view, the metal can be thought of as a plasma. Electrons moving rapidly in the metal plasma can sometimes behave collectively and oscillate with a single quantum of energy.⁷ Indeed, the collective oscillation of electron density in metals, known as plasmon resonance, can be induced by an external electric field and has been demonstrated for several metals.⁷ The plasmon resonance in a bulk metal propagates as a longitudinal wave with the plasmon frequency ω_p given by

$$\omega_p = \frac{Nq^2}{m \epsilon_0} \quad (1)$$

where N is the number of oscillating charges per unit volume, q is the electron charge, m is the effective electron mass, and ϵ_0 is the permittivity. For a typical free electron metal, the charge density $N \approx 10^{22} \text{ cm}^{-3}$ which results in $\omega_p \approx 5.7 \times 10^{15} \text{ sec}^{-1}$ or a wavelength of about 330 nm.⁶ Because the plasmon frequency varies from metal to metal, it provides a useful piece of spectral information about the material. It must be emphasized that the plasmon resonance is an optical property of bulk metals that is *independent* of the size of a metal structure, as noted from equation (1).

In addition to plasmon resonances in the bulk metal, lower energy resonances associated with surface-charge oscillations can be induced. Surface plasmon resonances, unlike those in the bulk, are strongly dependent on material size, shape, and interfacial properties. The geometrical shape can affect the frequency as well as the number of resonances. An elliptical particle, for example, may possess two spectrally distinct surface plasmon resonances corresponding to the short and long axes of the material.⁸ Interfacial conditions such as excess surface charge, surface-chemical modification, and the dielectric environment also influence the frequency and bandwidth of the plasmon resonance.^{2,9-11} Mulvaney reported that only 0.1 monolayer of a dielectric layer electrodeposited on a metal surface caused significant shifts in the energy of the surface plasmon resonance.⁹ Size, by far, has the largest impact on the nature of the surface plasmon. While metal structures of macroscopic dimensions (e.g. micrometers and larger) behave similarly to

bulk materials, nano-sized metal particles possess quite unique optical properties that are manifested in surface plasmon resonances.

Metal structures of dimensions much less than the wavelengths of light, such as the nano-sized silver colloidal particles shown in Figure 1, have been the subject of intense theoretical and experimental work since the early 1900's.⁶ Most of this work focused on understanding the various colors of colloidal metal solutions. One of the most successful theories was developed by Gustav Mie in 1908 to explain the colors of gold colloids in water.¹² A macroscopic approach was employed which used the classical Maxwell equations and essentially averaged the effects of an incident electric field over the volume of a nanostructure.¹³ By taking into account particle size-dependent dielectric functions, the Mie theory provided an exact solution for the efficiencies Q of light absorption (*abs*)

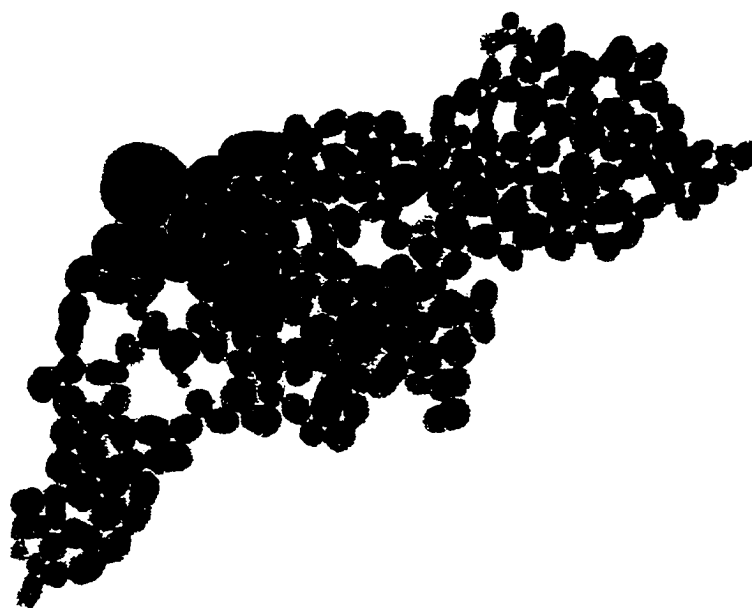


Figure 1. Transmission electron micrograph of nano-sized silver colloidal particles.

and scattering (*sca*) by small particles.¹³ The sum of the two contributions yields an experimentally measurable value given by

$$Q_{ext} = Q_{abs} + Q_{sca} \quad (2)$$

where Q_{ext} is known as the efficiency of extinction and describes the total attenuation of light by small particles. The particle size dependence of pure absorption, scattering, and extinction for a gold colloid according to the Mie theory is depicted in Figure 2.¹³ For spherical particles of radius 20 nm, the extinction band has a maximum around 530 nm and is comprised almost entirely of pure absorption (Q factor ≈ 2), there being only a small contribution from scattering ($Q \approx 0.1$), Figure 2(a). Under these conditions, the colloidal solution has a red color. For particles with a radius of 50 nm, the extinction band

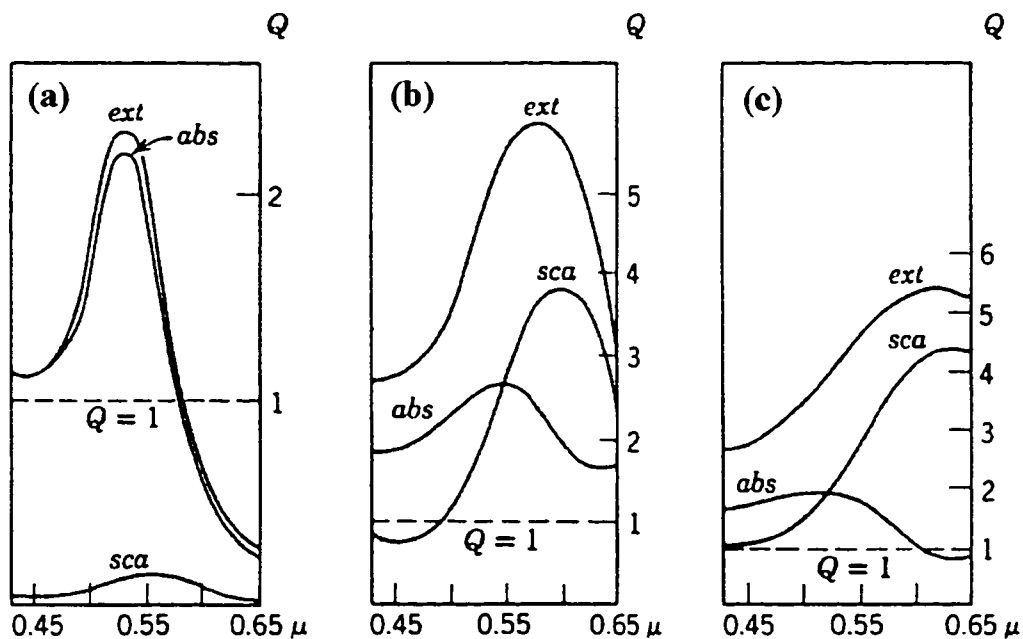


Figure 2. Extinction spectra according to Mie theory for different sizes of gold colloidal particles (from Ref. 13). The particle radii are (a) 20 nm, (b) 50 nm, and (c) 70 nm.

is shifted to a maximum around 580 nm and has a significantly increased efficiency of scattering ($Q \approx 4$) relative to the absorption, Figure 2(b). A colloidal solution of these particles has an orange-brown color. Finally, for particles with a radius of 70 nm, the extinction band is further shifted to around 610 nm and is dominated by the scattering component, Figure 2(c). The resultant Au colloidal solution has a blue color. The Mie theory has proven to yield accurate descriptions of the colors of nanostructured metals. It is therefore worth presenting some of the details of this theory.

As was apparent in Figure 2(a), the Mie theory predicts that the extinction cross section is dominated by pure absorption for spherical structures having a radius less than certain values ($R \cong 13$ nm for Au, $R \cong 8$ nm for Ag).¹⁰ The dipolar absorption cross-section is given by the relation

$$\sigma_{abs}(\omega) = 9 \frac{\omega}{c} \varepsilon_m^{3/2} V_0 \frac{\varepsilon_2(\omega)}{[\varepsilon_1(\omega) + 2\varepsilon_m]^2 + \varepsilon_2(\omega)^2} \quad (3)$$

where $\sigma_{abs}(\omega)$ is the frequency-dependent absorption cross-section, ω is the frequency of the incident radiation, c is the speed of light, V_0 is the spherical particle volume, and ε_m and $\varepsilon(\omega) = \varepsilon_1(\omega) + i\varepsilon_2(\omega)$ are the dielectric functions of the surrounding medium and of the particle material, respectively.¹⁰ In this size regime where the particle radius is much smaller than the wavelength of light, the instantaneous phase of the incident electric field is constant across the particle volume, which means that radiative damping terms due to retardation effects can be neglected. It is also interesting to note that higher order modes or multipoles can be optically excited.¹⁴ The probability of these resonances increases with increasing particle size.

A key result of equation (3) is that the optical properties of the sphere, in the small particle size regime, are determined solely by the real and imaginary parts of the complex dielectric function of the metal: $\epsilon_1(\omega)$ and $\epsilon_2(\omega)$, respectively. A peak appears in the Mie dipolar absorption cross-section at the frequency ω when the condition $\epsilon_1(\omega) = -2\epsilon_m$ is satisfied, as long as $\epsilon_2(\omega)$ is not too large and is slowly varying ($d\epsilon_2/d\omega \approx \text{small}$) near the resonance.¹⁰ Nanostructures of silver, gold, and the alkali metals are unique in that this condition is satisfied for incident light in the visible region of the spectrum.¹⁵ As an example, the particle size-dependent components $\epsilon_1(\omega)$ and $\epsilon_2(\omega)$ of the dielectric function for Ag particles ($R < 10$ nm) in an aqueous medium are shown in Figure 3.⁸ The above

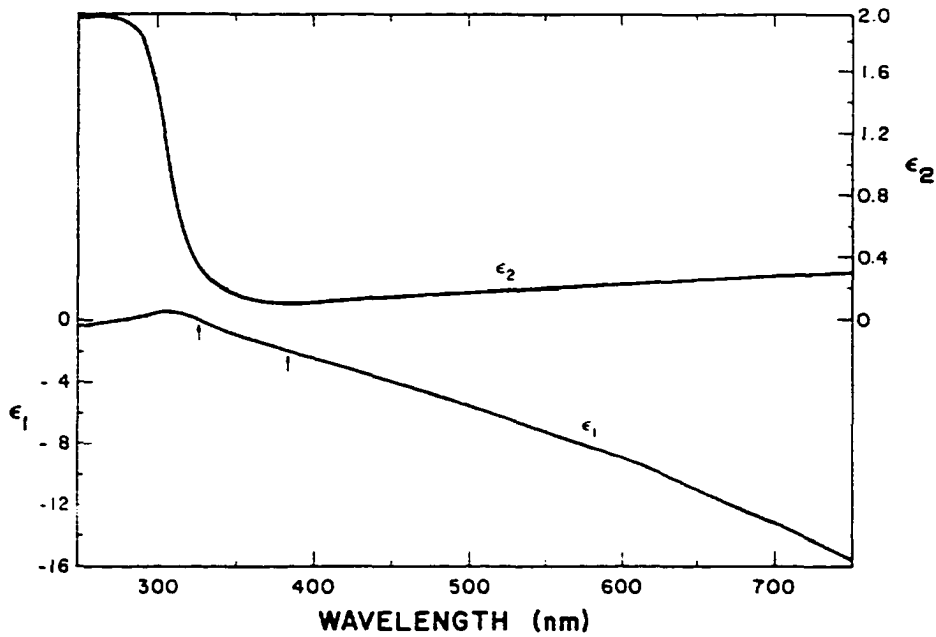


Figure 3. Real (ϵ_1) and imaginary (ϵ_2) parts of the complex dielectric function for silver particles (radius < 10 nm) in an aqueous medium (from Ref. 8).

condition is satisfied around the wavelength 380 nm where the Mie resonance peak occurs in the optical spectrum. Also noted is the position of the bulk plasmon resonance for Ag at 330 nm, well-resolved from the Mie absorption band. This Mie resonance band was recognized by Doyle as corresponding to the surface plasmon resonance of the free electron metal.¹⁶ The surface plasmon, when described as a dipole resonance, is pictured as oscillating positive and negative “caps” near the surface of the particle, Figure 4. The free electrons in the interior of the particle also participate in the resonance; however, the net electric field in the interior volume is zero as expected for a spherical conductor.

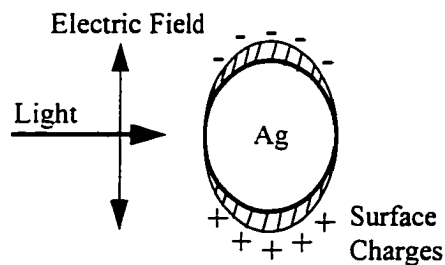


Figure 4. Polarization of a spherical silver particle under the influence of an incident, oscillating electric field, resulting in surface plasmon resonance.

So far the discussion has focused on the spectral position of the surface plasmon resonance band. However, this optical resonance of the metal nanostructure also has a predictable bandwidth. The homogeneous contribution to the bandwidth reflects the loss of phase coherence of the collective electron oscillation. Phase loss results in a decreased lifetime of the resonance, manifested in the optical spectrum by a decrease in overall intensity and broadening (“damping”) of the absorption band. Lamprecht and coworkers

measured the lifetime of the surface plasmon resonance to be 10 fs by second harmonic generation in lithographically designed, monodispersed Ag nanostructures of around 200 nm size.¹⁷ This fast decay accounted for nearly 74 nm of the bandwidth in the observed extinction spectra. Inhomogeneous contributions to the bandwidth are also generally present and are caused by the distribution of particle sizes, shapes, and matrix effects. These contributions are tedious to treat theoretically and will not be discussed here.

The homogeneous contribution to the absorption bandwidth has been described using a microscopic approach based on the Lorentz harmonic oscillator model for highly polarizable materials.⁶ In this model, the electrons and positive ion cores of the metal are viewed as a collection of independent, simple harmonic oscillators (i.e. “springs”). Each electron is thought to be connected by a spring to a stationary ion core. The equation of motion for the single oscillating electron is given by

$$m \frac{d^2x}{dt^2} + b \frac{dx}{dt} + kx = qE \quad (4)$$

where m is the mass of the oscillating electron, b is a damping constant, k is the spring constant, E is the force exerted by a uniform electric field on the charge q , and x is the displacement of the oscillator from equilibrium.⁶ If the electric field has a time-dependent frequency ω , then the displacement of the oscillator from equilibrium can be expressed as

$$x = \frac{(q/m)E}{\omega_0^2 - \omega^2 - i\gamma\omega} \quad (5)$$

where $\omega_0^2 = k m^{-1}$ is the resonant frequency of the electron oscillator and $\gamma = b m^{-1}$ is a phenomenological damping constant for the resonance.

The ensemble of independent, oscillating electrons in a metal also can be expected to oscillate collectively in response to an applied external electric field. As a result, there exists an induced dipole moment which is defined, normalized per unit volume, by

$$P = \frac{\omega_p^2}{\omega_0^2 - \omega^2 - i\gamma\omega} \epsilon_0 E \quad (6)$$

where P is the polarization of the collection of oscillators, ω_p is the classical bulk plasmon frequency previously given in equation (1), and ϵ_0 is the permittivity. This induced polarization can be related to the dielectric properties of the metal (and therefore to the optical properties) by using the following classical relations for the polarization (P) of a material and for the complex dielectric function (ϵ) given as

$$P = \epsilon_0 \chi E \quad (7)$$

$$\epsilon = 1 + \chi \quad (8)$$

where χ is the electric susceptibility.⁶ By combining equations (6), (7), and (8), the frequency-dependent dielectric function for a collection of harmonic, oscillating electrons can be derived as

$$\epsilon(\omega) = 1 + \frac{\omega_p^2}{\omega_0^2 - \omega^2 - i\gamma\omega} \quad (9)$$

Equation (9) is a fundamental relation of the Lorentz harmonic oscillator model for polarizable materials. It relates the complex dielectric constant, which was shown to directly determine the optical properties of metal nanostructures through the Mie resonance formula (equation 3), to the frequencies of the bulk plasmon resonance, the

incident electric field, the harmonic oscillator resonance, and a damping factor. The damping factor is important in that it determines the width of the Lorentzian lineshape.

For real systems of simple metals, however, the Lorentz model is not quite correct because the electron oscillators are “free” electrons and are not bound by a spring. Equation (9) can be modified to account for this fact simply by “clipping” the spring. In this case, known as the Drude model for a free electron metal, the spring constant $k = 0$ which results in the harmonic oscillator frequency $\omega_0^2 = 0$. The complex dielectric function now can be rewritten as

$$\varepsilon(\omega) = 1 - \frac{\omega_p^2}{\omega^2 + i\gamma\omega} \quad (10)$$

Again with the goal being to understand the bandwidth of Mie absorption features (surface plasmon resonances), the previously mentioned equation (3) which describes the absorption cross-section can be rewritten using the dielectric function in equation (10) and the condition $\omega \approx \omega_1$ yielding

$$\sigma_{abs}(\omega) = \sigma_0 \frac{1}{(\omega - \omega_1)^2 + \left(\frac{\gamma}{2}\right)^2} \quad (11)$$

where ω_1 is the frequency of the *undamped* Mie surface plasmon resonance given by

$$\omega_1 = \frac{\omega_p}{\sqrt{1 + 2\varepsilon_m}} \quad (12)$$

and ε_m is the dielectric constant of the surrounding medium.⁷ A key feature of equation (11) is that the Drude damping constant γ equals the real bandwidth, in frequency units, of the surface plasmon resonance of a nano-sized, free electron metal. In real systems,

damping of the plasmon results from scattering of the oscillating electrons with lattice phonons, neighboring electrons, or structural impurities.^{10,18}

Recent experimental results suggest that the original Drude damping constant γ is not sufficient for describing the observed bandwidth of surface plasmon resonances.¹⁰ While studying small silver clusters embedded in solid matrices, Kreibig and coworkers noted a significant increase in the plasmon bandwidth and small shifts in the plasmon frequency for decreasing particle sizes in the range 20 nm to 2 nm.¹⁰ The γ of equation (11) does not account for size-dependence. The authors also noted that the equation for Mie dipolar absorption (equation 3) contains only one size-dependent term, the spherical particle volume V_0 , which is in the prefactor and should not affect the plasmon resonance frequency or band shape. The experimental data was thus used to derive a new phenomenological damping parameter defined by

$$\Gamma_{\text{expt}}(R) = \Gamma_0 + a/R \quad (13)$$

where Γ_{expt} is the particle radius R dependent damping constant of the observed spectra, Γ_0 is the size-independent damping constant, and a is the slope of a fitted curve for the size dependence. The $1/R$ dependence of the damping constant was found to fit reasonably well with other data compiled from the literature (Ref¹⁰, Figure 3), assuming the adjustable parameter a is dependent on the surrounding matrix.

The above damping constant does not, however, successfully describe all systems. The surface plasmon resonance in many nanostructures exhibits strongly increased damping that appears to be independent of particle size. Several studies have focused on the phenomenon of “chemical interface damping” in which surface impurities, molecular

adsorption, or chemical reactions at the particle/matrix interface contribute to anomalously large damping factors.^{2,10,11} It should be emphasized that this is a relatively new area of research and broad theoretical descriptions have not yet evolved.

Surface-Enhanced Spectroscopies at Nanostructured Metals

The excitation of surface plasmon resonances in nanostructured metals results in a remarkable increase of the local electric field, relative to that of the incident electric field, near the structure's surface. It has been shown that this local electric field can cause the enhancement of various optical phenomena including Raman scattering, infrared absorption, fluorescence, second-harmonic generation, and four-wave mixing.¹⁹⁻²¹ Surface-enhanced Raman scattering spectroscopy was utilized extensively in the present work and is discussed in detail in the following section.

Of importance here is the form of the metal nanostructures generally employed for surface-enhanced spectroscopies. By far the most common structures are nano-sized colloidal metal particles, thin metal films, and roughened metal electrodes.²² Colloidal particles, like those shown previously in Figure 1, are advantageous for a number of reasons: (1) preparation is relatively easy, (2) fresh samples are continuously available by stirring the suspension, (3) particle size and shape are controllable, and (4) extinction spectra are readily measured in a standard spectrophotometer. Colloids are also an ideal system in that the isolated particles are well-described by the Mie theory. Unfortunately, many colloidal metals in the natural suspended state are unstable and readily form extended aggregates, whose optical properties can be different than those of the isolated

particles.¹⁸ To overcome this problem, Cotton et al. and Natan et al. independently developed colloidal metal films (CMF) as substrates for surface-enhanced spectroscopies.^{20,23} The CMFs are prepared by the spontaneous adsorption of monolayers of nano-sized particles to glass substrates derivatized with functional groups that have a high affinity for the metal, such as SH, COOH, and NH₃. A typical colloidal metal film is composed of isolated particles, as shown in the scanning electron micrograph in Figure 5.²⁴ CMFs are ideal substrates for several reasons: (1) the optical properties of the metal nanostructures are identical to those of the free particles in solution, (2) they can be readily transferred into any solution, and (3) they are stable over long periods of time.²⁰ Colloidal metal films formed from Ag nanostructures played an important role in the current studies of Chapters 3 and 4.

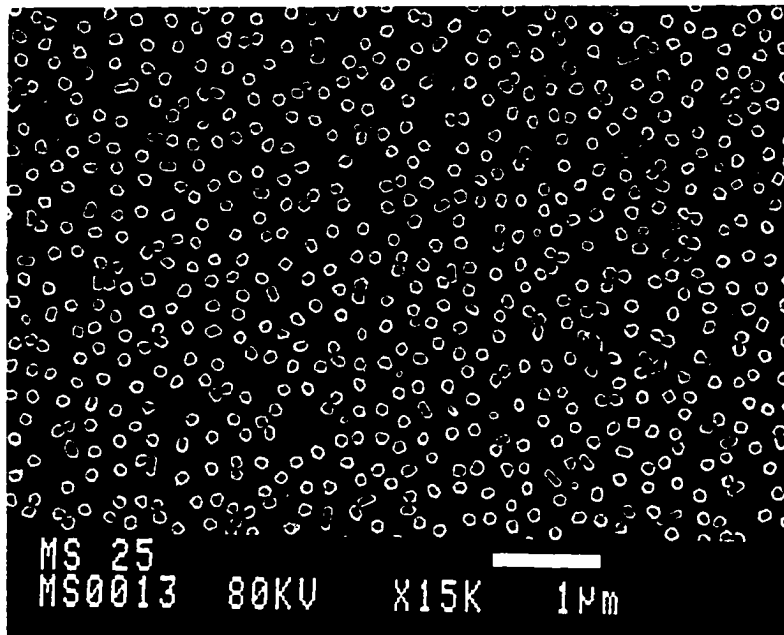


Figure 5. Scanning electron micrograph of a silver colloidal metal film (from Ref. 24).

Bulk metal electrodes and thin metal films are also useful as substrates for surface-enhanced spectroscopies. The latter are generally formed by lithographic techniques, in which highly-ordered periodic arrays are created, or by vapor-depositing the metal onto appropriate substrates.²² A thin silver film prepared by vapor-depositing ca. 1 μm equivalent mass thickness of the metal onto glass is shown in Figure 6.²⁴ From Figure 6 it can be clearly seen that the thin metal film is composed of nano-sized Ag structures, similar in two-dimensional shape to the colloidal metals. Surface plasmon resonances can be optically excited in these Ag structures, providing the high local fields for surface-enhancement. Even larger enhancement factors can be obtained, however, at roughened bulk metal electrodes and roughened thin metal films.²² The roughening is generally accomplished by immersing the metal into highly acidic solutions or, more preferably, by electrochemical procedures in which the metal is successively oxidized from the surface into an aqueous solution and then reduced back onto the metal surface. The application of an electrochemical roughening procedure to the thin Ag film of Figure 6 resulted in the silver surface shown in Figure 7.²⁴ The obvious result of the electrochemical procedure is that material is removed from the surface, creating atomically sharp and nano-scale roughness features. Appropriate theories have been developed to describe the optical properties (including surface plasmon resonances) in these roughened surfaces.²⁵

The unique optical properties of nanostructured metals, specifically surface plasmon resonances, play an important role in several modern analytical methods including surface-enhanced Raman scattering spectroscopy. In addition, extinction spectra

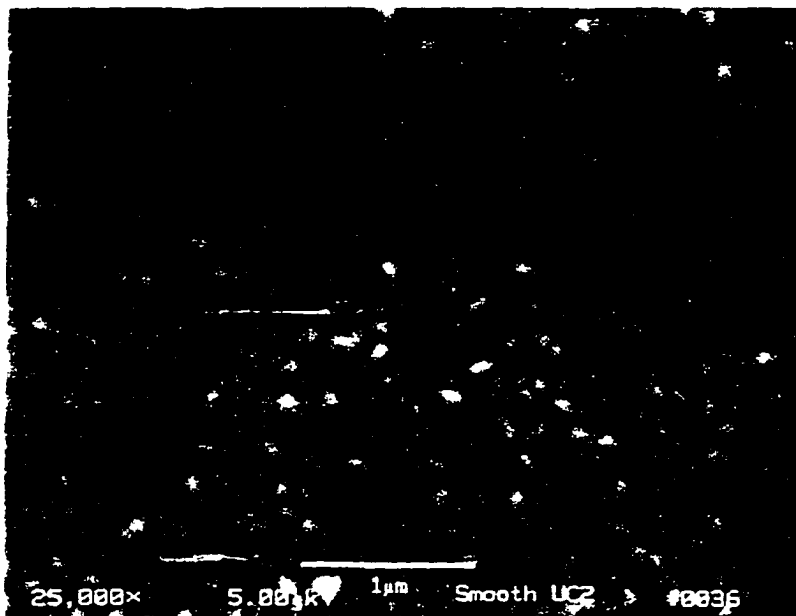


Figure 6. Scanning electron micrograph of a vapor-deposited thin Ag film (from Ref. 24).

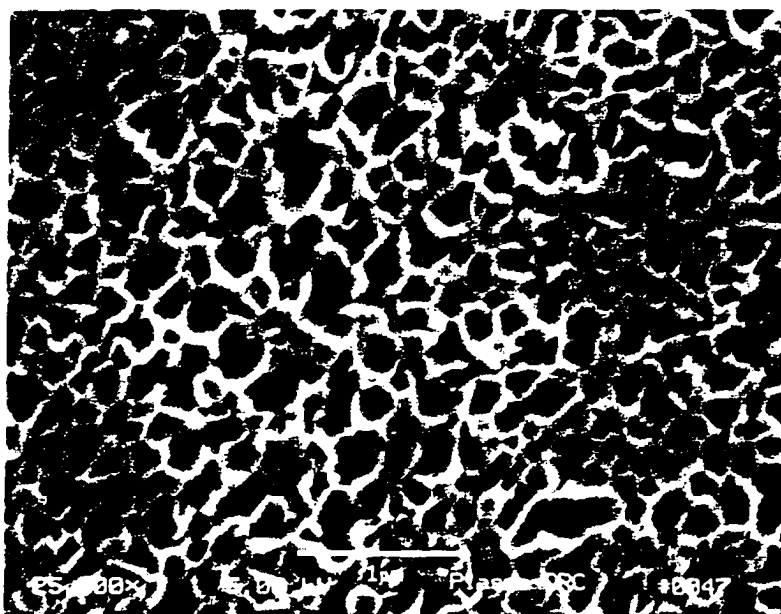


Figure 7. Scanning electron micrograph of a vapor-deposited thin Ag film, roughened by an electrochemical procedure (from Ref. 24).

of the plasmon resonances are extremely sensitive to interfacial properties of the metal, making them useful for the study of chemical reactions at the metal/solution interface.

Surface-Enhanced Raman Spectroscopy

Molecules and ions which are near or adsorbed on certain nanostructured metallic surfaces can exhibit unusually strong Raman scattering. In many cases, intensity enhancement factors of 10^5 to 10^6 have been observed relative to the Raman scattering from the same species in the absence of the surface.²² This phenomenon, known as surface-enhanced Raman scattering (SERS), plays an important role in the present dissertation research. SERS was employed as a spectroscopic method to characterize the interactions of protein molecules and small ions with Ag surfaces. The rich structural information provided by vibrational spectroscopies in addition to the inherent sensitivity to surface-adsorbed species make surface-enhanced Raman an appropriate choice for the current investigations.

Electrochemists in the early 1970's discovered the SERS effect while adapting Raman spectroscopy to study molecular adsorption processes at the aqueous solution-metal electrode interface.²⁶⁻²⁸ Fleischmann and coworkers observed changes in the frequencies and relative intensities of the normal vibrational modes of pyridine adsorbed on Ag as a function of electrode potential. From this work the authors concluded that pyridine adsorbed to the metal by coordination of the pyridyl N atom to the Ag surface. Then in 1977, while studying the same pyridine-silver system, two research groups

independently noted for the first time the significant enhancement of Raman scattering at the metal surface.^{27,28}

Through around 1985, a majority of the work in the SERS field consequently focused on understanding the enhancement mechanism(s).^{19,25,29} More modern studies have focused on *applying* SERS as a sensitive spectroscopic tool to address problems in such areas as chemistry, biochemistry, biophysics, and materials science.^{22,30,31} Through early 1997, over 3600 papers related to the SERS effect have been published including an average of around 130 papers per year from 1993 to 1996.

The following sub-sections are intended to provide a brief review of the basic theoretical understanding of the SERS effect as well as to highlight significant recent achievements in the application of SERS for chemical analysis and analytical detection.

Theoretical Considerations

In the classical electrostatic theory for scattering, particles that are small compared to the wavelength of light can be polarized in the presence of a uniform electric field.¹³ The extent of polarization, or induced dipole moment μ , depends on the polarizability α of the particle's electron density and the magnitude E of the applied electric field. The amplitude of the induced dipole moment is then given by the relation

$$\mu = \alpha \cdot E \quad (14)$$

where α is a tensor, a generalized vector having specified directional components, and the electric field E is assumed to be homogeneous. In the case where the particle is a molecule whose atoms can vibrate at a discrete frequency ω_k and where the applied field

varies with time as in the frequency of a monochromatic light source ω_L , equation (14) can be expanded to include the time-dependent terms and then simplified to the expression

$$\mu(\omega_L) = \alpha_0 E_0 \cos(\omega_L t) + (\frac{1}{2})\alpha_0 E_0 \cos(\omega_L - \omega_k)t + (\frac{1}{2})\alpha_0 E_0 \cos(\omega_L + \omega_k)t \quad (15)$$

where α_0 is the polarizability of the molecule in its equilibrium geometry.²² The first term of equation (15) describes light that is scattered by the molecule at the same frequency as the incident light, or “elastically,” and is referred to as Rayleigh scattering. The second and third terms describe radiation that is shifted in frequency, or “inelastically” scattered, relative to the incident light. These terms represent normal Stokes Raman scattering and Anti-Stokes Raman scattering, respectively, and inherently contain information about the vibrational frequencies of the molecule.

If the molecule of interest is near or adsorbed on certain metal surfaces, the intensity of the Raman scattered radiation can be significantly enhanced. The origin of this surface-enhanced Raman effect has been explained by two classes of theories, both evident from equation (14): the electromagnetic (EM) enhancement mechanism and the chemical enhancement or charge-transfer (CT) mechanism.^{19,25,29} Metal surfaces that exhibit either of these mechanisms for surface-enhancement are often referred to as “SERS-active.”

In the EM theory, the electric field which polarizes the molecule also interacts with the metal substrate to induce plasmon resonances.³² As discussed in the previous section on nanostructured materials, the excitation of surface plasmon resonances combined with

the incident electric field generates a very high local electric field E which can enhance all optical phenomena occurring near the metal surface. It has been both predicted and demonstrated experimentally that the high local field can lead to enhancement factors of 10^4 to 10^6 of the Raman scattered light.^{29,33}

The EM enhancement mechanism is also thought of as a long-range effect because the local field decays with a $1/r^{12}$ dependence, where r is the distance of the molecule from the metal surface.³⁴ Murray and coworkers elegantly demonstrated this long-range effect by using optically transparent polymer spacer layers between a roughened Ag surface and a monolayer of *p*-nitrobenzoic acid.³⁴ The Raman scattering intensity was found to decrease by an order of magnitude in about a 50 Å thick spacer layer. Two recent approaches to investigating this distance-dependence have employed Langmuir-Blodgett films and self-assembled monolayers of functionalized alkanethiols.³⁵⁻³⁷ Using self-assembled monolayers on an electrochemically roughened Ag surface, Tsen and Sun monitored the ring-breathing mode in the SERS spectrum from phenyl terminated mercapto-*N*-alkanamides of variable chain length, Figure 8.³⁷ The authors found that the

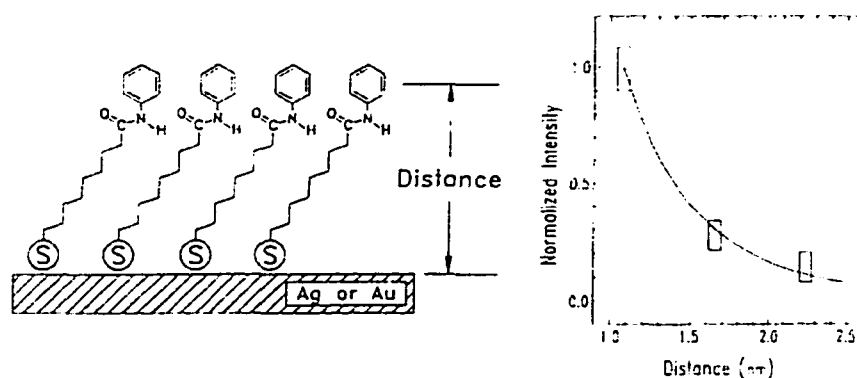


Figure 8. Distance-dependence of the SERS enhancement factor from a phenyl terminated mercapto-*N*-alkanamide self-assembled monolayer (from Ref. 37).

enhancement factor decayed by 50% in only 3.5 Å, nearly a factor of 10 faster than previous reports.^{34,35} Regardless of the slope of the decay curve, the important fact remains that, in the EM theory, molecules need not be in intimate contact with the metal surface for significant enhancement of Raman scattering to be observed. A consequence is that the observed SERS spectra are generally the same as those observed for free molecules in the vapor or condensed phases, making spectral interpretation straightforward.

The chemical enhancement or CT mechanism, on the other hand, requires some form of direct electronic interaction between the molecule of interest and the metal. This interaction can be due to σ - or π -bonding, temporary charge-transfer with metal “active sites” (adatoms, small clusters, or defect sites), or electrostatic attraction.³⁸⁻⁴⁰ The unique adsorbate-metal surface complex which is formed can significantly perturb the molecular polarizability α relative to the free molecule and can lead to SERS enhancement factors of 10 to 100.²² Chemical enhancement of Raman scattering is expected to be a short-range effect, generally confined to the first monolayer of adsorbates, and is highly sensitive to the specific adsorbate-metal interaction. The latter often results in SERS spectra that are different from Raman spectra of the free molecule. Band shifts, changes in relative band intensities, and even new features can be observed.³⁸

Moskovits and DiLella elegantly demonstrated the CT mechanism in studies of the adsorption of equimolar amounts of CO and N₂ on a Ag surface.⁴¹ The SERS spectrum for adsorbed CO was about 100 times more intense than that for adsorbed N₂, even though the polarizabilities of the free molecules are nearly the same. It was also noted in the

spectra that the band due to adsorbed CO was shifted nearly 30 cm^{-1} and broadened while the band due to adsorbed N_2 remained unchanged relative to the bands observed on a silver-free surface. This fact led the authors to conclude that CO formed a charge-transfer complex with the metal which gave rise to significant chemical enhancement of the Raman spectrum.

As an empirical model, the CT theory has been quite successful at explaining Raman data. It has proven difficult, however, to characterize experimentally the SERS “active sites” which give rise to chemical enhancement, often described using Otto’s adatom model.³⁹ In support of the adatom model, Choi et al. recently explained the time-dependent decay of SERS intensities using a “random walk” model for the surface diffusion of Ag adatoms.⁴² The intensity of the 3500 cm^{-1} band from H_2O adsorbed on a Ag electrode was monitored for 90 min. The irreversible loss of Raman intensity was found to follow a non-simple exponential decay and suggested that adatoms traveled only short distances (ca. 2 \AA) to become incorporated in non-SERS active large adatom clusters and surface defects. While the paper provided a nice explanation of the dynamics of SERS intensities, no direct spectroscopic evidence was provided for the existence of the described adatoms. Besides surface restructuring, the loss of “adatom” activity often has been attributed to surface passivation. For example, Rubim and Nicolai recently reported that O_2 effectively quenched the SERS signal from pyridine adsorbed on Ag, Cu, and Au electrodes in aqueous solution.⁴³ Uncontrolled processes such as surface oxidation and restructuring have proven to be significant obstacles to the continuous or long-term use of substrates for SERS-based analyses.

In another fundamental study, Campion and coworkers are working to prove that the CT mechanism actually involves *resonance* Raman scattering through a charge-transfer intermediate state.⁴⁴ The authors recorded spectra in ultrahigh vacuum of pyromellitic dianhydride (PMDA) on atomically smooth Cu(100) and Cu(111) single crystals, surfaces which are known to be inactive for the EM enhancement mechanism. First, the spectra were found to be strongly sensitive to the polarization on both surfaces, but in different ways. Molecular modeling indicated that these results could not be explained by simple reorientation effects. Second, the authors performed an excitation profile after discovering a strong resonance in the spectra of the PMDA monolayers in a spectral region where the free molecules did not absorb light. It was noted that the intensities of the resonant bands were not linearly affected by dosing the copper surfaces with multilayers of PMDA, consistent with the interpretation that a new adsorbate-surface electronic state was formed. Based on this work it is obvious that a complete understanding of the CT enhancement mechanism will require a thorough study of local electronic structure including both the adsorbate-metal complex and the bulk metal.

A recent review by Brandt and Cotton reminds practitioners of SERS spectroscopy that neither the EM theory nor the CT theory alone can account for all observations in surface-enhanced Raman scattering experiments.²² In most cases, the observed enhancement appears to be a product of the individual contributions of the EM and CT mechanisms.

Analytical Applications of SERS

Beyond the use of surface-enhanced Raman spectroscopy for the fundamental studies of molecules and surfaces, SERS has been quite successfully demonstrated as a sensitive analytical method for qualitative and quantitative analysis.³⁰ Some of the common problems to be dealt with in designing a SERS-based method of detection are (1) poor adsorption on the metal surface and/or fouling by strongly adsorbing species, (2) long-term stability of a surface, (3) reproducibility of SERS intensities both at different spots on a single substrate and among multiple substrates, and (4) concentration calibration curves that are useful over only a small dynamic range. A couple of these problems have been addressed in novel ways by the following authors.

Recent advancements in the use of SERS-based detection have been described for flow injection analysis, gas chromatography, planar chromatography, and complexation analysis. Pothier and Forcé developed a flow injection analysis method for biologically important molecules using a computer-controlled potential waveform to efficiently adsorb and desorb the analytes at an Ag electrode.⁴⁵ In an alternate approach, Rubim et al. demonstrated femtomol detection limits of Fe(II) using a novel spectroelectrochemical cell for flow injection analysis.⁴⁶ In this work, the authors prepared a fresh silver surface just prior to the injection of analyte by introducing Ag^+ ions to the flow system and electrodepositing the silver on a glassy carbon electrode. Anodic stripping to clean the carbon electrode between analytes thus maintained a clean, stable SERS-active surface.

SERS-based detection in planar chromatography was recently reviewed by Somsen and coworkers.⁴⁷ One notable study was by Caudin and coworkers in which sub-

femtogram amounts of all-*trans* crocetin were measured on TLC plates pre-coated with Ag colloid.⁴⁸ Roth and Kiefer demonstrated the use of SERS detection in gas chromatography by trapping a pyridine eluant in colloidal Ag solutions and on colloid-coated TLC plates.⁴⁹ A more sophisticated approach to GC-SERS was demonstrated by Carron and Kennedy in which *o,m,p*-xylenes were detected on a propanethiol-coated Ag foil.⁵⁰ The modified silver surface provided both a hydrophobic interface to promote adsorption of the organic molecules and prevented detrimental oxidation of the SERS “active sites.”

Surface-enhanced Raman spectroscopy also has been employed for quantitative host-guest complex and chelator-metal complex analyses. An interesting example of the former involved azo dye molecules which strongly interacted with thiol-derivatized cyclodextrin-modified Ag surfaces.⁵¹ Inclusion of the guest dye molecules into the host cyclodextrin cavity was monitored by predictable changes in the SERS spectra of the dyes. Examples of chelator-metal complex formation include a thiol-derivatized resorcinol-modified Ag surface for the detection of Cu, Pb, and Cd at ppb levels⁵², pyridyl and phenanthroline chelators adsorbed on Ag colloids for the detection of Co, Ni, and Fe also at ppb levels⁵³, and benzoic acid adsorbed on Ag colloids for the measurement of anion exchange constants with the metal.⁵⁴

Surface-enhanced Raman spectroscopy appears to be a useful practical technique for routine analysis providing molecular specificity, high sensitivities, and low limits of detection.

Single Molecule Detection

Pushing the limits of ultratrace detection, several authors have recently reported SERS from isolated single metal particles and, more impressively, SERS from single molecules.⁵⁵⁻⁵⁷ Xiao et al. claimed to demonstrate for the first time SERS from spatially isolated, single Ag particles.⁵⁵ The isolated nanostructures were lithographically prepared using a scanning probe microscope tip to etch a thiol self-assembled monolayer on a gold electrode followed by electrochemical reduction of Ag^+ preferentially into the etch “pits.” Using a focused laser, diffraction-limited spot, spectra with reasonable signal-to-noise were then obtained from *trans*-4-mercaptomethyl stilbene molecules adsorbed on the Ag surfaces. The authors calculated SERS enhancement factors of ca. 10^4 for the single particles and of ca. 10^6 for closely-spaced clusters of particles. The latter is an interesting result from which Xiao et al. speculated that additional enhancement occurred for molecules positioned in the space *between* particles due to electromagnetic coupling of plasmon resonances.

The detection of single molecules using SERS spectroscopy was recently reported independently by two groups.^{56,57} Kneipp and coworkers observed spectra from single crystal violet molecules under resonance conditions with near-IR excitation, thereby taking advantage of an estimated 10^{14} enhancement factor.⁵⁶ The low concentration limit was achieved by diluting the dye in a Ag colloid solution to 3.3×10^{-14} M and probing a volume of about 30 pL with a Raman microscope. This yielded an estimated 0.6 dye molecule and about 100 Ag particles in the probed volume, a ratio unlikely to yield the sampling of more than one molecule. The authors presented a sequential acquisition of

100 spectra measured in 1 sec intervals along with a time-profile of a single vibrational band. The latter showed the “on” and “off” behavior of the SERS scattering and, based on Poisson statistics, was consistent with an average of 0.5 molecules in the scattering volume per 1 sec integration time.

Using a different methodology, Nie and Emory observed spectra from single rhodamine 6G molecules on single Ag nanoparticles under resonance conditions with green excitation.⁵⁷ A unique feature of this study was the use of an integrated optical and atomic force microscope, which allowed sequential Raman scattering and topographical information to be recorded from the colloidal Ag particles immobilized on a polylysine-coated glass substrate. After incubating the substrates for about 3 hours with $\leq 2 \times 10^{-11}$ M dye solutions, each Ag particle was estimated to carry an average of ≤ 1 dye molecule. The authors collected wide-view SERS images by evanescent wave excitation which showed the distribution of “hot particles” that contained adsorbed dye. Nie and Emory also conducted measurements of the polarization dependence of the Raman scattering with respect to the single particle orientation. For example, ellipsoidal single particles were found to give only SERS spectra for excitation light polarized along the long axis of the given particle, as shown in Figure 9. SERS enhancement was thus considerably stronger for plasmon resonances excited along the particle long axis, relative to those excited along the short axis. To test if the observed polarization was purely due to the particle orientation and/or to dye molecule orientation, another experiment was performed in which the SERS spectra were excited with polarization-scrambled incident light and a dichroic polarizer prior to detection. This arrangement was then intended to eliminate the

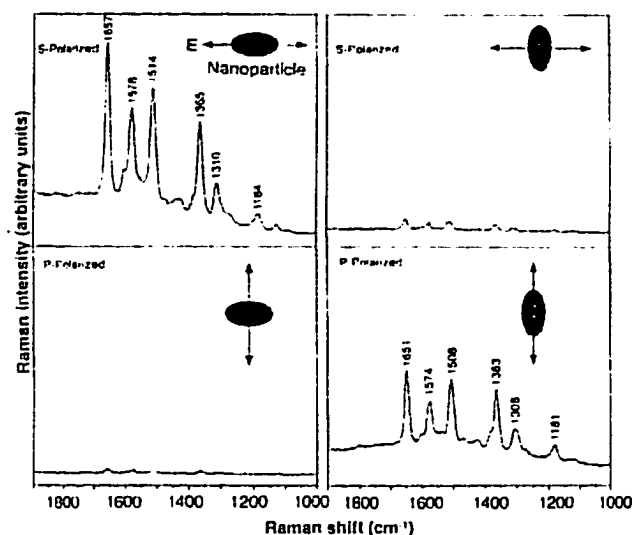


Figure 9. Surface-enhanced Raman spectra excited with linearly polarized light of single rhodamine 6G molecules on oriented single silver nanostructures (from Ref. 57).

orientation effect of the particle. The observed spectra seemed to indicate that the surface-enhanced Raman scattering from the dye was highly polarized, contrary to previous reports that SERS yields only depolarized scattering.⁵⁸ Several interesting results were presented in this work which demand further investigation.

The apparent observations of surface-enhanced Raman scattering from single nanostructures is a monumental achievement which should discount the belief that aggregates or clusters of particles are required for appreciable SERS. It also proverbially “opens the door” to a variety of particle size, shape, and structure dependent analyses. The further observations of SERS spectra from single dye molecules demonstrate the attainment of the ultimate limit of detection for an analytical method, that of the single molecule.

References

- (1) Ozin, G. A. *Adv. Mater.* **1992**, *4*, 612.
- (2) Henglein, A. *J. Phys. Chem.* **1993**, *97*, 5457.
- (3) Weller, H.; Eychmüller, A. In *Advances in Photochemistry*, Neckers, D. C., Volman, D. H. and Bünau, G. v., Eds.; Wiley: New York, 1995; Vol. 20, p 165.
- (4) Bard, A. J.; Abruña, H. D.; Chidsey, C. E.; Faulkner, L. R.; Feldberg, S. W.; Itaya, K.; Majda, M.; Melroy, O.; Murray, R. W.; Porter, M. D.; Soriaga, M. P.; White, H. S. *J. Phys. Chem.* **1993**, *97*, 7147.
- (5) Valmalette, J. C.; Lemaire, L.; Hornyak, G. L.; Dutta, J.; Hofmann, H. *Analysis* **1996**, *24*, M23.
- (6) Bohren, C. F.; Huffman, D. R. Ed.; Wiley: New York, 1983, Chap. 9.
- (7) Ferrell, T. L.; Callcott, T. A.; Warmack, R. J. *Amer. Sci.* **1985**, *73*, 344.
- (8) Kerker, M. *J. Colloid Interface Sci.* **1985**, *105*, 297.
- (9) Mulvaney, P. *Langmuir* **1996**, *12*, 788.
- (10) Hövel, H.; Fritz, S.; Hilger, A.; Kreibig, U.; Vollmer, M. *Phys. Rev. B* **1993**, *48*, 18178.
- (11) Rostalski, J.; Quinten, M. *Colloid Polym. Sci.* **1996**, *274*, 648.
- (12) Mie, G. *Ann. Physik* **1908**, *25*, 377.
- (13) Van de Hulst, H. C. *Light Scattering by Small Particles*, Dover: New York, 1981.
- (14) Kreibig, U.; Zacharias, P. *Z. Physik* **1970**, *231*, 128.
- (15) Creighton, J. A.; Eadon, D. G. *J. Chem. Soc., Faraday Trans.* **1991**, *87*, 3881.
- (16) Doyle, W. T. *Phys. Rev.* **1958**, *111*, 1067.
- (17) Lamprecht, B.; Leitner, A.; Aussenegg, F. R. *Appl. Phys. B* **1997**, *64*, 269.
- (18) Kreibig, U.; Quinten, M. In *Clusters of Atoms and Molecules II*, Haberland, H., Ed.; Springer Series in Chemical Physics Vol. 56; Springer-Verlag: Berlin, 1994, p 321.

- (19) Moskovits, M. *Rev. Mod. Phys.* **1985**, *57*, 783.
- (20) Chumanov, G.; Sokolov, K.; Gregory, B. W.; Cotton, T. M. *J. Phys. Chem.* **1995**, *99*, 9466.
- (21) Johnson, E.; Aroca, R. *J. Phys. Chem.* **1995**, *99*, 9325.
- (22) Brandt, E. S.; Cotton, T. M. In *Investigations of Surfaces and Interfaces-Part B*, 2nd ed.; Rossiter, B. W. and Baetzold, R. C., Eds.; Physical Methods of Chemistry Series; Wiley: New York, 1993, p 633.
- (23) Freeman, R. G.; Grabar, K. C.; Allison, K. J.; Bright, R. M.; Davis, J. A.; Guthrie, A. P.; Hommer, M. B.; Jackson, M. A.; Smith, P. C.; Walter, D. G.; Natan, M. J. *Science* **1995**, *267*, 1629.
- (24) Sibbald, M. S.; Cotton, T. M. *unpublished results*: **1996**.
- (25) Chang, R. K.; Furtak, T. E. *Surface Enhanced Raman Scattering*; Chang, R. K.; Furtak, T. E., Eds.; Plenum: New York, 1982.
- (26) Fleischmann, M.; Hendra, P. J.; McQuillan, A. J. *Chem. Phys. Lett.* **1974**, *26*, 163.
- (27) Jeanmaire, D. L.; Van Duyne, R. P. *J. Electroanal. Chem.* **1977**, *84*, 1.
- (28) Albrecht, M. G.; Creighton, J. A. *J. Am. Chem. Soc.* **1977**, *99*, 5215.
- (29) Otto, A.; Mrozek, I.; Grabhorn, H.; Akemann, W. *J. Phys.: Condens. Matter* **1992**, *4*, 1143.
- (30) Garrell, R. L. *Anal. Chem.* **1989**, *61*, 401A.
- (31) Rupérez, A.; Laserna, J. J. In *Modern Techniques in Raman Spectroscopy*, Laserna, J. J., Ed.; Wiley: New York, 1996, p 227.
- (32) Kerker, M. *Acc. Chem. Res.* **1984**, *17*, 271.
- (33) Zeman, E. J.; Schatz, G. C. *J. Phys. Chem.* **1987**, *91*, 634.
- (34) Murray, C. A. In *Surface Enhanced Raman Scattering*, Chang, R. K. and Furtak, T. E., Eds.; Plenum: New York, 1982, p 203.
- (35) Cotton, T. M.; Uphaus, R. A.; Mobius, D. *J. Phys. Chem.* **1986**, *90*, 6071.
- (36) Bercegol, H.; Boerio, F. J. *Langmuir* **1994**, *10*, 3684.

- (37) Tsen, M.; Sun, L. *Anal. Chim. Acta* **1995**, *307*, 333.
- (38) Cotton, T. M.; Kim, J.-H.; Chumanov, G. D. *J. Raman Spectrosc.* **1991**, *22*, 729.
- (39) Otto, A.; Pockrand, I.; Billmann, J.; Pettenkofer, C. In *Surface Enhanced Raman Scattering*, Chang, R. K. and Furtak, T. E., Eds.; Plenum: New York, 1982, p 147.
- (40) Birke, R. L.; Lombardi, J. R. In *Spectroelectrochemistry: Theory and Practice*, Gale, R. J., Ed.; Plenum: New York, 1988, p 263.
- (41) Moskovits, M.; DiLella, D. P. In *Surface Enhanced Raman Scattering*, Chang, R. K. and Furtak, T. E., Eds.; Plenum: New York, 1982, p 243.
- (42) Choi, Y.-S.; Kim, J.-J.; Miyajima, S. *Chem. Phys. Lett.* **1996**, *255*, 45.
- (43) Nicolai, S. H. A.; Rubim, J. C. *Vib. Spectrosc.* **1994**, *7*, 175.
- (44) Kambhampati, P.; Child, C. M.; Campion, A. *J. Chem. Soc., Faraday Trans.* **1996**, *92*, 4775.
- (45) Pothier, N. J.; Forcé, R. K. *Appl. Spectrosc.* **1994**, *48*, 421.
- (46) Gouveia, V. J. P.; Gutz, I. G.; Rubim, J. C. *J. Electroanal. Chem.* **1994**, *371*, 37.
- (47) Somsen, G. W.; Morden, W.; Wilson, I. D. *J. Chromatogr. A* **1995**, *703*, 613.
- (48) Caudin, J. P.; Beljebbar, A.; Sockalingum, G. D.; Angiboust, J. F.; Manfait, M. *Spectrochim. Acta* **1995**, *51*, 1977.
- (49) Roth, E.; Kiefer, W. *Appl. Spectrosc.* **1994**, *48*, 1193.
- (50) Carron, K. T.; Kennedy, B. J. *Anal. Chem.* **1995**, *67*, 3353.
- (51) Maeda, Y.; Kitano, H. *J. Phys. Chem.* **1995**, *99*, 487.
- (52) Crane, L. G.; Wang, D.; Sears, L. M.; Heyns, B.; Carron, K. *Anal. Chem.* **1995**, *67*, 360.
- (53) Hidalgo, M.; Montes, R.; Laserna, J. J.; Rupérez, A. *Anal. Chim. Acta* **1996**, *318*, 229.
- (54) Aubard, J.; Bagnasco, E.; Pantigny, J.; Ruasse, M. F.; Lévi, G.; Wentrup-Byrne, E. *J. Phys. Chem.* **1995**, *99*, 7075.

- (55) Xiao, T.; Ye, Q.; Sun, L. *J. Phys. Chem.* **1997**, *B101*, 632.
- (56) Kneipp, K.; Wang, Y.; Kneipp, H.; Perelman, L. T.; Itzkan, I.; Dasari, R. R.; Feld, M. S. *Phys. Rev. Lett.* **1997**, *78*, 1667.
- (57) Nie, S.; Emory, S. R. *Science* **1997**, *275*, 1102.
- (58) Van Duyne, R. P. In *Chemical and Biochemical Applications of Lasers*. Moore, C. B., Ed.; Academic Press: New York, 1979; Vol. IV, p 101.

CHAPTER 2. THE SHAPE AND STRUCTURE OF SERS ACTIVE SILVER NANOSTRUCTURES

A paper to be submitted to the *Journal of Solid State Chemistry*

Morgan S. Sibbald and Therese M. Cotton

ABSTRACT

Chemically-prepared nanostructures of silver were analyzed by transmission electron microscopy and were found to have a mean diameter of 99 ± 10 nm. These Ag structures had mostly regular polyhedral geometries including two-dimensional trigonal, square, pentagonal, and hexagonal shapes, indicative of the isotropic aqueous environment in which the crystals were grown. Quantitative analysis of the crystallographic structure using selected area diffraction and convergent beam electron diffraction techniques indicated that the Ag nanostructures were composed of a face-centered cubic phase and had a lattice constant $a = 4.05 \pm 0.11$ Å, consistent with previous studies of fcc silver.

INTRODUCTION

Suspensions of nanometer-sized silver particles have been studied as catalysts for condensed phase reactions and as substrates for enhancing Raman scattering from adsorbed molecules (1, 2). The latter, known as surface-enhanced Raman scattering (SERS), arises partially from the unique optical properties of colloidal metals such as silver, gold, and copper (3). For particles of dimensions less than the wavelengths of light, discrete surface plasmon resonances can be optically excited. Existence of a plasmon resonance produces a tremendous increase in the local electromagnetic field near the

particle's surface (4). This local field can function to enhance all light-dependent phenomena occurring at or near the metal surface. Signal enhancements of up to 10^7 have been observed in SERS measurements of adsorbed pyridine by several authors (5-7). In combined SERS and electrochemical experiments, Feilchenfeld *et al.* recently demonstrated a plasmon-assisted electron transfer process from the Ag metal to surface-adsorbed viologen cations (8). Plasmon resonances thus can serve to improve the sensitivity of analytical methods as well as to promote a variety of surface reactions.

Of fundamental importance to understanding these unique optical properties is the correlation between the observed optical extinction spectra, composed of contributions from absorption and scattering, and their crystalline structure including size, shape and uniformity. The crystal structure for particles of nanoscale dimensions can effectively be probed by using transmission electron microscopy (TEM) imaging and diffraction. Previous TEM work has shown a variety of crystal shapes exist for colloidal Ag including trigonal, pentagonal, and hexagonal structures (9, 10). Single Ag particles in a colloid formed by poly(ethylene imine) reduction of AgNO_3 were described by Duff *et al.* as either single crystalline or highly strained "multiple twins," particles composed of several single crystal components formed under stress during crystal growth (9).

In the present work, silver nanostructures prepared by citrate reduction of AgNO_3 in aqueous solution were studied by TEM. While the optical properties of these colloids were recently reported, nothing is known of their shape and crystal structure (11). These physical properties for Ag clusters and single Ag particles were studied using bright field imaging, selected area diffraction, and convergent beam electron diffraction methods.

EXPERIMENTAL METHODS

Colloidal silver particles were prepared by chemical reduction according to the Lee-Meisel method (12). Approximately 90 mg of silver nitrate (Aldrich, 99+%) was dissolved in 800 mL of deionized water (Millipore Milli-Q, 18 M- Ω resistivity) and was brought to boiling. The reducing agent tris-sodium citrate was then added as 10 mL of a 1% (w/w) solution. Boiling was continued for ca. 60 to 90 min with continuous stirring until the reduction of silver salt was complete. Typical colloids had a surface plasmon band $\lambda_{\max} \approx 450$ nm and an optical density > 8 .

Samples for electron microscopy were prepared by evaporating drops of the colloidal solutions on carbon-stabilized Formvar films (Ted Pella). The ca. 10 nm carbon overcoat served to minimize charging effects under the electron beam. The films were supported on 200 mesh copper grids.

Bright field imaging and selected area diffraction electron microscopies were performed on a JEOL 100CX microscope operating at 100 kV. Convergent beam electron diffraction and high resolution imaging on single particles was performed on a Phillips CM-30 microscope operating at 300 kV. For both instruments, the appropriate camera constants ($c\lambda$) were calibrated using selected area diffraction zones, also referred to as Debye rings, from polycrystalline gold. The accepted lattice constant for gold is $a = 4.079$ Å (13). The gold standard was prepared by depositing a thin film of the metal onto a Formvar-coated grid. CBED diffraction patterns were also computer simulated using the Macintosh software Desktop Microscopist (Virtual Laboratories Inc., Albuquerque, NM).

RESULTS AND DISCUSSION

Bright field images of the chemically-prepared, silver nanostructures were obtained to evaluate the crystal size, shape and structure. A representative cluster of particles is shown in Figure 1. The mean particle diameter was determined from several micrographs containing about 200 particles each to be 99 ± 10 nm. Most of the particles appeared to be highly geometrical in shape, although several irregular forms were also present. The typical two-dimensional shapes included trigonal, square, pentagonal and hexagonal structures. These regular polyhedra most likely reflect the isotropic aqueous environment in which the crystals were grown.

Several particles such as the one labeled (a) in Figure 1 had a pentagonal 2D shape with five sharp, dark contrast lines that met at a common point in the crystal. These contrast lines may be due to “twin” or grain boundaries, suggesting that the particle is not a single crystal. More likely the particle is composed of multiple crystal components, consistent with previous studies (10). However, one cannot rule out the possibility of stacking faults giving rise to the contrast lines, which could exist in a single crystalline phase (10). Based on several micrographs, approximately 80% of the particles appeared to be twinned with regular polyhedral shapes.

Other sources of intensity contrasts observed in Figure 1 included thickness fringes and bend contours. In the particle labeled (b) in Figure 1, the relatively sharp intensity oscillations near the crystal edges are thickness fringes. These fringes are caused by anomalous absorption of the transmitted electron wave with increasing crystal thickness.

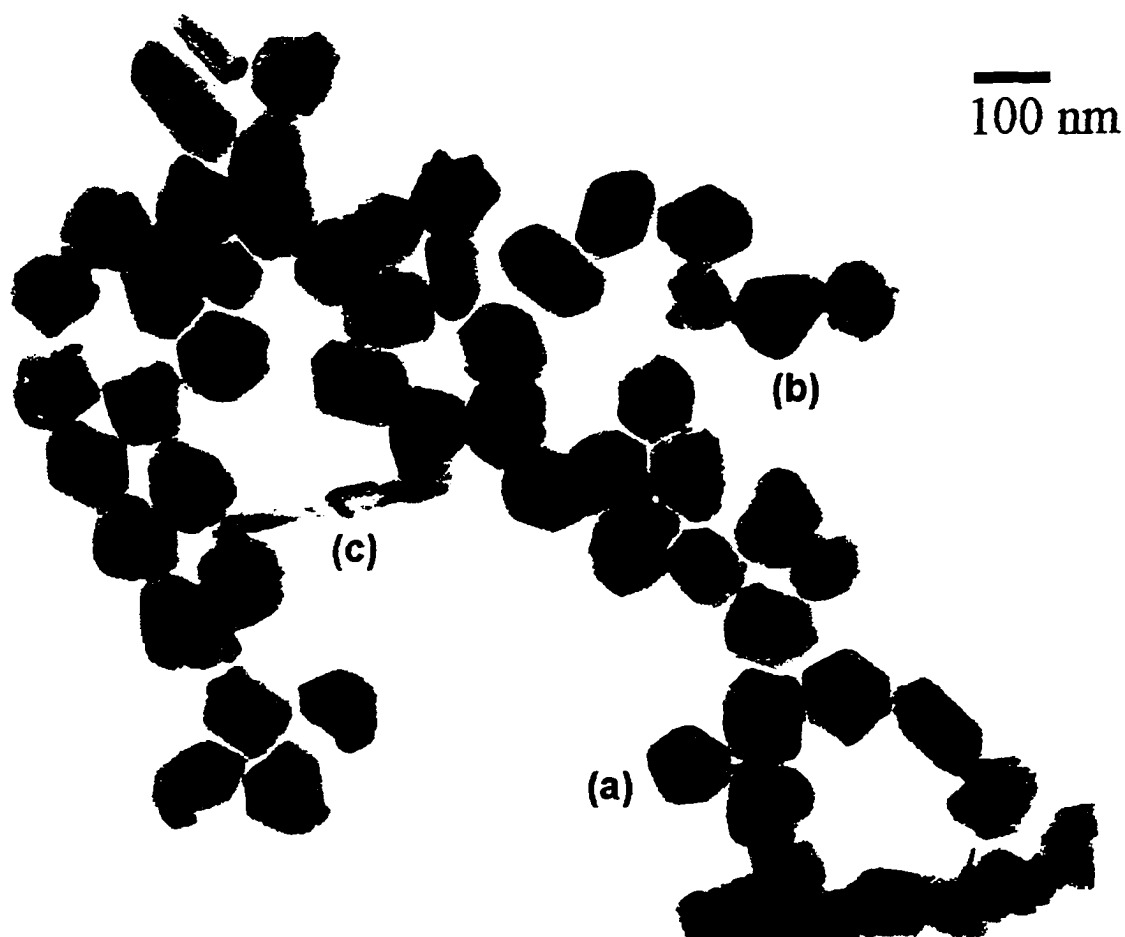


Figure 1. Transmission electron micrograph of a typical cluster of chemically-prepared, silver nanostructures; (a) Single particle having a 2D pentagonal shape and strong intensity contrasts at the twin boundaries; (b) Single particle exhibiting thickness fringes; (c) Single rod-like particle exhibiting bend contours at the regions of strain.

The presence of these thickness fringes is indicative of the three-dimensional particle shape. Bend contours, apparent in the rod-like particle labeled (c) in Figure 1, are caused by variations in orientation within the crystal and generally indicate local regions of strain.

In order to better evaluate the detailed structure of the nanoparticles, quantitative measurements of electron diffraction were performed. The selected area diffraction pattern from a cluster of several particles, shown in Figure 2, consisted of a series of concentric sharp rings. These rings, known as Debye rings, are characteristic of a polycrystalline phase or, in the case of single nanostructures, could be due to multiple randomly oriented single crystalline phases. Interplanar spacings (d-spacings) for the first four diffraction rings were calculated by the camera constant method and are given in Table 1 (14, 15). The experimental d-spacings agreed within 3% of the values predicted for a face-centered cubic Ag crystal (13). This fact strongly suggests that the chemically-prepared silver nanostructures are composed of a face-centered cubic phase. Assuming the fcc structure type, the lattice constant was then calculated to be $a = 4.05 \pm 0.11 \text{ \AA}$ from several diffraction measurements.

Table 1. Observed interplanar spacings taken from the selected area diffraction pattern of a cluster of silver nanostructures and predicted spacings for fcc silver.

Observed d_{hkl} (Å)	Predicted ^a d_{hkl} (Å)	Reflection Type
2.320	2.350	{111}
1.992	2.036	{200}
1.404	1.439	{220}
1.215	1.227	{311}

^a Based on fcc silver thin films, $a = 4.071 \text{ \AA}$ (13).

7607069

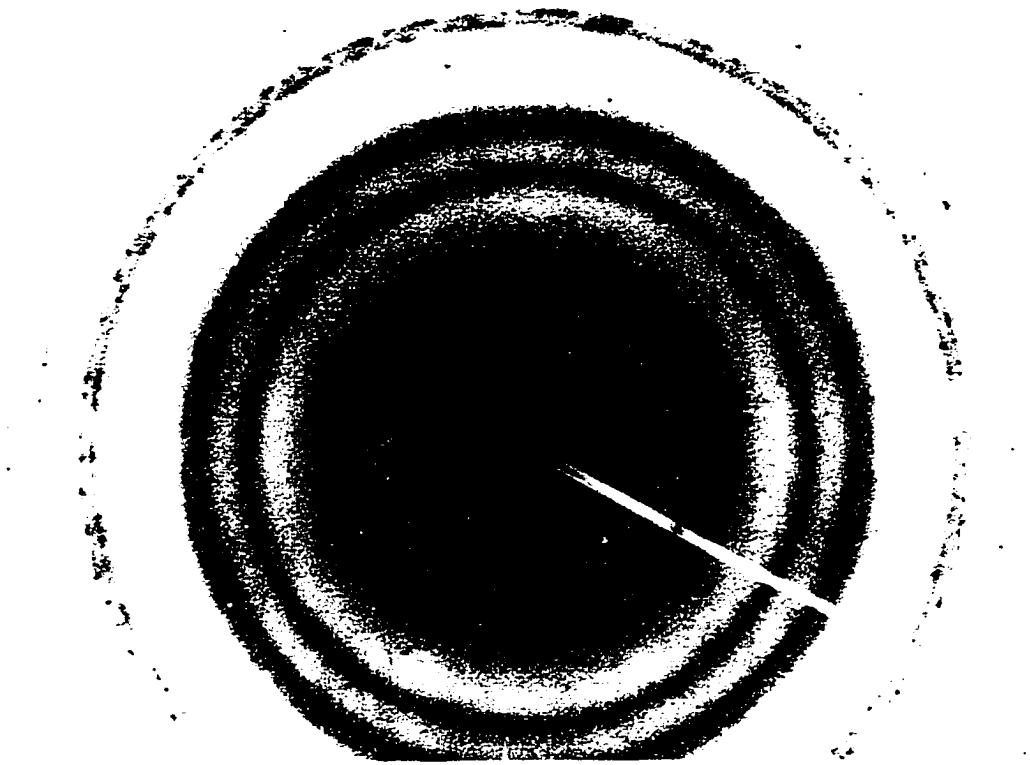


Figure 2. Selected area diffraction pattern from a cluster of silver nanostructures.

Additional confirmation of the fcc structure type was obtained using the convergent beam electron diffraction (CBED) method. The primary advantage of CBED over conventional selected area diffraction is the inherent ability to focus the beam down to cross-sectional dimensions comparable to or less than the size of the single particles. The single Ag nanostructure shown at high magnification (480,000x) in Figure 3 was analyzed using this technique. By converging the electron beam on the region which appeared dark in the image, the CBED pattern shown in Figure 4 was obtained. The sample was then physically tilted ca. 36° along a low-index Kikuchi line to obtain the diffraction pattern shown in Figure 5. The observed interplanar spacings in the CBED



100 nm

Figure 3. Bright field transmission electron micrograph of a single, multiply-twinned silver nanostructure at high magnification (480,000x).

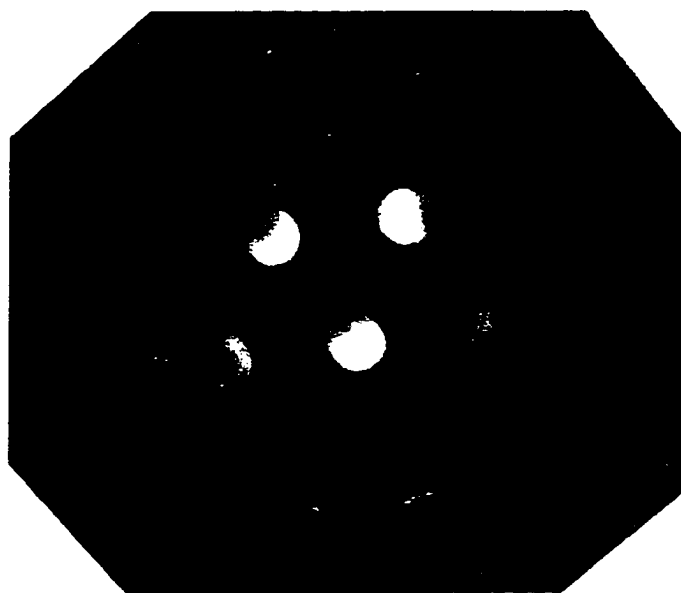


Figure 4. Convergent beam electron diffraction pattern taken along the $[111]$ zone axis of the single silver nanostructure of Figure 3.

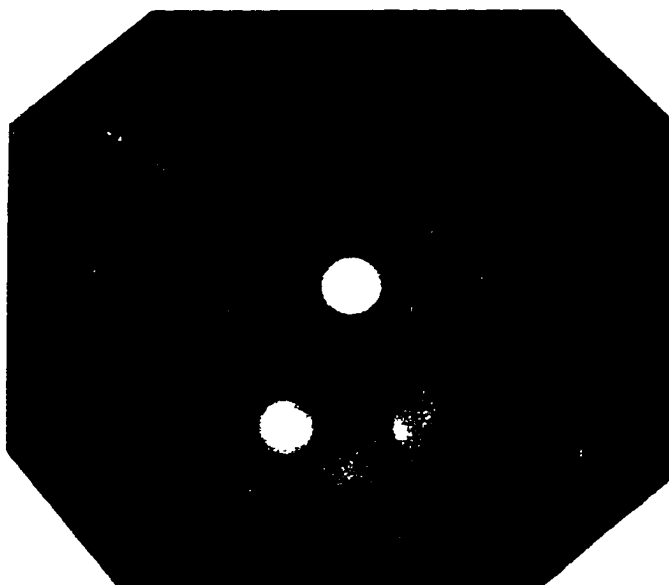


Figure 5. Convergent beam electron diffraction pattern taken along the $[101]$ zone axis of the single silver nanostructure of Figure 3.

Table 2. Observed interplanar spacings taken from the convergent beam electron diffraction pattern of a single silver nanostructures and predicted spacings for silver.

Zone Axis	Observed d_{hkl} (Å)	Predicted ^a d_{hkl} (Å)	Reflection Type
[111]	2.503	2.350	{111} ??
	1.446	1.439	{220}
[101]	2.405	2.350	{111}
	2.095	2.036	{200}

^a Based on fcc silver thin films, $a = 4.071$ Å (13).

patterns for reflections nearest the zero order disc along with those values predicted for fcc Ag are given in Table 2. The experimental d-spacings agreed within 3% of the predicted values. The forms of the CBED diffraction patterns were consistent with computer simulated CBED patterns for [111] and [101] zone axes of an fcc Ag crystal, Figure 6. Also, the observed interplanar angle of 36° was in good agreement with a predicted angle of 35.3° between [111] and [101] zone axes (13). Based on these results, the two experimental diffraction patterns are assigned as [111] and [101] zone axes of an fcc Ag crystal, Figures 4 and 5 respectively.

A curious result of the CBED experiments was the appearance of low intensity extra reflections on the [111] zone axis, Figure 4. The interplanar spacing for the six discs nearest the zero order disc was 2.503 Å. To a first approximation, these reflections could be of the {111} type. However, the observed d-spacing is considerably larger than the 2.350 Å expected for {111} planes. And more importantly, it is known that six different {111} type planes do not exist in an fcc phase. A computer simulated CBED pattern

centered on the $[111]$ zone axis for a thin silver crystal included similar extra reflections, shown in Figure 6. The simulation program also assigned these reflections as $\{111\}$ type, depicted by the spots labeled "x" in the $[111]$ zone axis pattern of Figure 6. At this time, no reasonable explanation for the extra reflections is apparent.

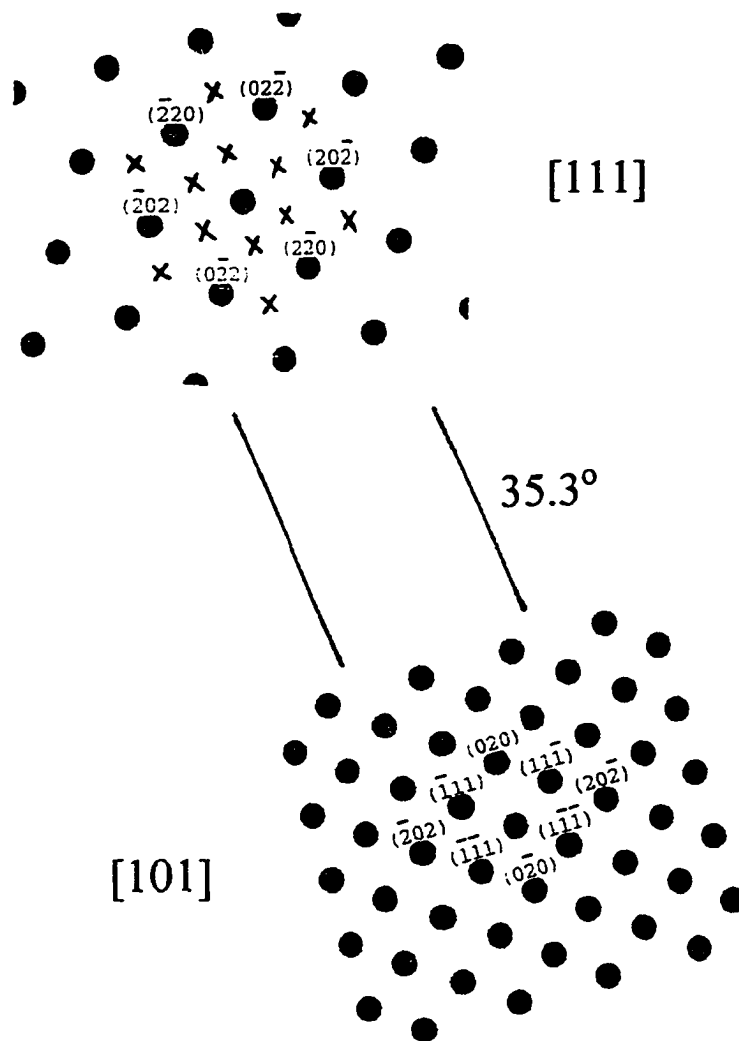


Figure 6. Computer simulated diffraction patterns for an fcc silver phase ($a = 4.079 \text{ \AA}$) taken along the $[111]$ and $[101]$ zone axes. The parallel lines labeled with a tilt angle of 35.3° represent the low-index Kikuchi line between the zone axis centers.

CONCLUSIONS

Chemically-prepared silver particles of mean 99 ± 10 nm diameter were analyzed by transmission electron microscopy. These nanostructures exhibited regular polyhedral shapes including two-dimensional trigonal, square, pentagonal, and hexagonal, indicative of the isotropic aqueous environment in which the crystals were grown. Intensity contrasts observed within single Ag particles included thickness fringes due to three-dimensional variations in particle thickness, bend contours due to crystal defects and regions of local strain, and sharp, dark lines due to phase boundaries. Quantitative analysis of the crystallographic structure using selected area diffraction and convergent beam electron diffraction methods indicated that the particles were composed of a face-centered cubic phase having a lattice constant $a \approx 4.05 \pm 0.11$ Å, consistent with previous studies of fcc silver.

In future experiments, CBED and centered dark field imaging techniques will be used to probe the three-dimensional forms of the single Ag nanoparticles. The latter should help distinguish between simple crystal defects such as stacking faults and multiple single crystal components defined by twin boundaries.

ACKNOWLEDGMENT

The authors wish to thank Scott Chumbley for several helpful discussions. Research at the Ames Laboratory was supported by the Division of Chemical Sciences, Office of Basic Energy Sciences, U.S. Department of Energy. Ames Laboratory is operated for the U.S. Department of Energy by Iowa State University under Contract No. W-7405-Eng-82.

REFERENCES

- (1) P. Mulvaney, F. Grieser, and D. Meisel, in M. Grätzel and K. Kalyanasundaram, eds. "Kinetics and Catalysis in Microheterogeneous Systems", Vol. 38, pp 303-373, Marcel Dekker, New York, 1991.
- (2) E. S. Brandt and T. M. Cotton, in B. W. Rossiter and R. C. Baetzold, eds., "Investigations of Surfaces and Interfaces-Part B", p. 633, Wiley, New York, 1993.
- (3) M. Kerker, *J. Colloid Interface Sci.*, **105**, 297 (1985).
- (4) T. L. Ferrell, T. A. Callcott, and R. J. Warmack, *Amer. Sci.*, **73**, 344 (1985).
- (5) M. Fleischmann, P. J. Hendra, and A. J. McQuillan, *J. Chem. Soc., Chem. Commun.*, **80** (1973).
- (6) D. L. Jeanmaire and R. P. V. Duyne, *J. Electroanal. Chem.*, **84**, 1 (1977).
- (7) M. G. Albrecht and J. A. Creighton, *J. Am. Chem. Soc.*, **99**, 5215 (1977).
- (8) H. Feilchenfeld, G. Chumanov, and T. M. Cotton, *J. Phys. Chem.*, **100**, 4937 (1996).
- (9) D. G. Duff, A. C. Curtis, P. P. Edwards, D. A. Jefferson, B. F. G. Johnson, A. I. Kirkland, and D. E. Logan, *Angew. Chem. Int. Ed. Engl.*, **26**, 676 (1987).
- (10) S. M. Heard, F. Grieser, C. G. Barraclough, and J. V. Sanders, *J. Colloid Interface Sci.*, **93**, 545 (1983).
- (11) G. Chumanov, K. Sokolov, B. W. Gregory, and T. M. Cotton, *J. Phys. Chem.*, **99**, 9466 (1995).
- (12) P. C. Lee and D. Meisel, *J. Phys. Chem.*, **86**, 3391 (1982).
- (13) P. Villars and L. D. Calvert, "Pearson's Handbook of Crystallographic Data for Intermetallic Phases", American Society of Metals, Metals Park, 1985.
- (14) L. S. Chumbley, personal communication, (1996).
- (15) M. H. Loretto, "Electron Beam Analysis of Materials", 2nd ed., 1984.

CHAPTER 3. REDUCTION OF CYTOCHROME C BY HALIDE-MODIFIED, LASER-ABLATED SILVER COLLOIDS

A paper published in the *Journal of Physical Chemistry*¹

Morgan S. Sibbald, George Chumanov, Therese M. Cotton

ABSTRACT

Silver colloids of 20 nm mean particle diameter were prepared by laser-ablation and modified by adsorption of iodide and bromide ions. Addition of cytochrome *c* to this colloid resulted in the reduction of the protein, which was monitored by surface-enhanced resonance Raman scattering and absorption spectroscopies. Colloidal metal films, prepared from the same Ag colloid, were employed in order to minimize contributions from aggregation. Effects of surface modification on the Ag plasmon resonance was studied in both colloidal suspensions and colloidal metal films. The conclusion was made that adsorption of I⁻ and Br⁻ results in charging of the Ag particle as a whole and a shift of its potential to more negative values. The donated charge is delocalized in a thin surface layer and does not significantly affect the plasmon resonance frequency of the particle.

INTRODUCTION

Colloidal platinum, gold and silver are known to catalyze various reduction reactions in aqueous solution.¹⁻³ In these reactions, an electron is transferred from a sacrificial donor molecule to a metal particle and further to an acceptor species. The role

¹ Reprinted with permission from *J. Phys. Chem.* 1996, 100, 4672-4678. Copyright American Chemical Society.

of the metal particles is to accumulate electrons and build up potentials sufficient for reduction.⁴ When homogeneous electron transfer between the donor and acceptor is thermodynamically allowed but is kinetically slow, the metal particles can also increase the overall efficiency of the reaction by trapping those species at the surface.¹

Organic radicals have been the most widely used species as electron donors for the colloidal metal particles because they are easy to prepare and react readily with metals. A variety of methods for radical generation have been employed. Miller et al.⁵ electrochemically generated the methyl viologen cation radical ($MV^{\bullet+}$) which transfers an electron to colloidal platinum. The resulting reaction was the decomposition of water to chemisorbed hydrogen at the Pt surface, ultimately producing molecular hydrogen. Although electron transfer from $MV^{\bullet+}$ to water is energetically favorable, in the absence of colloidal metal the reaction does not proceed to an appreciable extent. The platinum is required to trap hydronium ions at the metal surface, thereby increasing the efficiency of the reduction reaction. McLendon and Miller⁶ produced reducing radicals in the presence of colloidal Pt by utilizing metalloporphyrins as photosensitizers. In this scheme, the porphyrin absorbs visible light and subsequently undergoes excited state quenching by electron transfer to the methyl viologen dication producing $MV^{\bullet+}$. The viologen cation radical is then oxidized at the colloidal Pt surface, yielding H_2 as a final product. Henglein and coworkers⁴ utilized γ -radiation from a ^{60}Co source to produce 2-propanol- or 1-hydroxy-1-methylethyl radicals which also generate molecular hydrogen in the presence of silver colloids. The efficiency of this process was found to depend strongly on particle size, metal composition as well as the donor species reduction potential.⁴

In more recent work, the same authors showed that adsorption of nucleophiles such as CN^- , SH^- , $\text{C}_6\text{H}_5\text{S}^-$, I^- and PH_3 strongly influences the catalytic as well as optical properties of Ag colloid.^{7,8} An observed decrease in intensity and a broadening of the Ag colloid plasmon resonance band was attributed to damping of the resonance by adsorbed species. Additionally, its spectral shift was assigned to changes in the charge distribution in the surface layer of the particle as a consequence of charge transfer from the adsorbed species to the metal.⁸ It was also found that in the absence of an electron acceptor, charge is accumulated on the particles. For particles of 70 Å mean diameter, the capacitance was determined to be 43 μF per square centimeter of particle surface⁹, which is comparable to that of bulk electrodes. By generating a potential difference between the metal particles and the solution, methyl viologen dication or protons from water are reduced at the expense of silver oxidation to Ag^+ ions.⁷

Colloidal metal particles that are employed for catalysis are most frequently prepared by chemical reduction of aqueous metal salts.¹⁰ In the preparation of colloidal Ag, sodium borohydride or sodium citrate are common reducing agents for AgNO_3 , although a variety of other reductants have been employed as well. Silver colloids are also prepared using organic radicals and hydrated electrons, formed under γ -radiation, as reducing agents of the metal ions.⁷ All of these methods suffer from one common disadvantage: the presence of oxidation products and extraneous ions in the suspension of metal particles. These will interfere with surface reactions and can cause uncontrolled aggregation. To minimize aggregation, a variety of stabilizers including polymers can be

added to the colloid.³ However, the stabilizers can interfere with surface reactions as well. A new and highly promising method for colloid preparation involves laser-ablation from bulk metal into high purity aqueous solution.¹⁰ In this method, the metal in water or other solvents is irradiated with a pulsed Nd:YAG laser for a period of time. As a result, finely dispersed metal particles form a stable colloid which is free from chemical reagents or ions associated with their surface. The optical density and size distribution function can be controlled by varying the pulse energy and the time of ablation.

In the present work, the addition of halide ions to an aqueous suspension of nanosized Ag particles prepared by laser-ablation is shown to reduce the native-oxidized form of cytochrome *c* (Cyt *c*). To our knowledge, this is the first demonstration of the direct reduction of a protein by chemically-modified Ag colloid. Evidence for the reduction of Cyt *c* was obtained from surface-enhanced resonance Raman scattering (SERRS) and light absorption spectroscopies. Particular attention was given to the effects of halide modifiers on the Ag plasmon resonance. The effects of halide-modification on Ag colloid were also compared with halide-modification of Ag colloidal metal films (CMF)¹¹ and roughened Ag electrodes. CMFs are composed of an optical glass slide uniformly coated with isolated Ag particles. This is accomplished by covalent bonding of nanosized metal particles to the glass through functional groups with a high affinity for the metal such as -SH, -COOH, -NH₃, -CN and -pyridyl.¹¹ The use of CMFs was intended to minimize aggregation effects on the extinction spectra of modified colloidal particles.

EXPERIMENTAL SECTION

Chemicals and Materials. Water for the experiments was purified using a Millipore Milli-Q system and had a nominal resistivity of 18 M Ω -cm. Silver metal (99.99%, Aesar (Johnson Matthey)) was sonicated in water prior to colloid preparation. Cytochrome *c* (Horse Heart, Type VI) was used as received from Sigma or purified according to published procedures.¹² Purification did not noticeably influence the results. Bromide and iodide salts were dried at >100 °C under vacuum prior to use. Crystalline silver-iodide was prepared by adding a slight excess of KI to a solution AgNO₃; the AgI precipitate was washed several times in water to remove excess ions. Molecular iodine solution was prepared by dissolving I₂ in chloroform (HPLC grade). Triiodide solution was produced by mixing I₂ with a slight excess of KI in methanol (HPLC grade) and yielded the characteristic I₃⁻ absorption spectrum.¹³ All other reagent grade chemicals were used without further purification. Unless otherwise stated, solutions were purged with high purity nitrogen gas prior to experiments.

Colloid Preparation. Suspensions of nanosized Ag particles in water were prepared as described previously.¹⁰ Silver metal was ablated from a thin plate using 1064 nm radiation (Nd:YAG laser, Quanta Ray DCR2A, Spectra Physics) with 55 mJ pulse energy at a 10 Hz repetition rate. Ablation proceeded for approximately 15 min. The total silver concentration in a colloid was determined by atomic absorption (Perkin-Elmer 305B) measurements of samples dissolved in 1% (v/v) nitric acid. The concentration of Ag for a colloid with an optical density 3.6 measured at 396 nm was determined to be 3.2

$(\pm 0.1) \times 10^{-4}$ M. The pH value of the Ag colloids was 6-7. When appropriate, suspensions were centrifuged at 12,000 g.

Electron micrographs were obtained using a JEOL 1200 STEM instrument operating at 100 kV. Samples for TEM were prepared by evaporating a drop of colloidal solution on a Formvar coated nickel mesh grid (Electron Microscopy Sciences). The laser-ablated Ag colloid employed in this study had a particle size distribution of 20 ± 4 nm as determined from the analysis of several micrographs (Figure 1).

Colloidal Metal Film (CMF) Preparation. Films were prepared on a glass substrate modified with a molecular adhesive (3-mercaptopropyl trimethoxysilane, MPS) according to the procedure described by Goss et al.¹⁴ Briefly, a coating solution was prepared containing 300 mL of 2-propanol, 6 mL of water and 6 mL of MPS. The adhesive layer was prepared by repeating the following steps three times: reflux the substrates in the coating solution for 10 min, remove and rinse in 2-propanol and dry at 110 °C in an oven for 10 min. After the MPS-coated slides were cooled, they were immersed in a colloidal Ag solution for several days. Formation of uniform thin films of Ag particles was achieved in this manner.¹¹ In the present study, all CMFs were prepared from the same suspension of laser-ablated Ag colloid.

Raman Spectroscopy. Resonance Raman and surface-enhanced resonance Raman scattering spectra were obtained using the following excitation sources: (a) the 514.5 nm line of an Ar⁺ laser (Coherent, Innova 200), (b) the 647.1, 752.5 or 799.3 nm lines of a Kr⁺ laser (Coherent, Innova 100) or (c) the 640.0 nm line from an Ar⁺ pumped-dye laser (Coherent CR-599, R6G). The laser light was focused on the sample by a

cylindrical lens ($f = 100 \text{ nm}$). The power at the sample was maintained at less than 10 mW for all measurements. Scattered light was collected by a camera lens ($f/1.2$) in a backscattering geometry and dispersed by a triple spectrometer (Spex, Triplemate 1877) equipped with a CCD detector (Princeton Instruments, LN 1152 x 298). The total accumulation time was typically 400 seconds. in the spectral region ca. $1650\text{-}500 \text{ cm}^{-1}$

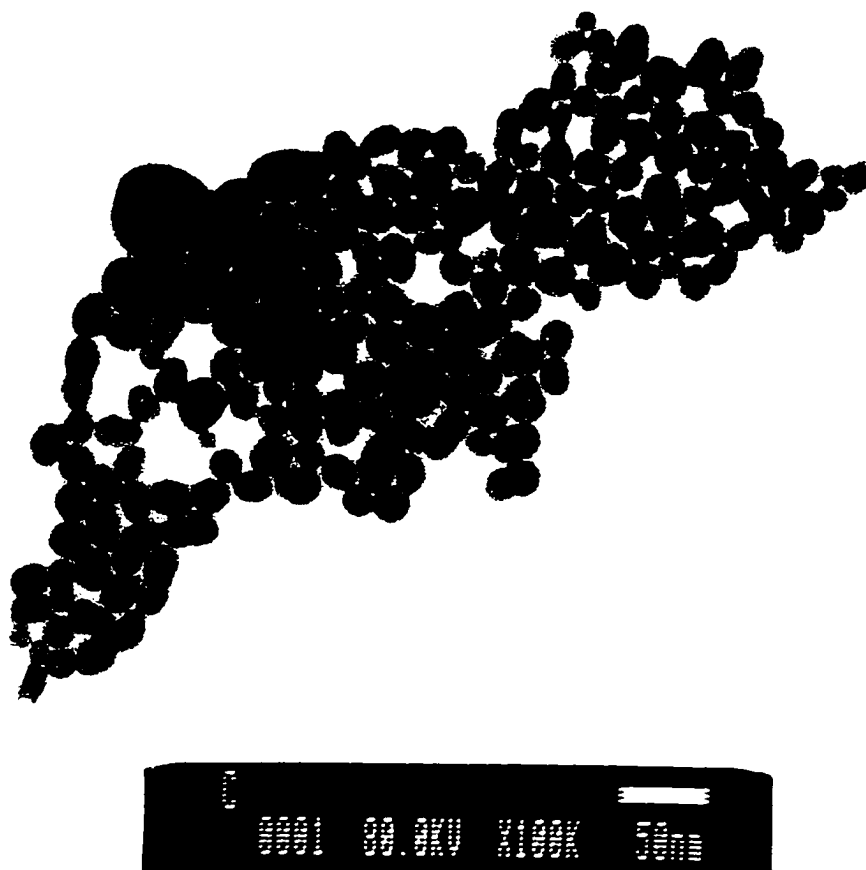


Figure 1. Electron micrograph of Ag colloidal particles prepared by laser-ablation.

data were calibrated with indene and in the region ca. 400-0 cm^{-1} with a mixture of chloroform and bromoform in combination with the laser line. All Raman spectra are reported with a spectral resolution of 0.14 nm.

Electronic Absorption Spectroscopy. Absorption spectra were recorded on a UV-Vis spectrophotometer (Perkin-Elmer, Lambda 6) in a 1 cm pathlength quartz cuvette. Spectra were acquired at a scan rate of 120 nm/min, slit width of 1.0 nm and were background corrected. The UV-Vis spectra for Cyt *c* solutions contained contributions to the absorbance from both oxidized and reduced forms of the heme. To quantitatively identify each constituent, a linear combination of equations was solved assuming the validity of Beer's Law. The constituent concentrations were determined using the molar absorptivities at the peak maxima of the α band in each form of cytochrome *c* ($\text{Fe}^{\text{III}} \epsilon_{528} = 11,200 \text{ M}^{-1} \text{ cm}^{-1}$, $\text{Fe}^{\text{II}} \epsilon_{550} = 27,700 \text{ M}^{-1} \text{ cm}^{-1}$) as reported by Margoliash and Frohwirt.¹⁵

RESULTS

Cytochrome *c* reduction in modified Ag colloid. Cytochrome *c* was found to undergo reduction when introduced into a suspension of colloidal Ag mixed with aqueous Γ^- or Br^- in micromolar concentrations. Other halides such as Cl^- and F^- at concentrations up to 100 mM did not affect the redox state of Cyt *c* under similar conditions. Reduction of Cyt *c* was also observed upon addition of S^{2-} to the Ag colloid at concentrations similar to those of Γ^- . (The data with sulfide are not discussed in this paper.)

Surface-enhanced resonance Raman scattering spectroscopy was used to monitor the reduction of Cyt *c*, Figure 2. These spectra were excited at 514.5 nm, which is in

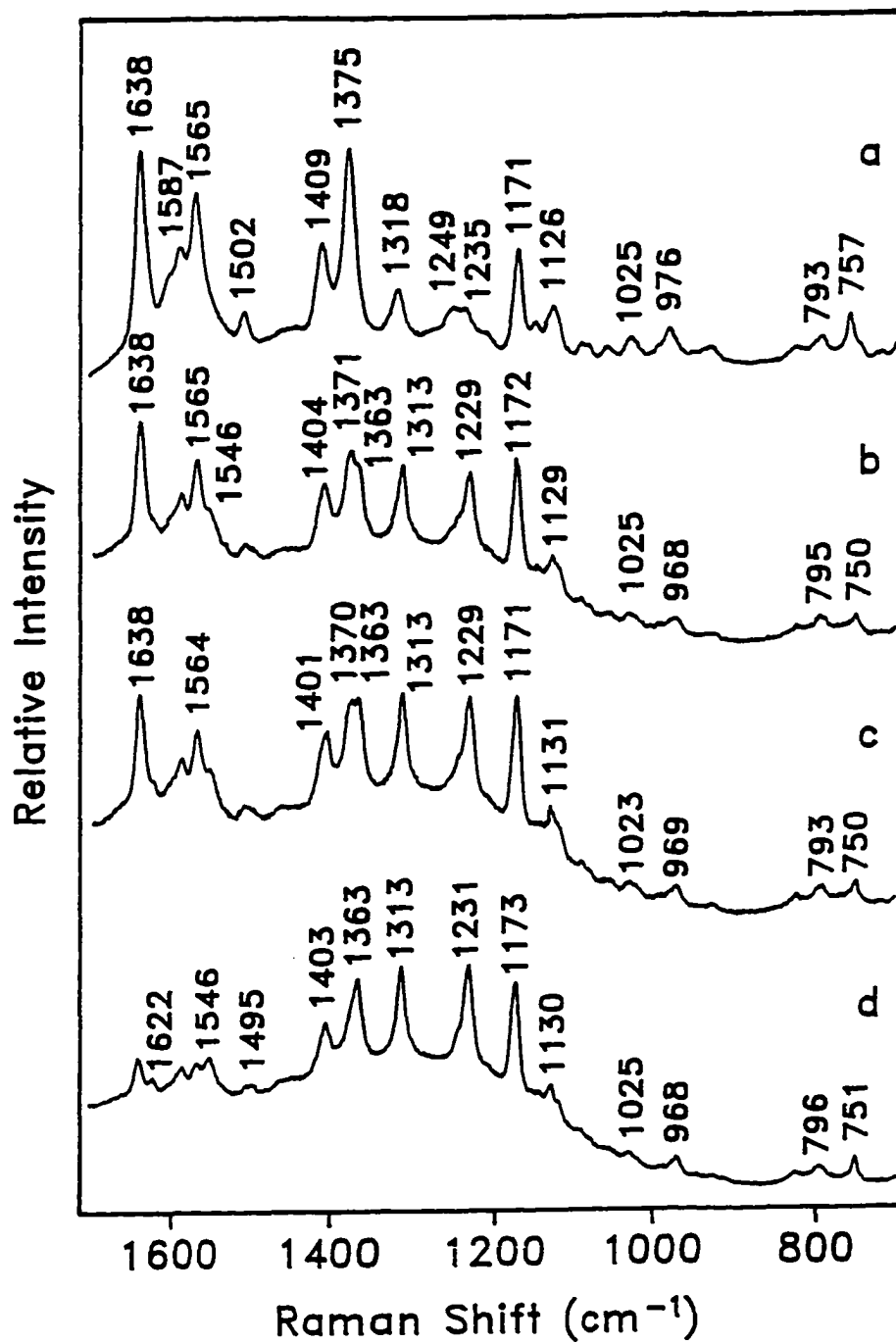


Figure 2. SERRS spectra of cytochrome *c* (7.4 μM) in aqueous Ag colloid (optical density 7.2 at 396 nm) with different concentrations of iodide: (a) 30 μM , (b) 60 μM , (c) 75 μM and (d) 120 μM . Excitation wavelength 514.5 nm.

resonance with the β absorption band of both oxidized and reduced forms of Cyt *c*. At the concentration of cytochrome *c* employed, no significant contributions to the Raman signal was observed from the Cyt *c* in solution. The bands at 1375 cm^{-1} and 1363 cm^{-1} , attributed to the C_{α} -N breathing mode of the pyrrole macrocycle (ν_4), are commonly used as markers for the redox state of cytochrome *c* and correspond to oxidized and reduced forms, respectively.¹⁶ Assignment of these and other bands in SERRS spectra were reported by Hildebrandt and Stockburger.¹⁷

The total amount of reduced Cyt *c* depended linearly on the concentration of Ag colloid, once the molar ratio of halide to Ag exceeded a certain value. In other words, cytochrome *c* reduction occurred only after the concentration of halide became two to three times greater than that predicted for saturation coverage of the Ag surface (threshold behavior, *vide infra*). SERRS spectra of mixtures of oxidized and reduced forms of Cyt *c* at different iodide concentrations are presented in Figure 2. For convenience, the halide concentration at which the two bands 1375 cm^{-1} and 1363 cm^{-1} are equal in intensity was chosen as a reference point, Figure 2c. However, it should be emphasized that this reference point does not represent equal concentrations of oxidized and reduced forms. The contribution of each form to the observed signal depends on the resonance conditions, their molar absorptivity at the excitation wavelength and their affinity to the Ag surface. At the reference point, the concentration of I^- added to the colloid was ca. 40 times lower than that for Br^- .

It is known that Cyt *c* interacts directly with various anions, including halides.¹⁸⁻²⁰ Therefore, competition may exist between Ag and Cyt *c* for iodide binding. We observed

slightly more (ca. 10%) reduced cytochrome *c* based on the intensity ratio of the 1375 cm^{-1} and 1363 cm^{-1} bands when Γ and Ag colloid were premixed before cytochrome *c* addition, relative to the case where Γ and Cyt *c* were mixed first and then added to Ag colloid.

In order to address the possible role of light in the reduction of Cyt *c* on the surface of halide-modified Ag colloids, electronic absorption (UV-Vis) spectroscopy was employed. As silver/halide complexes are often photosensitive, photoreduction of Cyt *c* might occur under the high laser light intensities which are required for Raman measurements. Because UV-Vis measurements are typically performed under low light intensities, the effects of light can be minimized. Absorption spectroscopy also permits a quantitative determination of reduced Cyt *c*. It allows the measurement of reduced cytochrome *c* in solution, whereas SERRS spectroscopy, because of the inherent surface selectivity, detects primarily the surface species.

Absorption spectra of Ag colloid mixed with Γ before and after addition of Cyt *c* are shown in Figure 3. The intense band at 396 nm in spectrum (a) is due to plasmon resonance in isolated Ag particles of 20 nm mean diameter. The peak at 226 nm is the charge-transfer-to-solvent transition of the hydrated iodide ion.¹³ Upon adsorption of Γ to the metal surface, this band is no longer observed due to the loss of solvent supported excited states. The charge-transfer band of aqueous Γ was used as a marker for saturation coverage of the Ag surface by iodide. For colloids with a plasmon maximum at 396 nm and an optical density 0.70, saturation coverage of the Ag surface was achieved at about 4 μM KI concentration. The lowest concentration of aqueous Γ which can be accurately

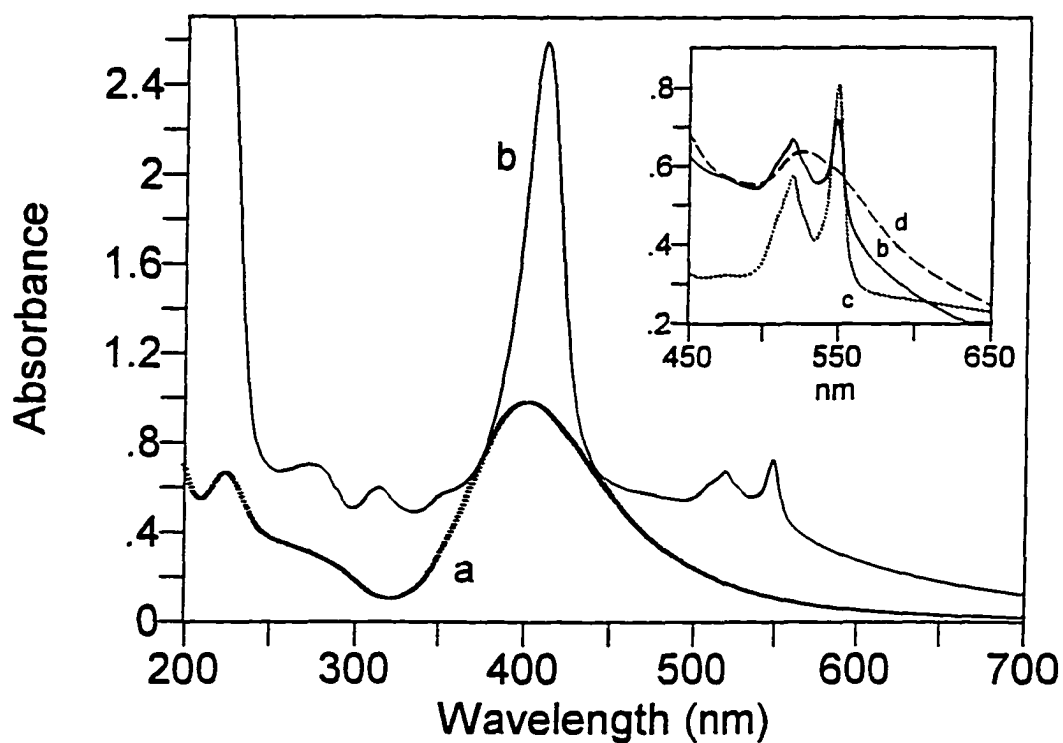


Figure 3. Extinction spectra of iodide-modified Ag colloid (a) before and (b) after the addition of Cyt *c* (25.1 μM). The iodide concentration was 25.3 μM . Insert: (b) Cyt *c* in I-modified Ag colloid, (c) Cyt *c* reduced by sodium dithionite and (d) Cyt *c* in unmodified Ag colloid.

determined by absorption measurements is $< 0.5 \mu\text{M}$, providing an accuracy of $\leq 10\%$ in these measurements.

Addition of Cyt *c* to the colloidal suspension caused aggregation of the Ag particles. As a result, the distinct plasmon band at 396 nm was no longer observed and the Cyt *c* spectrum appeared on top of a broad background due primarily to scattering from aggregates, Figure 3b. From the spectral features between 500 and 600 nm, it is clear that Cyt *c* becomes more reduced upon Γ addition.¹⁵ For comparison, spectra of cytochrome *c* without Γ (oxidized form) and sodium dithionite reduced are presented in Figures 3c and 3d, respectively. In these experiments, the samples were prepared in the dark.

An attempt was also made to correlate the amount of reduced Cyt *c* with Γ and Ag colloid concentrations. The amount of reduced Cyt *c* was determined from UV-Vis spectra taken after the Ag particles were precipitated by centrifugation. Spectra were corrected for cytochrome *c* coprecipitated with the metal particles and were then compared to those of dithionite reduced Cyt *c* of equivalent concentration. For a constant Ag colloid concentration, it was found that the molar ratio of reduced Cyt *c* to iodide varied significantly for different sample preparations. These variations are attributed to differences in colloid aggregation, as initiated by addition of iodide. Aggregation affects the surface potential of individual particles²¹ and, as a result, influences their reducing power.

Cytochrome *c* reduction on modified CMFs. The films were immersed in 1.0 mM KI solution for 30 min. to insure that saturation of the Ag surface by iodide was achieved, followed by a thorough rinse in water to remove excess Γ . The CMF was then

Table 1. Optical densities of colloidal metal films and equilibrium concentrations of cytochrome *c*.

OD ^a , au (λ_{\max} , nm)	OD ^b , au (λ_{\max} , nm)	Initial Cyt., μM	OD ^c , au (λ_{\max} , nm)	Final Cyt., μM Oxidized State	Final Cyt., μM Reduced State
0.509 (388)	0.467 (389)	3.35	0.471 (394)	2.75	0.36
0.487 (396)	0.452 (398)	2.97	0.450 (404)	2.00	0.52
0.483 (395)	0.457 (397)	2.59	0.455 (405)	1.60	0.47
0.528 (394)	0.501 (398)	2.97	0.504 (403)	2.40	0.25
0.549 (396)	0.527 (397)	3.08	0.526 (404)	2.71	0.37
0.591 (388)	0.540 (389)	3.22	0.556 (395)	2.61	0.32

^a Clean CMF in water. ^b CMF in water after exposure to 1.0 mM KI. ^c CMF in water after exposure to 1.0 mM KI and cytochrome *c*.

exposed to ca. 3 μM Cyt *c* for 15 min. Longer immersion times in KI or Cyt *c* solutions did not significantly influence the amount of reduced Cyt *c*. All manipulations were performed under an argon atmosphere and with continuous N₂ purging of solutions. The amount of reduced cytochrome *c* was measured by UV-Vis spectroscopy after removal of the CMF. The data are summarized in Table 1.

The extinction spectra of the CMFs were examined after exposure to I⁻ and Cyt *c*. Only small changes were observed in the spectra following adsorption of iodide. After exposure to Cyt *c* solution, the plasmon band decreased in intensity, broadened by less than 10% and shifted 6-10 nm to the red spectral region. These changes are attributed to

the effect of the local dielectric environment on the plasmon resonance of the metal particles, which has been described previously.¹¹

Iodide adsorption on silver. A series of experiments were performed to elucidate the role of the halide-metal interaction in the Cyt *c* reduction phenomenon. Upon addition of Γ in concentrations up to several hundred micromolar to the Ag colloid, a red-shift, broadening and decrease in intensity of the plasmon resonance band was observed, Figure 4. These changes were found to be independent of the monovalent cation and are typical of partially aggregated colloids, when small irregular clusters of particles are formed. At higher Γ concentrations, the plasmon band shifted back toward the blue spectral region but remained broader and weaker in intensity relative to the band of the unmodified Ag colloid, Figure 4a. The blue-shift of the plasmon band is due to etching of the silver, as confirmed at longer times by the appearance of the bulk AgI absorption band at 428 nm²² (insert of Figure 4). Etching reduces the mean particle diameter and, according to Mie theory²³, results in a shift of the plasmon resonance band to the blue spectral region. This effect is promoted by oxygen and was found to be more rapid in air-saturated solutions.

If the red-shift of the Ag Plasmon band at low Γ concentrations is in fact caused by aggregation, then colloidal metal films are an ideal substrate for testing this hypothesis. A CMF was exposed stepwise for 30 min. to increasing concentrations of KI solution under continuous N_2 purging. Extinction spectra were measured after each exposure. As the surface coverage of Γ on the Ag particles was increased, a decrease in intensity and broadening of the plasmon resonance band was observed, Figure 5. All significant changes in the spectra occurred at Γ concentrations below saturation coverage of the

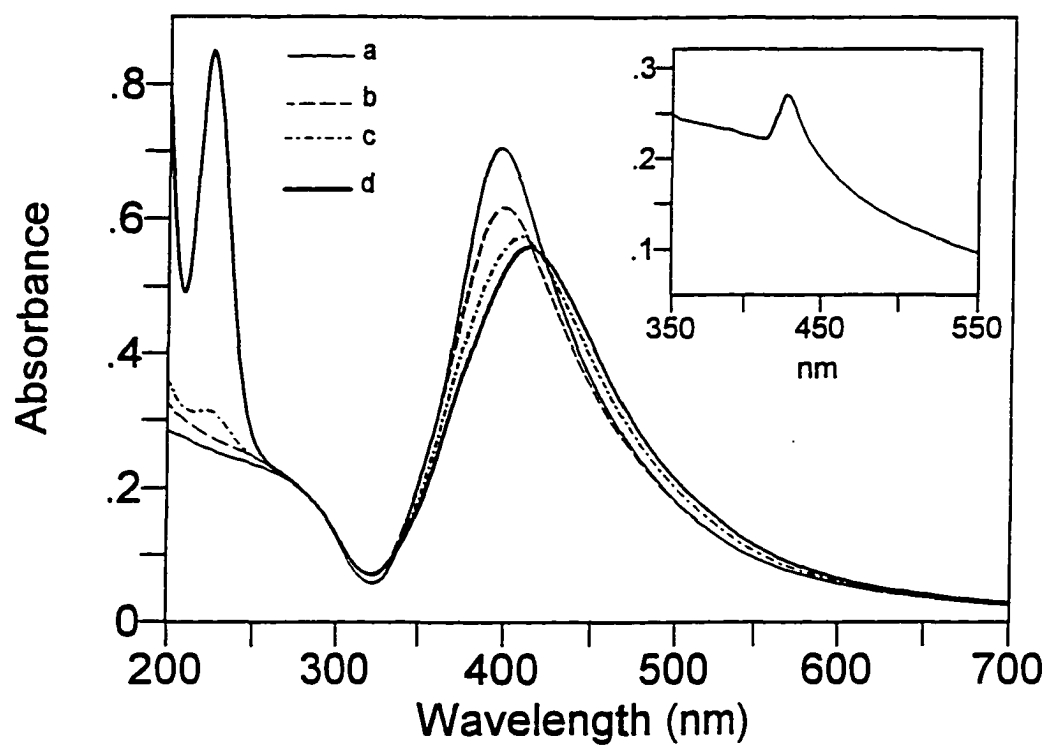


Figure 4. Extinction spectra of iodide-modified Ag colloid as a function of KI concentration: (a) 0 μM , (b) 4 μM , (c) 8 μM and (d) 48 μM . Insert: extinction spectrum of AgI formed by exposure of Ag colloid to air-saturated, 1.6 mM KI solution.

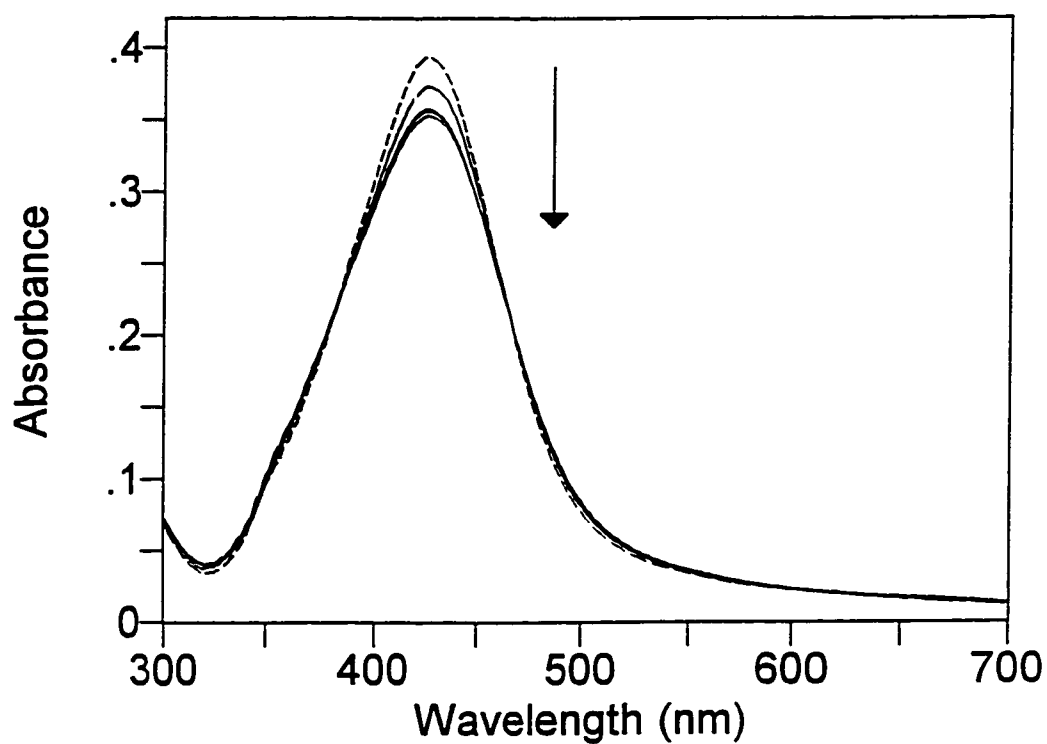


Figure 5. Extinction spectra of Ag colloidal metal film as a function of KI concentration: 0, 0.6, 1.8, 5.0 and 84.0 μM KI, where the arrow indicates the direction of changes with increasing concentrations of Γ .

surface. Small changes in the spectra which occurred at higher Γ concentrations (up to 20 times saturation) are attributed to slow adsorption kinetics. It is also important to note that the CMF plasmon resonance did not shift significantly after exposure to iodide, in contrast to what was observed in the colloidal suspensions.

Adsorption of halides at the metal surface was also monitored by surface-enhanced Raman Spectroscopy (SERS). The metal-halide stretch was manifested in the spectrum as a broad band (full-width at half-maximum $\sim 30 \text{ cm}^{-1}$) at 246 cm^{-1} for $\text{Ag}_s\text{-Cl}$, 156 cm^{-1} for $\text{Ag}_s\text{-Br}$ and 112 cm^{-1} for $\text{Ag}_s\text{-I}$, where Ag_s represents the silver surface.²⁴⁻²⁶ The SERS spectrum of Ag colloid mixed with KI solution and SERS spectra obtained from Ag electrode exposed to I_2 and I_3^- solutions are shown in Figure 6. The Ag electrode, roughened by a double-potential step oxidation-reduction cycle according to published procedures²⁷, was used for SERS measurements of I_2 and I_3^- because these species were prepared in chloroform and methanol to insure the highest concentration of their pure forms. These solvents are incompatible with aqueous colloids. The spectra were obtained at open circuit potential where iodine species are known to adsorb strongly to noble metals. SERS spectra shown in Figure 6 were nearly identical to those obtained at the other excitation wavelengths used in this study.

The Raman spectrum of chemically prepared, polycrystalline AgI is shown in Figure 7a. This spectrum is very similar to those of iodide species adsorbed on the silver surface (compare with Figure 6). However, it was noted that a darkening of the initially yellow AgI powder occurred upon exposure to the laser light, presumably as a result of photoreduction of AgI to metallic silver. Precautions were undertaken to minimize

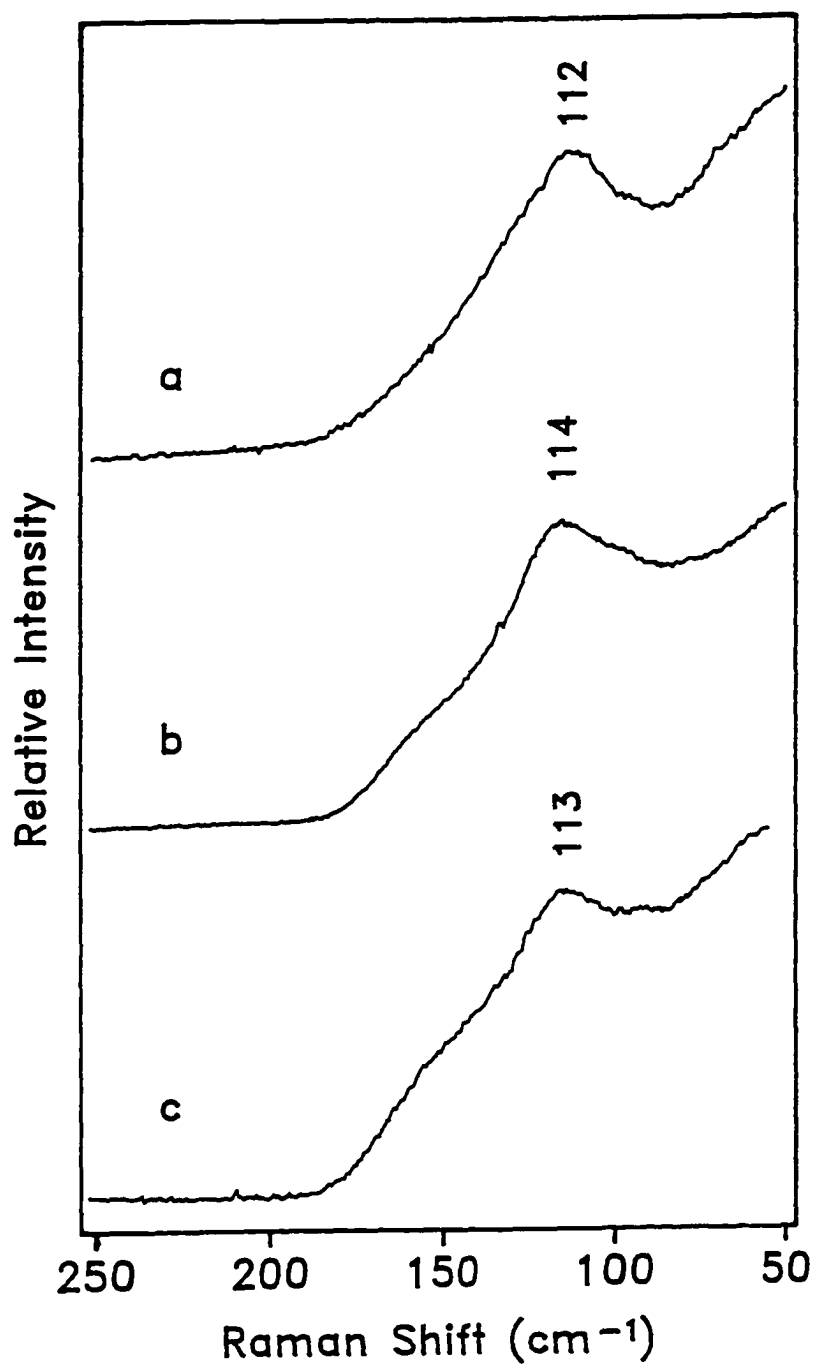


Figure 6. SERS spectra of (a) Ag colloid mixed with KI solution: excitation wavelength 647.1 nm; (b) Ag electrode exposed to I₂ in chloroform: excitation wavelength 752.5 nm; (c) Ag electrode exposed to I₃⁻ in methanol: excitation wavelength 640.0 nm.

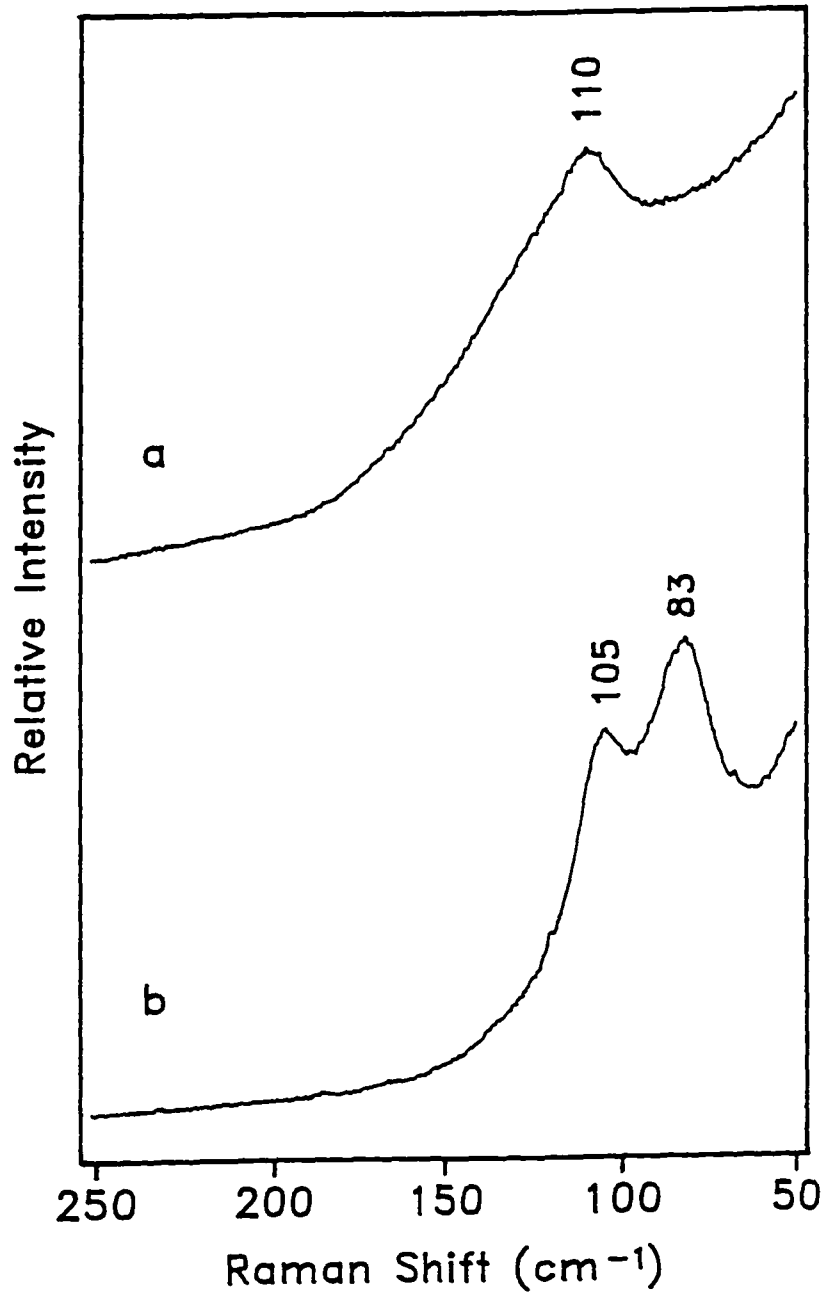


Figure 7. Raman scattering spectra of chemically-prepared, polycrystalline silver-iodide as (a) dry powder and (b) aqueous suspension in a rotating cell. Excitation wavelength 799.3 nm.

photochemistry which included excitation with low energy photons (799 nm) and the use of a rotating cell containing the AgI crystals suspended in water. The Raman spectrum obtained under these conditions is shown in Figure 7b. A new band at 83 cm^{-1} was present in the spectrum together with a weaker band around 105 cm^{-1} . When the rotation of the cell was stopped, the latter band grew in intensity with time whereas the former decreased.

DISCUSSION

Bromide- and iodide-modified silver colloids and CMFs are shown to reduce cytochrome *c* at their surface. Neither the Ag particles alone nor a solution of these halide salts reduces the Cyt *c*. Therefore, it can be concluded that the potential of the particles is shifted to values sufficient for Cyt *c* reduction as a result of the halide-metal interaction. Because silver-halides are known to be photosensitive²², the effect of light must be considered. Based on the following experimental observations, it appears that the role of light is minimal in the reduction process. First, we observed reduction of Cyt *c* at the low light intensities typical for UV-Vis measurements. Second, no change in the amount of reduced Cyt *c* was observed after prolonged exposure to intense laser light. However, we cannot rule out entirely the possibility that this process is extremely photosensitive and is already completed under low light intensities.

A shift in the potential of the particles upon adsorption of the halide ions is a result of charge transfer from the adsorbate to the metal. The extent of the charge transfer is dependent upon the nature of the silver-halide bond, or in other words, the degree of ionic

or covalent character.²⁵ The nature of the silver-halide bond can be probed by Raman spectroscopy. Adsorption of iodide from KI, I₂ and I₃⁻ on silver resulted in nearly identical features at 112 cm⁻¹ in the SERS spectra. This indicates that iodide, independent of its source, forms the same surface-bound species and 112 cm⁻¹ represents the metal-iodide (Ag_s-I) vibration. In contrast, the Raman spectrum of chemically prepared, polycrystalline AgI contains two bands one of which is near 83 cm⁻¹, probable due to a lattice vibration. A second band around 105 cm⁻¹ results from photodecomposition of AgI to metallic silver and iodine which further reacts to form Ag_s-I. This reaction is similar to the reduction of silver-halides in the photographic process. Two similar bands at 85 cm⁻¹ and 107 cm⁻¹ were previously observed in the Raman spectrum of a wurtzite-type AgI single crystal.²⁸ Both bands were assigned to phonon modes, but no photochemistry was discussed in this study. Based on the present work, most likely there are two overlapping bands in the region 105-112 cm⁻¹ in the Raman spectrum of crystalline AgI: one at a lower frequency due to phonon vibrations and a second at a somewhat higher frequency due to Ag_s-I formed as a result of photodecomposition.

The frequency of the metal-halide vibration was used by Gao and Weaver²⁵ to estimate the force constant for the chemical bond. In combined Raman-electrochemical measurements, the metal-iodide vibrational frequency was determined as a function of the surface charge on gold and silver electrodes.²⁵ The authors concluded that the Au_s-I bond is totally covalent, whereas the Ag_s-I is less covalent. The latter conclusion is based on the smaller force constant, as well as the observation that the vibrational frequency of Ag_s-I decreased as the electrode potential was made more negative. This result is expected if

the Ag_s-I bond has some degree of ionic character. On the other hand, ultrahigh vacuum studies on halide-modified Ag(111) employing x-ray photoelectron spectroscopy indicate that iodide exists in a nearly zero-valent state upon adsorption to the metal.^{29,30} Wertheim and coworkers²⁹ estimated an upper limit for the charge on iodide to be 0.035 electron. Based on these results, it is reasonable to assume that nearly one electron is donated to the colloidal Ag particle per I adsorbed.

In the case of Br⁻, Cyt *c* reduction was observed at concentrations ca. 40 times higher than those for I⁻. This difference in concentration is attributed to two reasons. First, the Ag_s-Br bond is more ionic than that of Ag_s-I which means that less charge is transferred to the metal.²⁵ Second, the lower affinity of Br⁻ toward the Ag surface relative to I⁻ requires a higher concentration to achieve an equal surface coverage.^{31,32} Chloride and fluoride anions weakly associate with the metal surface forming predominantly ionic species with Ag and even at saturation coverage cannot charge the particles sufficiently to reduce Cyt *c*.

In experiments involving a colloidal metal film, it is possible to calculate the equilibrium potential of the system using the Nernst equation and the reduction potential of Cyt *c*. The latter is assumed to be identical to the value for Cyt *c* in solution (+0.02 V vs. SCE³³). This assumption is based on the observation that the protein maintains its native conformational state on the surface of the halide-modified Ag colloid, as supported by SERRS spectra in which bands at 1502 cm⁻¹ and 1493 cm⁻¹ in Figure 2 are characteristic of the native, six-coordinated low-spin state of oxidized and reduced heme, respectively³³. For the different stoichiometric ratios of reduced and oxidized Cyt *c*

(Table 1), the equilibrium potential varied between +0.031 V and +0.054 V. In these experiments, monolayer coverage by Γ was insured by comparing the amount of adsorbed iodide, measured experimentally, to that calculated assuming $\sqrt{3} \times \sqrt{3}$ packing on the Ag surface.^{30,34} The variations in the equilibrium potential are explained by differences in the initial potential of the silver particles which depends strongly on various factors such as the particle diameter (size distribution function), charging/discharging processes to the solution during CMF storage, local ion environment, etc. The discharging of iodide-modified Ag colloid is demonstrated in the following experiment. Cytochrome *c* was added at different times after the Ag colloid was modified with iodide. Because the solutions were not degassed, dissolved oxygen removed charge from the particles and, as a result, the efficiency of the iodide-modified Ag particles toward Cyt *c* reduction was decreased, Figure 8. This effect was not observed when all solutions were purged with nitrogen.

An important issue regarding the mechanism of Cyt *c* reduction on the halide-modified Ag particles is whether the electron donated by the halide ion is localized near the $\text{Ag}_s\text{-I}$ complex or is delocalized in a thin layer near the surface. If the charge is localized, the reduction of Cyt *c* would be governed by the potential of the Ag/AgI couple, -0.394 V vs. SCE³⁵, which is sufficient to reduce cytochrome *c*. In this case, a stoichiometry of 1:1 is expected for $\Gamma/\text{Cyt } c$, assuming that all added Γ is adsorbed on the Ag particles. It is not clear, however, how the initial charge on the particles will affect their reducing capabilities. On the other hand, if the charge is delocalized, each Γ donates one electron to the Ag particle, thereby raising the potential of the particle as a whole. The

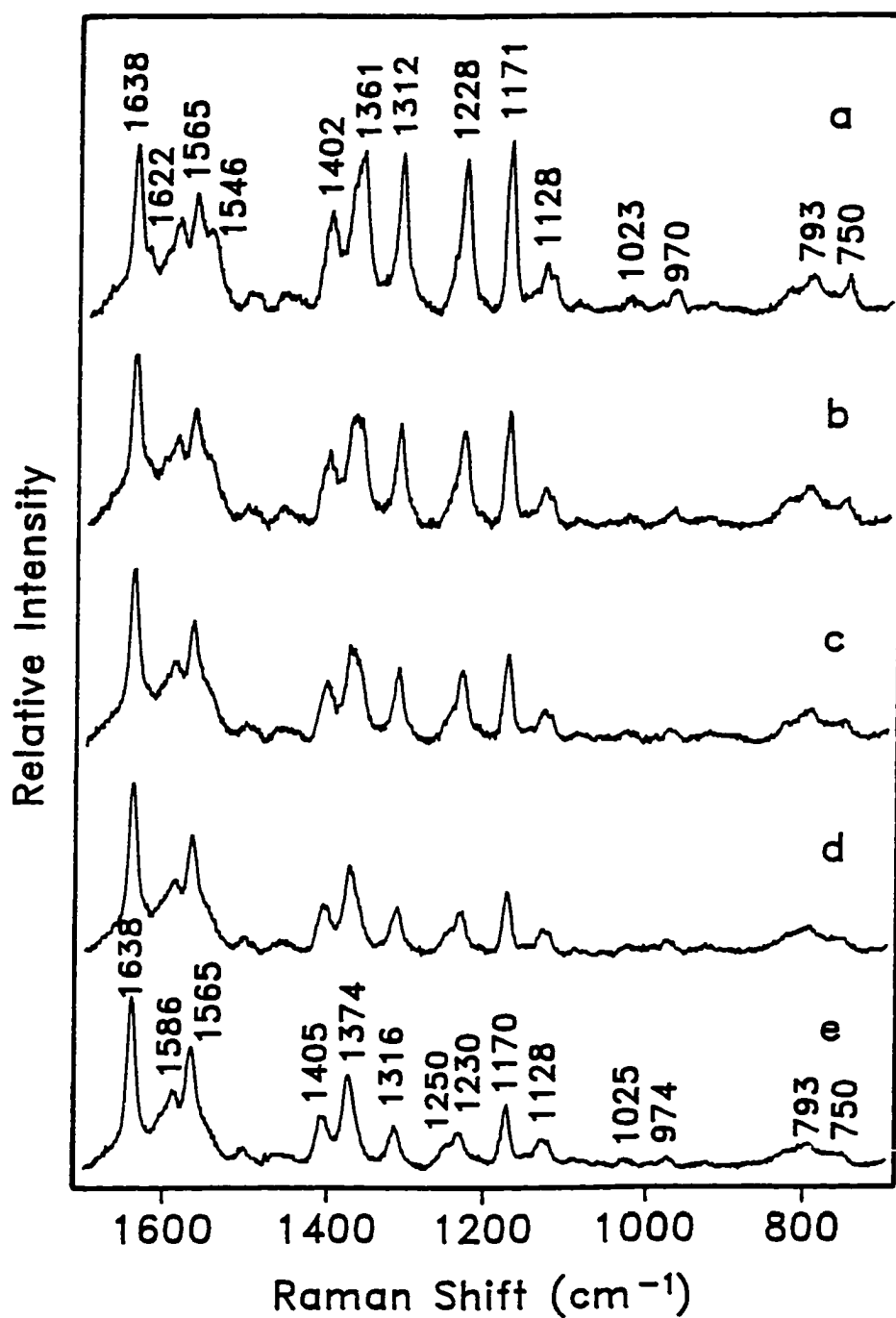


Figure 8: SERRS spectra of Cyt *c* (7.0 μM) added at different times after the Ag colloid was modified with iodide: (a) 0.5 min., (b) 5.5 min., (c) 10.5 min., (d) 15.5 min. and (e) 20.5 min. Excitation wavelength 514.5 nm.

particles store charge and function as “microelectrodes.”^{1,7} In this scenario, the potential of the particle depends on its capacitance and the amount of charge donated, as well as its starting potential; Cyt *c* reduction is expected to exhibit threshold behavior with increasing surface coverage by Γ . In our experiments, preadsorption of a certain amount of Γ on the Ag surface was always required before any Cyt *c* reduction was observed. (Note that the reduction of Cyt *c* was monitored by SERRS which provides extreme sensitivity for monitoring the reduced species at the surface.) A stoichiometry of 1:1 was never achieved even though stringent precautions were taken to eliminate oxygen and other oxidizing impurities. These results support the model in which the potential of the Ag particles is gradually built-up by the adsorbed ions to a level sufficient for Cyt *c* reduction.

Adsorption of iodide on nanosized Ag particles is expected to affect their plasmon resonance especially when Γ donates an electron to the metal. It also should be recognized that charging of a conducting metal sphere leads to accumulation of charge mainly in the surface layer. In experiments with silver colloids of 70 Å mean diameter, Heinglen et al.⁸ observed a dramatic red-shift of nearly 30 nm in the position of the maximum together with a decrease in intensity and broadening of the plasmon band upon addition of KI sufficient only for monolayer. Further increase in Γ concentration had no effect on the extinction spectrum. The authors explained the red-shift in the plasmon resonance upon Γ adsorption by a decrease in the free electron density in the surface layer. In this model, the donated electrons remain bound to the coordinatively-unsaturated Ag surface atoms and, as a result, a fraction of the *free* electron density from the surface layer is “squeezed” into

the interior of the particle.⁷ Assuming that excitation of the plasmon leads to an oscillation of the charge distribution in the surface layer of the particle, the authors conclude that electron depletion of this layer is manifested in the red-shift of the plasmon resonance.

According to the above, it would appear that the interior electrons of the particle do not significantly influence the plasmon resonance. However, when the diameter of the particle is much less than the wavelength of visible light (retardation effects are neglected), the particle can be described as a cavity for *free* electron oscillation.³⁶ This means that, even though the plasmon excitation creates only oscillating positive/negative caps near the surface, the interior electron density also participates in the collective motion. Interior electrons together with boundary conditions at the surface determine the electron wave function in the particle as a whole.³⁷ Changes in the surface layer do not strongly affect the plasmon frequency, but will influence its intensity and half-width due to changes in the boundary conditions for resonance. These changes occur as a result of donation or withdrawal of charge as well as adsorption of highly polarizable species such as iodide. Our experiments with colloidal metal films, where aggregation of the particles is believed to be insignificant, support this model. Addition of Γ up to twenty times greater than that required for monolayer coverage resulted only in a decrease in intensity by ca. 10% and broadening of the plasmon resonance (Figure 5); however, practically no red-shift was observed.

CONCLUSIONS

Adsorption of iodide and bromide on the surface of silver in a colloidal suspension and a colloidal metal film causes a charging of the metal particles and a shift in their potential to more negative values. At certain surface coverages, the potential reaches a value sufficient for the reduction of cytochrome *c*. In the absence of oxidizing agents, charge is stored within the particle for an extended period of time. Upon adsorption to the metal surface, each Γ donates nearly one electron which is delocalized within a thin surface layer. Charging of the Ag particles does not affect their plasmon frequency but causes damping (a decrease in intensity and broadening) of the plasmon resonance.

ACKNOWLEDGMENT

Funding for this research was provided by the National Institutes of Health (GM 35108, TMC). The authors gratefully acknowledge this support. Fruitful discussions with Professor Katsumi Niki are especially appreciated.

REFERENCES AND NOTES

- (1) McLendon, G. In *Energy Resources Through Photochemistry and Catalysis*, Grätzel, M., Ed.; Academic Press: New York, 1983, pp 99-122.
- (2) Fendler, J. H. *Membrane-Mimetic Approach to Advanced Materials*, Advances in Polymer Science Series Vol. 113; Springer-Verlag: Berlin, 1994; pp 96-111.
- (3) Mulvaney, P.; Grieser, F.; Meisel, D. In *Kinetics and Catalysis in Microheterogeneous Systems*, Grätzel, M. and Kalyanasundaram, K., Eds.; Surfactant Science Series; Marcel Dekker: New York, 1991; Vol. 38, pp 303-373.
- (4) Henglein, A. In *Topics in Current Chemistry*, Steckhan, E., Ed.; Springer-Verlag: Berlin, 1988; Vol. 143, pp 115-180.

- (5) Miller, D. S.; Bard, A. J.; McLendon, G.; Ferguson, J. *J. Am. Chem. Soc.* **1981**, *103*, 5336.
- (6) McLendon, G.; Miller, D. S. *J. Chem. Soc., Chem. Commun.* **1980**, *11*, 533.
- (7) Henglein, A. *J. Phys. Chem.* **1993**, *97*, 5457.
- (8) Linnert, T.; Mulvaney, P.; Henglein, A. *J. Phys. Chem.* **1993**, *97*, 679.
- (9) Henglein, A.; Lilie, J. *J. Am. Chem. Soc.* **1981**, *103*, 1059.
- (10) Neddersen, J.; Chumanov, G.; Cotton, T. M. *Appl. Spectrosc.* **1993**, *47*, 1959.
- (11) Chumanov, G.; Sokolov, K.; Gregory, B. W.; Cotton, T. M. *J. Phys. Chem.* **1995**, *99*, 9466.
- (12) Brautigan, D. L.; Ferguson-Miller, S.; Margoliash, E. *Meth. Enzymol.* **1978**, *53*, 128.
- (13) Awtrey, A. D.; Connick, R. E. *J. Am. Chem. Soc.* **1951**, *73*, 1842.
- (14) Goss, C. A.; Charych, D. H.; Majda, M. *Anal. Chem.* **1991**, *63*, 85.
- (15) Margoliash, E.; Frohwirt, N. *Biochem. J.* **1959**, *71*, 570.
- (16) Spiro, T. G.; Li, X.-Y. In *Biological Applications of Raman Spectroscopy*, Spiro, T. G., Ed.; Wiley: New York, 1988; Vol. III, pp 1-37.
- (17) Hildebrandt, P.; Stockburger, M. *J. Phys. Chem.* **1986**, *90*, 6017.
- (18) Barlow, G. H.; Margoliash, E. *J. Biol. Chem.* **1966**, *241*, 1473.
- (19) Margoliash, E.; Barlow, G. H.; Byers, V. *Nature* **1970**, *228*, 723.
- (20) Gopal, D.; Wilson, G. S.; Earl, R. A.; Cusanovich, M. A. *J. Biol. Chem.* **1988**, *263*, 11652.
- (21) Heimenz, P. C. *Principles of Colloid and Surface Chemistry*, 2nd ed.; Marcel Dekker: New York, 1986.
- (22) Marchetti, A. P.; Eachus, R. S. In *Advances in Photochemistry*, Volman, D., Hammond, G. and Neckers, D., Eds.; Wiley: New York, 1992; Vol. 17, pp 145-216.

- (23) Born, M.; Wolf, E. *Principles of Optics*, 6th ed.; Pergamon: Oxford. 1980; pp 633-664.
- (24) Garrell, R. L.; Shaw, K. D.; Krimm, S. *J. Chem. Phys.* **1981**, *75*, 4155.
- (25) Gao, P.; Weaver, M. J. *J. Phys. Chem.* **1986**, *90*, 4057.
- (26) Wetzel, H.; Gerischer, H.; Pettinger, B. *Chem. Phys. Lett.* **1981**, *78*, 392.
- (27) Holt, R. E.; Cotton, T. M. *J. Am. Chem. Soc.* **1987**, *109*, 1841.
- (28) Bottger, G. L.; Damsgard, C. V. *J. Chem. Phys.* **1972**, *57*, 1215.
- (29) Wertheim, G. K.; DiCenzo, S. B.; Buchanan, D. N. E. *Phys. Rev. B* **1982**, *25*, 3020.
- (30) Berry, G. M.; Bothwell, M. E.; Bravo, B. G.; Cali, G. J.; Harris, J. E.; Mebrahtu, T.; Michelhaugh, S. L.; Rodriguez, J. F.; Soriaga, M. P. *Langmuir* **1989**, *5*, 707.
- (31) Garrell, R. L.; Shaw, K. D.; Krimm, S. *Surf. Sci.* **1983**, *124*, 613.
- (32) Weaver, M. J.; Hupp, J. T.; Barz, F.; Gordon, J. G., II; Philpott, M. R. *J. Electroanal. Chem.* **1984**, *160*, 321.
- (33) Hildebrandt, P.; Stockburger, M. *Biochemistry* **1989**, *28*, 6710.
- (34) Salaita, G. N.; Lu, F.; Laguren-Davidson, L.; Hubbard, A. T. *J. Electroanal. Chem.* **1987**, *229*, 1.
- (35) Weast, R. C. *CRC Handbook of Chemistry and Physics*; 62nd ed.; Weast, R. C., Ed.; CRC Press: Boca Raton, 1981, pp D136-137.
- (36) Kerker, M. *Acc. Chem. Res.* **1984**, *17*, 271.
- (37) Kreibig, U.; Quinten, M. In *Clusters of Atoms and Molecules II*, Haberland, H., Ed.; Springer Series in Chemical Physics Vol. 56; Springer-Verlag: Berlin, 1994, pp 321-359.

CHAPTER 4. REDUCTIVE PROPERTIES OF IODIDE-MODIFIED SILVER NANOPARTICLES

A paper accepted by the *Journal of Electroanalytical Chemistry*¹

Morgan S. Sibbald, George Chumanov, Therese M. Cotton

ABSTRACT

Reduction of cytochrome *c* and 2,6-dichloroindophenol was observed on iodide-modified colloidal silver films. Two different processes were identified: reduction at sub- to monolayer coverages by Γ on the Ag surface and reduction in the presence of free iodide in solution. In the former, only about 5% of the electron acceptor molecules relative to surface-bound Γ underwent reduction, whereas in the latter a 1:1 stoichiometry was observed. Emission around 425 nm indicated the formation of molecular silver iodide. It was concluded that, in the absence of an electron acceptor, binding of iodide to the silver surface forms a complex which is different from molecular AgI. The electron derived from partial charge transfer between Γ and the Ag metal resides near the silver-iodide complex and does not contribute to the “free” electron density of the silver nanoparticles.

1. INTRODUCTION

At bare metal surfaces, many redox-active proteins exhibit irreversible electron transfer reactions and significant deviation from their native redox potential. This

¹ Reprinted with permission from *J. Electroanal. Chem.* 1997, in press (ref. JEC 5131).

behavior has been attributed to structural alterations of the protein following its adsorption on the surface. Modification of metal surfaces with small organic molecules or inorganic anions prevents direct interaction of proteins with the metal, thereby preserving their structure. The modifiers are not electroactive in the potential range where protein reduction occurs and, therefore, do not function as mediators of electron transfer. For example, adsorption of 4,4'-bipyridine, 4-mercapto-pyridine or iodide result in nearly reversible electron transfer kinetics for cytochrome *c* at gold and silver electrodes [1-3]. At the same time, the reduction potential on the bare metals was shifted about 440 mV more negative than that in the solution. Surface-enhanced resonance Raman scattering (SERRS) was employed to monitor the structure of adsorbed cytochrome *c*. Bands sensitive to the spin state and coordination number of the heme prosthetic group provided direct evidence for the native protein structure at the modified surface [4].

An important question to be addressed is how modifiers influence interfacial properties of metals, in particular the open circuit potential and the electron tunneling characteristics. Henglein and coworkers studied the adsorption of CN^- , SH^- , $\text{C}_6\text{H}_5\text{S}^-$ and PH_3 on colloidal silver and their effect on the reductive properties of the metal particles [5, 6]. It was found that in the absence of an electron acceptor, a potential difference was generated between the particles and the solution resulting from charge transfer from the adsorbed species to the metal. This potential was used to reduce methyl viologen dication or protons from water at the expense of silver oxidation to silver ions. Porter et al. measured a shift of nearly 700 mV in the open circuit potential of a gold electrode upon adsorption of butanethiol and butyl sulfide [7]. The authors also noted that the open

circuit potential was extremely sensitive to fortuitous electron acceptors, especially oxygen. Berry et al. discussed changes in the tunneling current when iodide is adsorbed onto an atomically smooth Au(111) surface resulting from the higher density of states at sites where iodide atoms are located [8].

Halide adsorption on the surface of silver nanoparticles and its effect on plasmon resonances and cytochrome *c* reduction was recently studied by Sibbald and coworkers [9]. Formation of an iodide monolayer on the Ag particles was shown to cause a decrease in intensity and broadening of the plasmon resonance. No shift in the resonance frequency was observed for this case, in contrast to the dramatic shift reported by Henglein et al. in similar experiments [5]. It was suggested that reduction of cytochrome *c* resulted from a charging of the metal particles and a shift in their potential to more negative values [9]. In the current study, quantitative measurements of the reductive properties of iodide-modified Ag nanoparticles arranged in two-dimensional arrays were undertaken in order to establish the molecular details of the reduction mechanism. Both cytochrome *c* and a redox active dye were used as electron acceptors in this work.

2. EXPERIMENTAL METHODS

2.1. Reagents

Cytochrome *c* (Horse Heart, Type VI, Sigma Chemical), 2,6-dichloro-indophenol-sodium salt (Fisher) and all other reagent grade chemicals were used as received. Water was purified using a Millipore Milli-Q system and had a nominal resistivity of 18 M Ω cm. All solutions were prepared in phosphate buffered pH 7.12 solution. The buffer contained

0.100 M potassium phosphate monobasic (EM Science) adjusted to pH 7.12 using 6 M NaOH. Solutions were purged with high-purity nitrogen (99.995%) using copper transfer lines for at least 15 min prior to measurements. All manipulations with samples were performed under an argon (99.996%) atmosphere.

2.2. Colloidal Metal Film (CMF) Preparation

The monolayer of Ag nanoparticles was prepared on a glass substrate modified with (3-mercaptopropyl)trimethoxysilane [10]. Upon immersing the substrates into Ag suspensions, the particles were spontaneously adsorbed due to strong covalent bonding between silver and the thiol headgroup of the modifier, producing two-dimensional semi-regular arrays. The mean particle diameter was determined by transmission electron microscopy to be ca. 100 nm. CMFs prepared in this manner were analyzed by scanning electron microscopy and appeared to be uniform across the entire substrate.

2.3. Electronic Absorption Spectroscopy

UV/Vis spectra were recorded using a Perkin-Elmer Lambda 6 dual-beam spectrophotometer with 2 nm spectral resolution. Because the cytochrome *c* absorption spectra typically contained contributions from both oxidized and reduced states of the heme, a linear combination of equations was solved utilizing Beer's Law and the reported molar absorptivities for each form of the protein at the wavelengths 528 and 550 nm in order to determine the concentration of each constituent [11]. The molar absorptivity of 2,6-dichloroindophenol in the oxidized state was reported by Heineman and coworkers to be $20,600 \text{ M}^{-1} \text{ cm}^{-1}$ at 600 nm [12].

Extinction spectra of colloidal metal films were obtained from the films immersed in water using a bare glass substrate as a reference.

2.4. Raman Spectroscopy

Raman scattering, surface-enhanced resonance Raman scattering and emission spectra were excited using 413.1 nm radiation from a Coherent Innova 100 Krypton laser. Laser power at the sample was less than 10 mW. Scattered light was collected by a $f/1.2$ camera lens in a back-scattering geometry and analyzed by a Spex 1877 Tripletmate spectrograph equipped with a Princeton Instruments LN 1100 x 330 CCD detector. Spectral resolution was 9 cm^{-1} . The spectra were calibrated using indene.

2.5. Electrochemical Measurements

Voltammetry experiments were performed using a BAS 100 electrochemical analyzer (Bioanalytical Systems) and a conventional three-electrode cell. The working electrode was a silver film prepared by vacuum deposition on a glass substrate. The exposed area was about 25 mm^2 . Platinum mesh was used as the auxiliary electrode. A saturated calomel electrode (SCE) served as the reference electrode. The working electrode was sequentially polished to a mirror-like surface with 0.3 and $0.05\ \mu\text{m}$ alumina + water slurries and sonicated in water prior to use. The electrolyte contained 0.50 M sodium sulfate and 0.10 M phosphate buffer, pH 7.12. All potentials described in the present work are reported with respect to the saturated calomel electrode.

3. RESULTS AND DISCUSSION

The evolution of the cytochrome *c* absorption spectrum as a function of increasing iodide concentration in the presence of a colloidal silver film is shown in Fig. 1. Colloidal

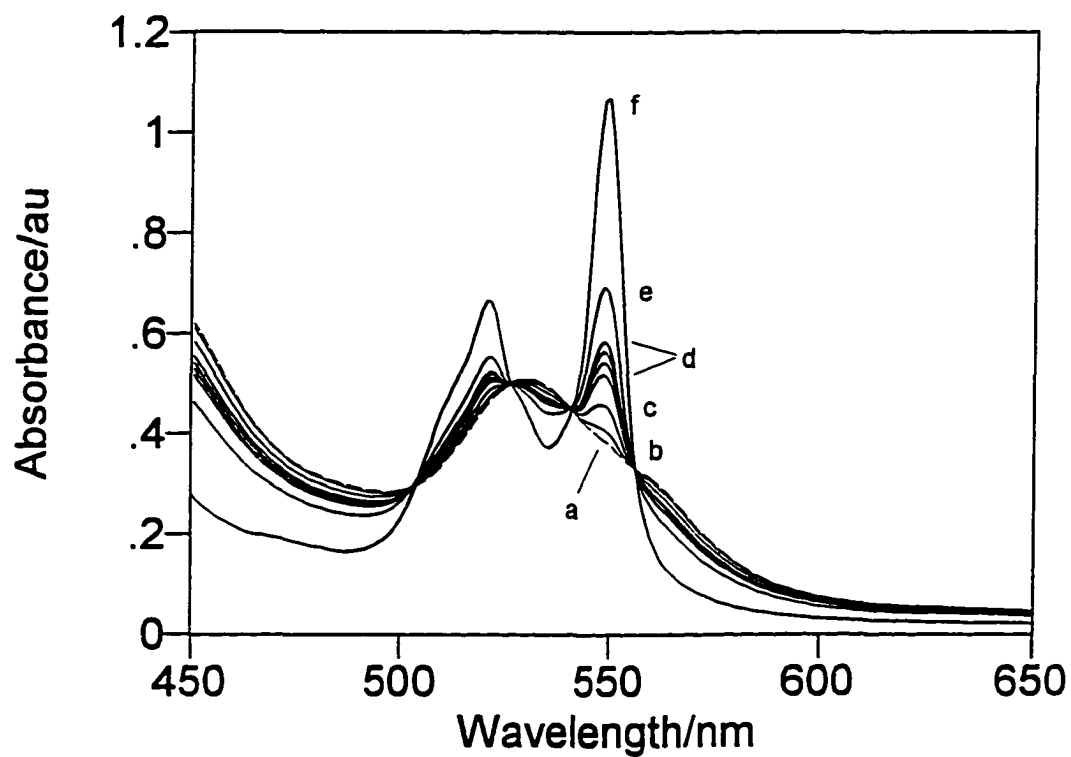
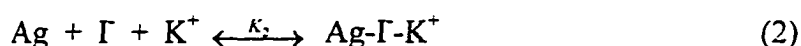
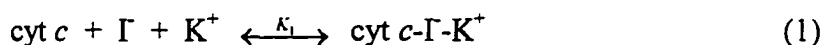


Figure 1. Absorption spectra of cytochrome c (45.40 μM) for different concentrations of KI in the presence of a colloidal silver film: (a) 0, (b) 3.0, (c) 12.1, (d) 21.2, and (e), (f) 48.5 μM . Spectra (a), (b), (c), and (e) were recorded at 15 min after mixing. Spectra in (d) were recorded at 15, 30, 45, and 60 min after mixing. Spectrum (f) was recorded at 18 hours after mixing.

films were used as a silver substrate because plasmon resonances of nanosized particles, which are sensitive to surface modification and redox reactions involving the Ag, can be easily monitored by absorption spectroscopy [9]. In addition, high concentrations of phosphate buffer did not cause aggregation of the silver particles in CMFs, in contrast to an aqueous colloidal suspension. The experiment for cyt *c* reduction was performed as follows. A colloidal film was immersed in 1.2 mL of 30 μM potassium iodide solution (pH 7.12) for 15 min to saturate the surface with iodide. Monolayer coverage in this case was insured by comparing the adsorbed amount of Γ , measured from decreased absorption at 226 nm assigned to an iodide charge-transfer-to-solvent band [13], with the calculated surface area of the Ag. For all films used in this study, monolayer coverage was equivalent to $8.3 \pm 0.4 \mu\text{M}$ of iodide and was consistent with $\sqrt{3} \times \sqrt{3}$ packing of Γ on the silver surface [8, 14]. The film was then rinsed to remove non-bound Γ , and immersed in 1.2 mL of a known concentration of cyt *c* in the oxidized state. At this point, less than 0.5 μM of reduced cyt *c* was observed, which was independent of the initial cyt *c* concentration. Addition of free iodide to the solution resulted in a significant increase in reduced cyt *c* (Fig. 1). A slow time-dependence was observed for this reduction process. When the solution was stirred for several hours in an oxygen-free atmosphere at a given Γ concentration, more reduced form appeared. After 18 h, the amount of reduced cyt *c* was nearly equivalent to the amount of iodide added, including Γ which was required for monolayer coverage of the metal surface (Fig. 1f).

After the metal surface was saturated with bound iodide, reduction of cytochrome appeared to be dependent on the formal cyt *c* concentration. In other words, more absolute

amounts of reduced cyt *c* were observed for lower initial concentrations, even though the same iodide concentration was present and the system was incubated for the same period of time. This behavior is illustrated in Fig. 2. The concentration and time dependence of the reduction process can be explained by a direct interaction between iodide and cytochrome. It is known that cyt *c* interacts electrostatically with various anions, including halides [15-17]. Therefore, competition exists between the Ag surface and cytochrome for Γ binding. When iodide is added to the solution, some ions are bound to cytochrome while others immediately interact with Ag, causing reduction of the protein.



Because the covalent bond of iodide to silver is stronger than the electrostatic interaction between iodide and cyt *c*, i.e. $K_2 \gg K_1$, the equilibrium will be shifted over time towards all iodide “pulled away” from cytochrome. As a result, after 18 h the ratio of reduced cyt *c* and added iodide approached one-to-one (Fig. 1).

Interaction of cytochrome with Γ requires long times for the system to reach equilibrium and interferes with quantitative measurements of the reductive properties of the Ag surface. In addition, cytochrome itself adsorbs on the silver surface, which has been shown to affect its standard reduction potential [18]. To overcome these complications, 2,6-dichloroindophenol (DCIP) dye was chosen as a redox indicator for studying the reductive properties of the iodide-modified Ag particles. This dye undergoes a reversible two-electron reduction which is accompanied by strong changes in the

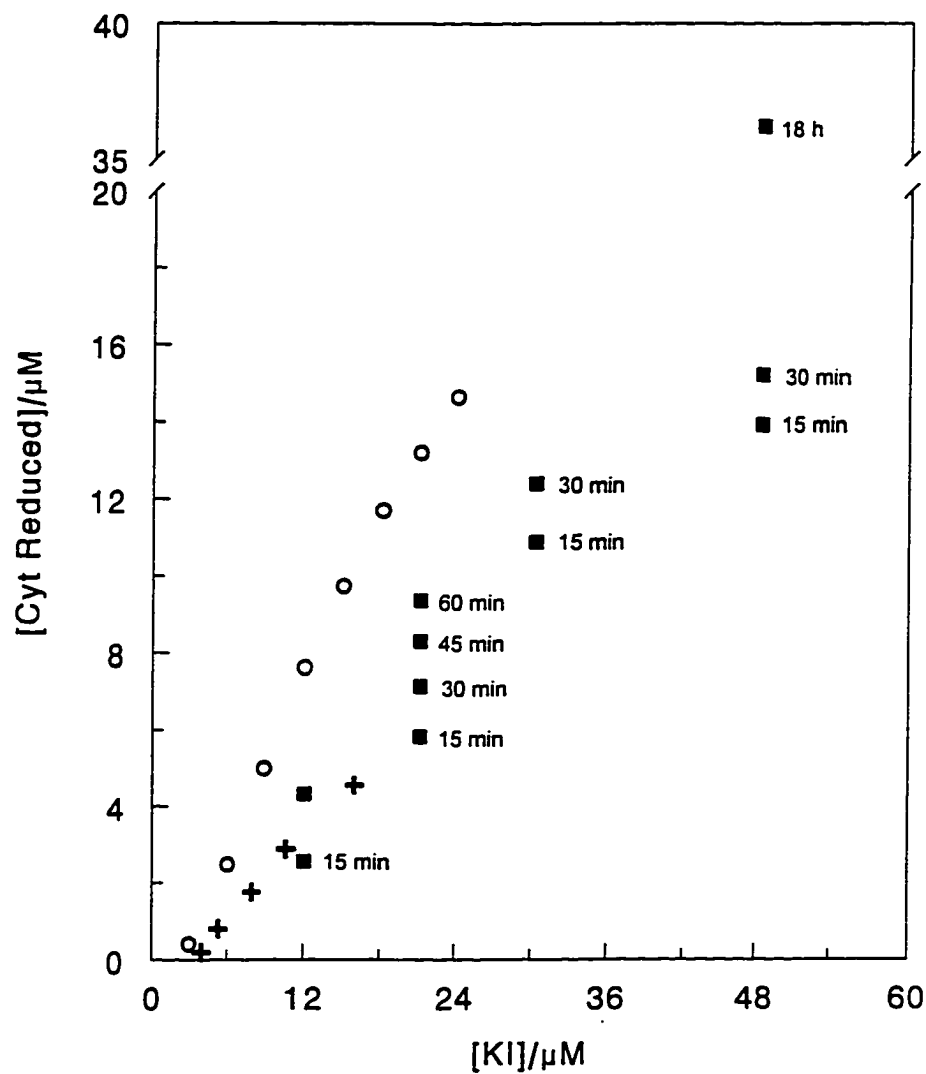
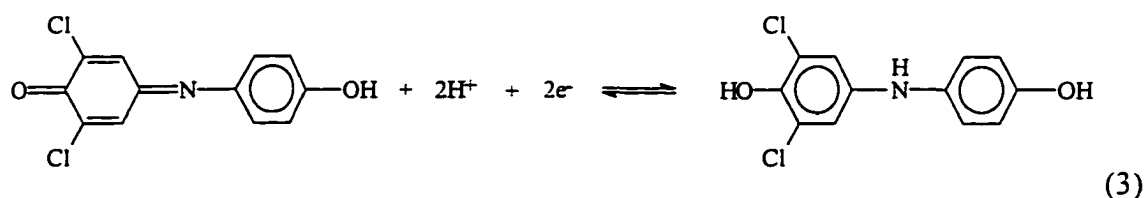


Figure 2. Dependence of reduced cytochrome c on the formal concentration of KI in the presence of a colloidal silver film for different concentrations of cytochrome: (o) - 16.4 μM; (+) - 51.2 μM; (■) - 45.4 μM.



absorption spectrum [12]. In the oxidized state, a broad band is observed around 600 nm. When DCIP becomes reduced, the chromophoric properties of this molecule are destroyed and visible absorption disappears. The cyclic voltammetric current-potential curves exhibited only one pair of cathodic/anodic waves revealing a midpoint potential of +0.021 V (Fig. 3). Although this is a two-electron reduction process, the potentials for each single electron transfer were indistinguishable even at scan rates up to 1 V s^{-1} . Because the reduction potential of DCIP is pH sensitive, all measurements were performed at pH 7.12 in phosphate buffer solution [19].

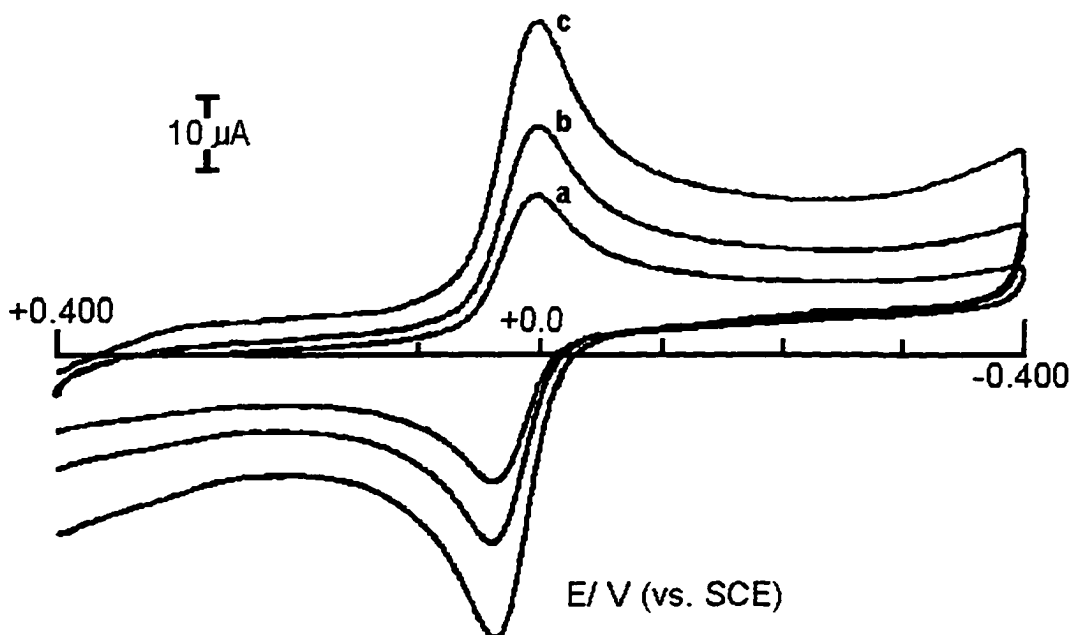


Figure 3. Cyclic voltammograms of 0.26 mM 2,6-dichloroindophenol at a freshly polished Ag electrode in 0.10 M phosphate buffer solution (pH 7.12) containing 0.50 M Na_2SO_4 . Scan rates: (a) 0.010, (b) 0.050, and (c) 0.100 V/s; Initial potential, +0.400 V.

A suspension of colloidal silver was utilized to test for interaction between DCIP and a Ag surface because such interactions might perturb the dye's midpoint potential. The frequency of the plasmon resonance in nanosized particles is directly influenced by molecules adsorbed on the surface as well as aggregation induced by this adsorption. Because addition of up to 30 μM of the dye to the Ag colloid did not cause any discernible changes in the extinction spectrum, the conclusion was made that DCIP does not adsorb on the silver surface. In addition, no SERS spectrum was observed even after intentional aggregation of the colloid in the presence of dye.

Ions of the phosphate buffer also adsorb on the silver surface, thereby interfering with DCIP adsorption and/or with the overall reduction phenomenon. SERS spectra of phosphate from the phosphate buffer solution in silver colloid displayed a downshift of the P-O stretching band from 990 cm^{-1} to 912 cm^{-1} [20], indicating a direct interaction between the ion and the metal surface. The addition of iodide to Ag colloid containing adsorbed phosphate resulted in loss of the 912 cm^{-1} band from the SERS spectra, consistent with displacement of the weakly bound phosphate from the metal surface by iodide. The conclusion is made that the presence of phosphate buffer does not significantly interfere with the reduction process. Also, no difference was observed for cytochrome *c* reduction on iodide-modified colloidal films in the presence or absence of phosphate buffer.

Reduction of DCIP on colloidal silver films was performed according to the protocol described above for cyt *c*. Absorption spectra were recorded in differential mode, in which the sample and reference cells contained the same formal concentrations of dye.

As the concentration of iodide was increased, bleaching was observed in the visible and near-uv spectral regions corresponding to disappearance of the oxidized form, as shown in Fig. 4. The new band around 225 nm ($\epsilon \approx 26,700 \text{ M}^{-1} \text{ cm}^{-1}$) is assigned to the reduced form of DCIP. The reaction was found to be extremely oxygen sensitive. Both reduced DCIP and the modified silver particles can be oxidized by traces of oxygen (and possibly other electron acceptors), resulting in a lower yield for the reaction. Precautions were made to minimize these factors. It is important to emphasize that no time evolution of this reduction process was observed, unlike that found in the experiments involving cytochrome. The absolute amount of reduced dye was also independent of its formal concentration and was directly proportional to iodide concentration.

In Fig. 5, the amount of reduced DCIP is plotted as a function of iodide concentration for different concentrations of dye. Reduction was highly reproducible and, as can be seen in the Fig., independent of DCIP concentration. This reaction is limited by iodide, which means that the Γ concentration determines the absolute amount of dye reduced. The stoichiometry of Γ to reduced DCIP was established from the slope of the line in Fig. 5 to be 1.87 to 1. The ratio was expected to be 2 to 1 because reduction of the dye is a two-electron process. This discrepancy could arise if not all DCIP molecules undergo two-electron reduction; the one-electron reduced semiquinoid intermediate could be formed [21]. However, no obvious indication of a third component was found in the UV/Vis spectra.

As can be seen, the nearly 2 to 1 reaction stoichiometry was observed only after saturation of the Ag surface by iodide (Fig. 5). The amount of Γ required for saturation

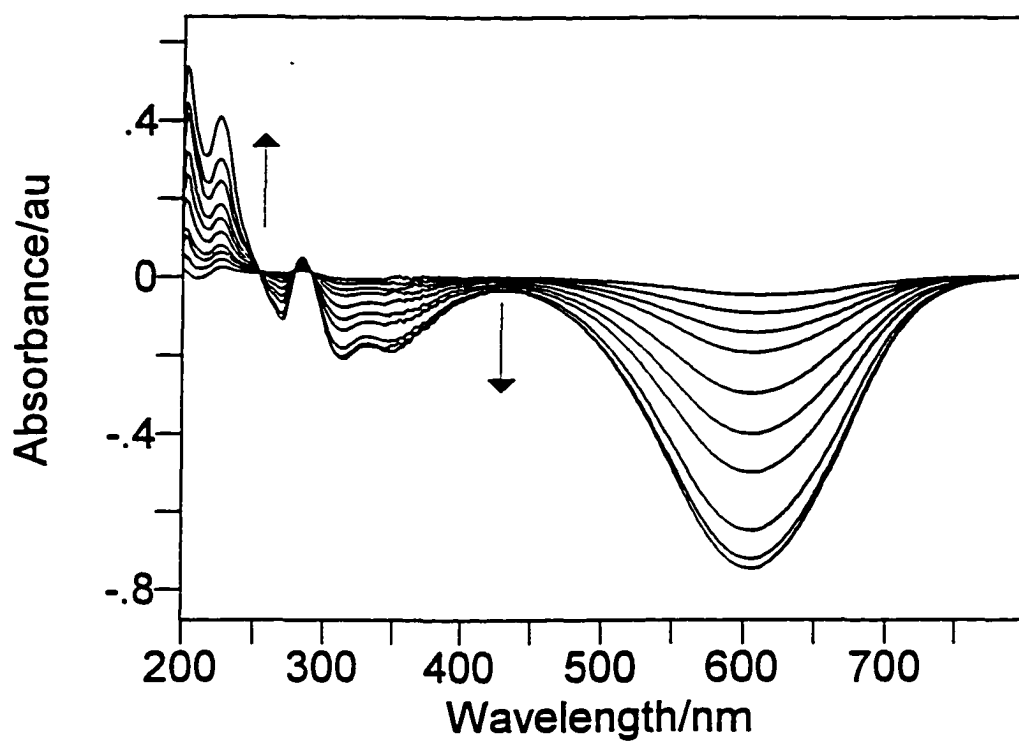


Figure 4. Absorption difference spectra of 2,6-dichloroindophenol ($91.2 \mu\text{M}$) in the presence of a colloidal silver film as a function of KI concentration. The arrows indicate the direction of changes with increasing concentrations of iodide.

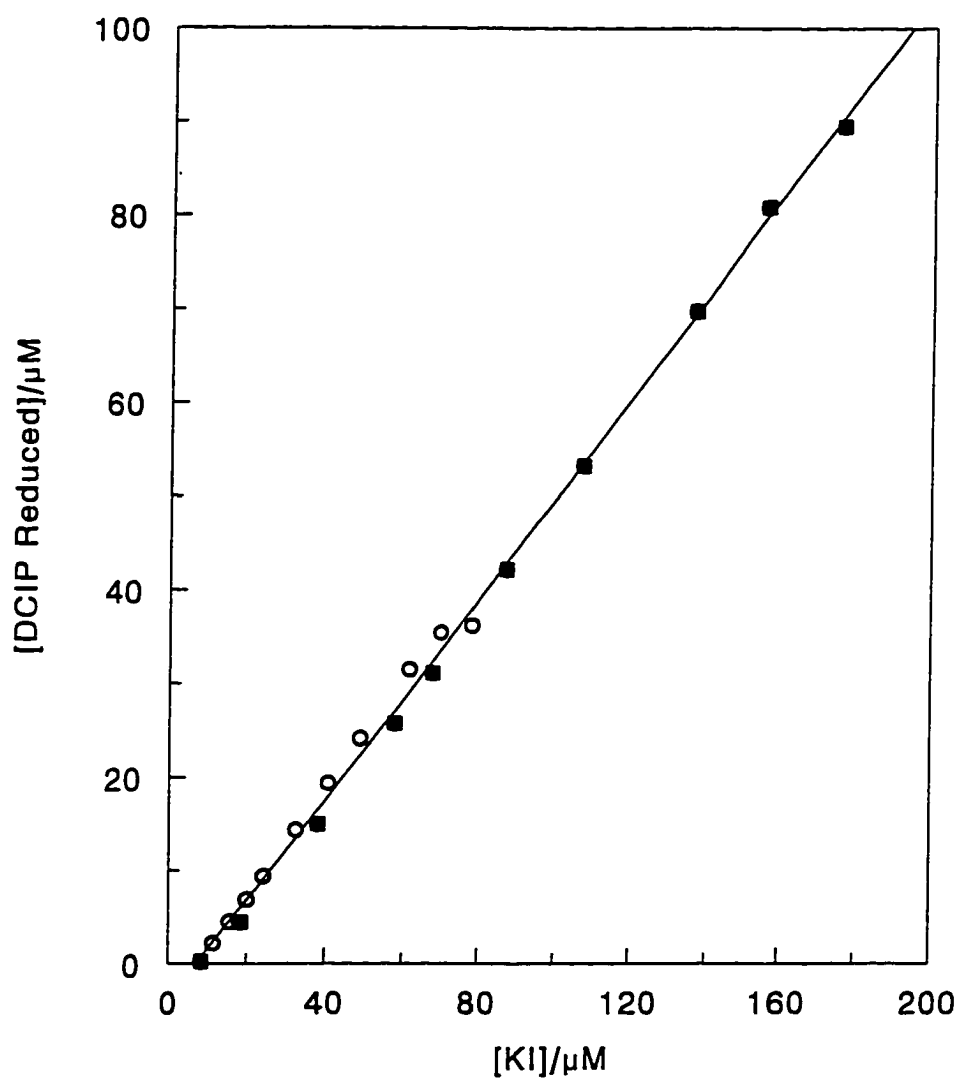


Figure 5. Dependence of reduced 2,6-dichloroindophenol on the formal concentration of KI in the presence of a colloidal silver film for different concentrations of dye: (o) - 37.0 μM ; (■) - 91.2 μM .

corresponds to monolayer coverage and is represented by the intercept of the plot with the x-axis. At this coverage, ca. 0.25 μM of reduced DCIP was observed even though the films were thoroughly rinsed to remove traces of non-bound iodide. In contrast, monolayer coverage on a continuous silver surface (e.g. silver electrode) normalized in surface area to the colloidal Ag films did not result in observable amounts of DCIP or cytochrome reduction. The latter was established by both UV/Vis and SERS measurements. Reduction at sub- to monolayer coverages is a unique property of the colloidal metal films composed of isolated Ag nanosized particles. Therefore, the reduction can be arbitrarily divided into two processes: reduction at sub- to monolayer coverages when all added iodide is adsorbed on the metal surface and reduction in the presence of free iodide in solution.

Reduction of cytochrome *c* and DCIP dye at sub- to monolayer iodide coverages on colloidal silver films can be assumed to result from a shift in the particles' potential to more negative values upon iodide adsorption. Upon adsorption, Γ is expected to donate nearly one electron into the Ag particle [9]. This electron, however, does not contribute to the "free" electrons of the metal; instead, it remains mostly bound to the Ag surface-I complex. Otherwise, the potential of the metal particle would be shifted to unrealistic negative values which can be seen from the following consideration.

The potential of a spherical capacitor can be calculated from the amount of stored charge and its capacitance. Weaver et al. measured a capacitance of ca. 15 $\mu\text{F cm}^{-2}$ for polycrystalline silver in electrolyte containing KI at potentials positive of the potential of zero charge (ca. - 0.95 V), where the capacitance is relatively independent of the applied

potential [22, 23]. Valette et al. measured the potential dependence of the capacitance for different crystal faces of silver around the potential of zero charge in iodide solution [24]. In the potential region between -0.7 V and -1.5 V, the capacitance for all crystal faces increased to maxima of up to $360 \mu\text{F cm}^{-2}$ and then rapidly decreased to a plateau around $30 \mu\text{F cm}^{-2}$. For the present calculation, the capacitance in the potential regions positive of -0.7 V and negative of -1.5 V was assumed to be $20 \mu\text{F cm}^{-2}$, whereas in the region between -0.7 V and -1.5 V it was approximated by an average value of $200 \mu\text{F cm}^{-2}$. The amount of charge donated by iodide to one Ag particle of 1000 Å diameter was calculated to be ca. 5.8×10^5 electrons. This value was determined from the total amount of adsorbed iodide, which was measured spectroscopically as described above, normalized to the number of silver particles in the colloidal Ag film, which was obtained from electron micrographs.

The calculation yields an unrealistic value of -7.5 V for the potential of the iodide-modified Ag particle. Actually, the particle will not be charged to such an extent; the evolution of hydrogen around the potential -1.1 V would limit the charging at sub-monolayer coverages and further build up of the monolayer would continue to produce hydrogen gas. No gas production was observed as the monolayer of iodide was formed on the colloidal films nor during prolonged exposure of the films to millimolar KI solutions. A second limiting factor for charging is the potential of iodide desorption from the Ag surface which is ca. -0.9 V [25]. This potential would also be reached at small fractions of monolayer coverage which would prevent further monolayer formation. From experiments it is known that a full monolayer of iodide on the Ag particles is formed.

Another concern regarding the concept of charging of the Ag nanoparticles by adsorbed iodide is the continuous discharging which can take place by traces of fortuitous electron acceptors, in particular oxygen. Oxygen is known to convert iodide in the presence of silver metal to molecular silver iodide. In the case of colloidal silver films, this reaction can be monitored by changes in the plasmon resonance of the nanoparticles as the metal is converted to AgI (described below). Precautions taken in this work were sufficient to minimize oxygen such that no significant changes in the plasmon resonance were observed after immersing a silver colloidal film overnight in millimolar KI solution.

The above considerations lead to the conclusion that the electron which is delivered upon Γ adsorption is mainly localized near the Ag surface-I complex. The negative charge which builds up in the surface layer could be compensated by cation coadsorption in the inner Helmholtz layer or by the inherent positive charge of the surface silver atoms. Cation coadsorption with iodide anions in a 1:1 stoichiometry on Au(110) was recently determined by in situ surface x-ray scattering [26]. The potential due to adsorbed Γ drops very rapidly across the coadsorbed cation layer and is not accessible to electron acceptors from the bulk solution. However, the fact that small reduction of the dye and cyt *c* is observed at monolayer Γ coverages strongly suggests that the potential of the system has been changed after iodide adsorption. Two reasons for the change in the effective potential can be suggested. First, if the adsorption of iodide on the Ag surfaces causes a change in the electron density in terms of the number of electrons N per unit volume V , then the Fermi energy E_f of the electrons will also be affected according to the equation,

$$E_f = \frac{\hbar^2}{2m} \left(\frac{3\pi^2 N}{V} \right)^{2/3} \quad (4)$$

altering the electrochemical potential of the particle [27]. Second, adsorption of iodide and its cation can reduce the barrier for electron tunneling to the acceptor. Neumann et al. reported that the work function on iodide-modified Au(100) at 300 K was up to 10% lower relative to the unmodified gold surface due to adsorbate-induced surface reorganization [28]. Even though reducing the barrier does not directly affect the potential of the particle, it will increase the electron transfer rate for a spontaneous reaction resulting in an increased amount of reduced species.

For reduction of *cyt c* and the dye in the presence of non-bound iodide in solution, it is conceivable that the potential of the system is governed by the silver/silver iodide couple. This means that the system reaches a potential at equilibrium which is determined by the Γ concentration and can be calculated from the Nernst equation. When the reduction reaction occurs, this potential changes in response to the decreasing concentration of iodide, establishing a new equilibrium potential which can be calculated using the Nernst equation and the ratio of reduced to oxidized dye. Because the potential of the Ag/AgI couple (-0.396 V at unit activity) is much more negative than the midpoint potential of DCIP (+0.021 V), the reaction appeared to “consume” all available iodide. Strictly speaking, a small amount of iodide could still remain in solution, but quantitation is limited by the detection limit in our UV/Vis measurements, 5×10^{-7} M for iodide. The concentration of Γ in solution at equilibrium was calculated to be 5×10^{-9} M for a few

percent of reduced dye, whereas this value was ca. 6×10^{-7} M for nearly one hundred percent reduction.

There are, however, two major concerns in applying the Nernst equation for determining the potentials of this reaction. First, the potential of the silver/silver iodide couple requires a certain amount of molecular silver iodide adsorbed on the silver metal and free Γ in solution. As will be discussed below, in the absence of an electron acceptor, no molecular silver iodide is formed on the silver surface. This factor makes the reported value of -0.396 V for the Ag/AgI couple inappropriate for determining the initial potential of the iodide-modified silver surface. Second, the Nernst equation is correctly applied under equilibrium conditions for a reversible reaction. This implies that the reduced DCIP can be reoxidized by AgI, producing Ag^0 and Γ in solution. Because both the dissociation constant of AgI in water (ca. 10^{-16}) and its solubility as a molecular species (ca. 10^{-7} M) are very low [29], silver iodide will exist as a precipitate and the formation of Ag^0 and Γ will be kinetically slow if not forbidden.

Adsorption of iodide on the silver surface resulted in the formation of a complex which is different from molecular AgI. This complex can be converted to AgI by a suitable electron acceptor in the presence of non-bound Γ in solution. The reverse reaction can be achieved by irradiating AgI with visible or ultraviolet light at room temperature; photodecomposition occurs which yields a silver cluster with a layer of adsorbed iodine, as in the photographic process. Formation of the complex appeared to be independent of the iodine source, i.e. whether Γ , I_2 or I_3^- , is added to the silver metal. In previous experiments, it was determined by Raman spectroscopy that the vibrational frequency of

surface-bound iodide, 112 cm^{-1} , is different from the vibrational signature of bulk AgI, 105 cm^{-1} and 83 cm^{-1} [9]. The Raman spectrum of bulk AgI was obtained in a rotating cell with near-infrared excitation to minimize photodecomposition.

The reduction process on the iodide-modified silver surface in the presence of Γ in solution can be followed by an emission near 425 nm upon 413.1 nm excitation. This emission is characteristic of exciton recombination in AgI [30, 31]. A series of emission spectra of Ag colloid in the presence and absence of cytochrome *c* and iodide are shown in Fig. 6. The spectra were obtained at 77 K in order to minimize photodecomposition effects. A strong SERRS spectrum characteristic of the native-oxidized cyt *c* was observed on Ag colloid in the absence of Γ (Fig. 6a) [9]. Iodide itself on Ag colloid exhibits weak emission at 426 nm, the intensity of which is comparable to the SERRS spectrum (Fig. 6b). Upon addition of cyt *c* to the iodide-modified Ag colloid in the presence of Γ in solution, an intense band appeared around 427 nm. Its intensity was typically ca. 20 times higher than that in the absence of cytochrome, clearly indicating the formation of molecular AgI (Fig. 6c). The weak emission which was observed in the absence of cyt *c* is attributed to oxidation of the iodide-modified Ag surface due to fortuitous electron acceptors, most likely oxygen. It is necessary to emphasize that no emission was observed at monolayer coverages of the silver surface by iodide in the presence of electron acceptors. Oxidation of the surface-bound silver-iodide complex on colloidal films causes etching of the Ag nanoparticles which results in a decrease in intensity and shift to the blue spectral region of the plasmon resonance peak (Fig. 7). The sloping background in the resultant spectrum in Fig. 7 is due to scattering by insoluble AgI particles.

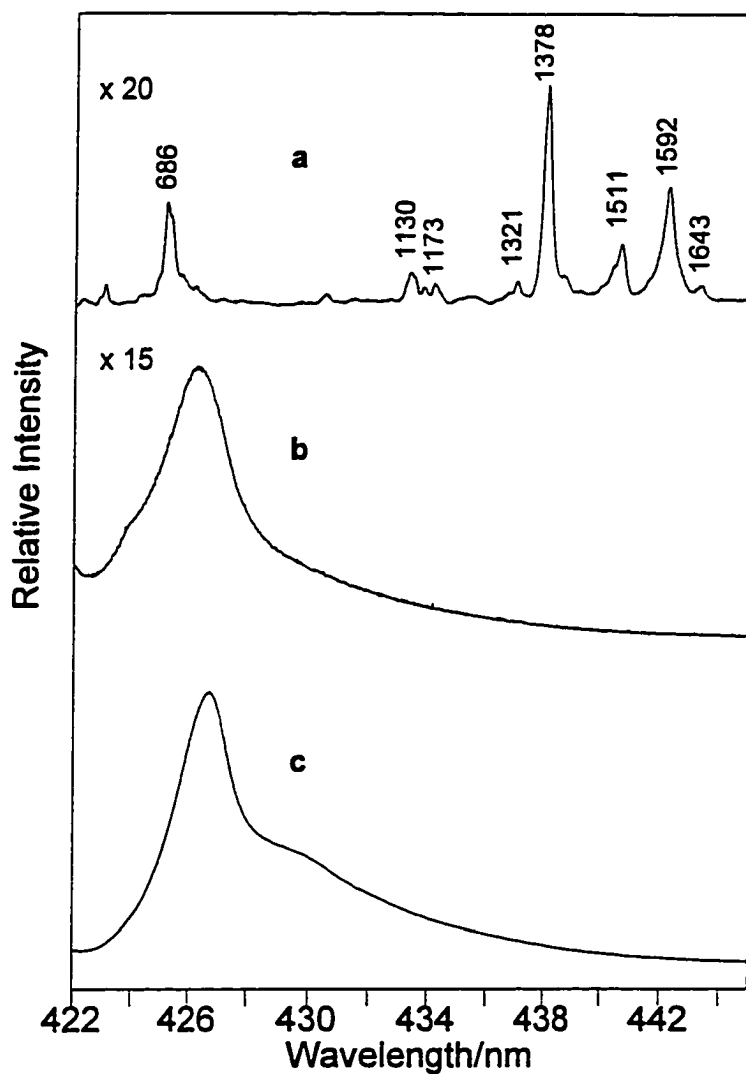


Figure 6. SERRS spectrum of cytochrome c (8 μM) in Ag colloid (a), and emission spectra from iodide-modified Ag colloid in the absence (b) and presence (c) of cytochrome at 77 K. Excitation wavelength 413.1 nm. Peaks in SERRS spectrum are labeled in relative wavenumbers.

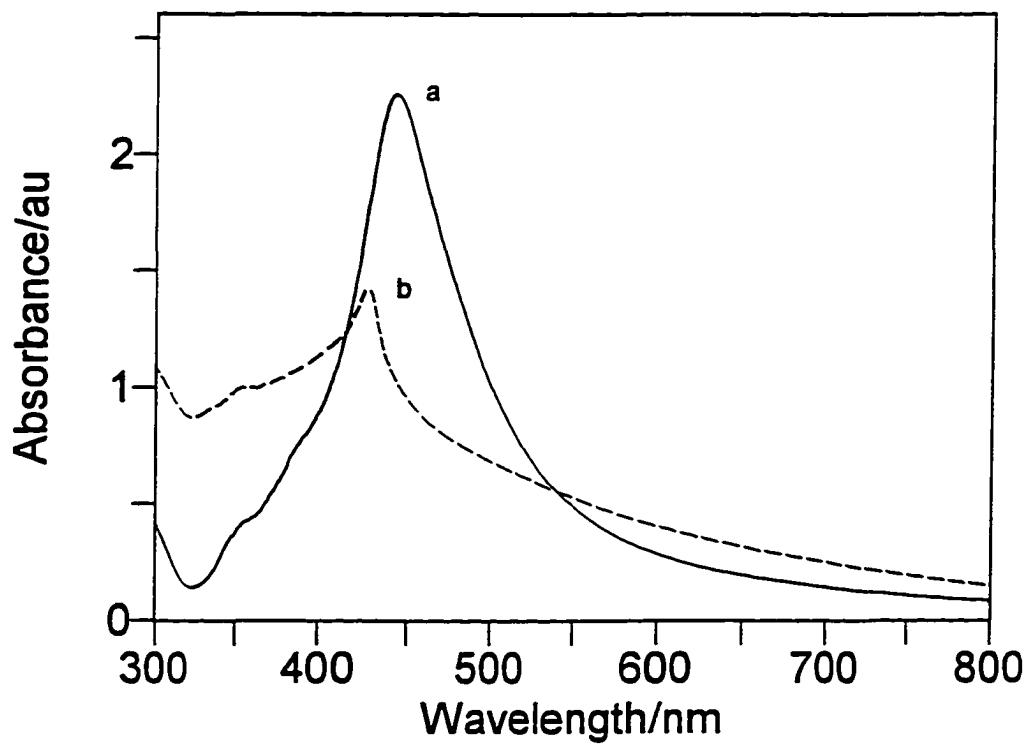


Figure 7. Extinction spectra of iodide-modified colloidal silver film before (a) and after (b) the reduction of 2,6-dichloroindophenol (91.2 μM).

4. CONCLUSIONS

Adsorption of iodide on a colloidal silver film causes reduction of cytochrome *c* and 2,6-dichloroindophenol. Reduction of the cytochrome exhibits a complex dynamic attributed to a competition between iodide binding to cyt *c* and to silver. The reduction can be arbitrarily divided into two parts: reduction at sub- to monolayer coverages when all added iodide is adsorbed on the metal surface and reduction in the presence of free iodide in solution. The former process is specific for nanosized silver particles, whereas the latter can be observed on the bulk metal surface. Reduction at monolayer coverage was rationalized to arise from a shift in the Fermi energy of electrons in the silver particles due to a change in the electron density and from a decrease in the barrier for electron tunneling. In the presence of Γ in solution, the potential of the system is controlled by the Ag/AgI couple, and the reduction process appeared to follow a 1:1 stoichiometry. It was concluded that upon adsorption of Γ on the silver surface, the donated electron resides near the silver-iodide bond and does not contribute to the "free" electron density of the metal. Spectroscopic evidence indicates that iodide bound to the silver surface forms a complex which is different from molecular silver iodide.

ACKNOWLEDGMENTS

Research at the Ames Laboratory was supported by the Division of Chemical Sciences, Office of Basic Energy Sciences, U.S. Department of Energy. Ames Laboratory is operated for the U.S. Department of Energy by Iowa State University under Contract No. W-7405-Eng-82.

REFERENCES

- [1] M. J. Eddowes and H. A. O. Hill, *J. Chem. Soc., Chem. Commun.* (1977) 771.
- [2] T. Sagara, K. Niwa, A. Sone, C. Hinnen, and K. Niki, *Langmuir*, 6 (1990) 254.
- [3] T. Lu, X. Yu, S. Dong, C. Zhou, S. Ye, and T. M. Cotton, *J. Electroanal. Chem.*, 369 (1994) 79.
- [4] D. Hobara, K. Niki, C. Zhou, G. Chumanov, and T. M. Cotton, *Colloids and Surfaces*. A93 (1994) 241.
- [5] T. Linnert, P. Mulvaney, and A. Henglein, *J. Phys. Chem.*, 97 (1993) 679.
- [6] A. Henglein, *J. Phys. Chem.*, 97 (1993) 5457.
- [7] N. Tani, C. Zhong, and M. D. Porter, unpublished results, (1996).
- [8] G. M. Berry, M. E. Bothwell, B. G. Bravo, G. J. Cali, J. E. Harris, T. Mebrahtu, S. L. Michelhaugh, J. F. Rodriguez, and M. P. Soriaga, *Langmuir*, 5 (1989) 707.
- [9] M. S. Sibbald, G. Chumanov, and T. M. Cotton, *J. Phys. Chem.*, 100 (1996) 4672.
- [10] G. Chumanov, K. Sokolov, B. W. Gregory, and T. M. Cotton, *J. Phys. Chem.*, 99 (1995) 9466.
- [11] E. Margoliash and N. Frohwirt, *Biochem. J.*, 71 (1959) 570.
- [12] W. R. Heineman, B. J. Norris, and J. F. Goelz, *Anal. Chem.*, 47 (1975) 79.
- [13] A. D. Awtrey and R. E. Connick, *J. Am. Chem. Soc.*, 73 (1951) 1842.
- [14] G. N. Salaita, F. Lu, L. Laguren-Davidson, and A. T. Hubbard, *J. Electroanal. Chem.*, 229 (1987) 1.

- [15] G. H. Barlow and E. Margoliash, *J. Biol. Chem.*, 241 (1966) 1473.
- [16] E. Margoliash, G. H. Barlow, and V. Byers, *Nature*, 228 (1970) 723.
- [17] D. Gopal, G. S. Wilson, R. A. Earl, and M. A. Cusanovich, *J. Biol. Chem.*, 263 (1988) 11652.
- [18] P. Hildebrandt and M. Stockburger, *Biochemistry*, 28 (1989) 6710.
- [19] H. D. Gibbs, B. Cohen, and R. K. Cannan, *Public Health Repts. (U.S.)*, 40 (1925) 649.
- [20] N. B. Colthup, L. H. Daly, and S. E. Wiberley, *Introduction to Infrared and Raman Spectroscopy*, 3rd ed., Academic Press, New York, 1990.
- [21] G. Schwarzenbach and L. Michaelis, *J. Am. Chem. Soc.*, 60 (1938) 1667.
- [22] D. Larkin, K. L. Guyer, J. T. Hupp, and M. J. Weaver, *J. Electroanal. Chem.*, 138 (1982) 401.
- [23] J. O. M. Bockris and A. K. N. Reddy, *Modern Electrochemistry* Plenum Press, New York, 1970.
- [24] G. Valette, A. Hamelin, and R. Parsons, *Zeit. Physikal. Chem.*, 113 (1978) 71.
- [25] M. J. Weaver, J. T. Hupp, F. Barz, J. G. Gordon, II, and M. R. Philpott, *J. Electroanal. Chem.*, 160 (1984) 321.
- [26] J. X. Wang, G. M. Watson, and B. M. Ocko, *J. Phys. Chem.*, 100 (1996) 6672.
- [27] C. Kittel, *Solid State Physics* Wiley, New York, 1976.
- [28] A. Neumann, K. Christmann, and T. Solomun, *Surf. Sci.*, 287 (1993) 593.
- [29] R. C. Weast, ed., *CRC Handbook of Chemistry and Physics*, CRC Press, Boca Raton, 1981.
- [30] A. P. Marchetti and R. S. Eachus, in D. Volman, G. Hammond, and D. Neckers, eds. *Advances in Photochemistry*, Vol. 17, Wiley, New York, 1992, p. 145.
- [31] A. Henglein, M. Gutierrez, H. Weller, A. Fojtik, and J. Jirkovsky, *Ber. Bunsenges. Phys. Chem.*, 93 (1989) 593.

CHAPTER 5. MULTIPLE-OVERTONE RESONANCE RAMAN SCATTERING AND RESONANCE FLUORESCENCE FROM IODIDE ADSORBED ON SILVER SURFACES

A paper to be submitted to the *Journal of Chemical Physics*

Morgan S. Sibbald, George Chumanov, Therese M. Cotton

ABSTRACT

A detailed excitation profile of the resonance emission (Raman and fluorescence) from iodide adsorbed on an electrochemically roughened Ag surface was obtained in the spectral range from 409 to 433 nm. The excitation wavelength was tuned in small steps (ca. 0.25 nm) resulting in a total of 77 spectra. At the temperature 20 K, the most intense emission features were from a vibrational progression having a fundamental band at 123 cm^{-1} and up to six overtones. This spectrum was previously assigned to the $\nu(\text{I-I})$ stretch of a unique I_2 species adsorbed on small Ag clusters. From the Raman excitation profile, a picture of the electronic structure of the surface-adsorbed I_2 species was developed. Vibronic spacing of ca. 123 cm^{-1} was observed in both the ground and excited electronic states. In addition, significant displacement of the potential energy surfaces along the nuclear coordinate was suggested by the ca. 370 cm^{-1} spacing (three quanta) of the two resonance maxima in the excitation profile for each band in the progression.

INTRODUCTION

The distinction between resonance Raman (RR) scattering and resonance fluorescence (RF) has been the subject of numerous theoretical and experimental investigations.¹⁻³ Many of the early advances concerning the assignment of resonance

emission as RR or RF were made in the 1970's. In one study, Holzer and coworkers demonstrated both RR and RF from various halogen gases including Cl_2 , Br_2 , I_2 , and ICI .⁴ The authors found that the resonance fluorescence consisted of very sharp doublet lines having irregular overtone sequences, often with some lines completely missing. The resonance Raman features were broadened, relative to the fluorescence, due to allowed rotational transitions. Overtones in the Raman progressions exhibited continuous broadening and a decrease in intensity with higher vibrational quantum number. Holzer et al. noted the unique opportunity in these halogen gases to observe both resonance Raman and resonance fluorescence, where the latter is generally much more intense and can overwhelm the detection system.

One of the clearest examples of both RR and RF was shown by Hochstrasser and Nyi.⁵ In this study, the wavelength of the exciting radiation was tuned through single vibronic levels of azulene in a naphthalene matrix at 2 Kelvin. Several overtone progressions were observed from the different normal vibrational modes depending on the excitation wavelength. Progressions assigned to a resonance Raman transition were found to always shift in absolute frequency with changes in the incident laser frequency. On the other hand, progressions assigned to a resonance fluorescence transition remained at a fixed set of frequencies independent of the incident laser frequency. Similar studies were recently performed by Zeigler in which the wavelength and pressure dependence of the RR and RF features in resonance-excited spectra of gas phase methyl iodide in a methane matrix.¹ The spectra elegantly showed a broad fluorescence feature which remained fixed

in wavelength position while a sharp Raman feature tracked with the excitation wavelength.

Resonance emission was recently reported by Sibbald and coworkers from iodide adsorbed on silver surfaces.⁶ At room temperature the Raman spectrum from the iodide-modified Ag surface contained a single, broad band around 112 cm^{-1} which has been assigned to the metal-iodide stretch.⁷ At liquid nitrogen temperature, a vibrational progression appeared in the Raman spectrum with a fundamental band at 123 cm^{-1} and as many as six overtones. A model was developed in which at low temperatures, under irradiation, a bond is formed between neighboring iodine adatoms producing a new I_2 species adsorbed on a small Ag cluster.⁶

In a preliminary excitation profile of the iodide-modified Ag surface, a strong dependence on the excitation wavelength was revealed based on the relative intensities of the overtone bands at the wavelengths 406.7, 413.1, and 415.4 nm.⁶ With excitation of the Raman spectrum at 457.9 nm, however, no progression appeared suggesting the existence of an electronic resonance transition in this spectral region. The strong Raman signal which was observed from no more than one monolayer of iodide adsorbed on the Ag surface further suggested a significant contribution from surface-enhanced phenomena, i.e. surface-enhanced Raman scattering.⁸

The present work was undertaken in order to determine if the silver surface-adsorbed I_2 species might be an ideal system for theoretical modeling of resonance emission processes. It is a simple case of a diatomic species exhibiting only one totally symmetric mode in which only diagonal components of the transition polarizability are

non-zero. This diatomic molecule has only one resonant excited state which can be described by Albrecht's *A*-term scattering mechanism.^{9,10} It exists at low temperatures at which all molecules are in the lowest vibrational level of the ground electronic state and interactions with the matrix environment (or "bath") are expected to be minimal.

EXPERIMENTAL METHODS

Modification of Silver Surfaces. The iodide-modified silver substrates were prepared according to previously reported procedures.⁶ Briefly, the thin films of silver, prepared by vapor depositing ca. 1 μm equivalent mass thickness of Ag on glass substrates, were first treated in an RF plasma cleaner for 2 min to produce a hydrophilic surface. After rinsing in water, the Ag film was immersed in a vial containing 0.10 M Na_2SO_4 (or 0.10 M NaClO_4) electrolyte solution. The film was then subjected to an electrochemical roughening procedure using double-potential step oxidation-reduction cycles. A standard three-electrode cell was employed with the silver as working electrode, a platinum foil as the auxiliary electrode, and a saturated-calomel electrode (SCE) as the reference. All potentials are reported with respect to the SCE reference. Roughening of the Ag film was performed in the dark and under an argon gas atmosphere. Three cycles of the following procedure were performed: the potential was initially stepped to +0.55 V, 25 mC/cm^2 of charge was allowed to pass, and then the potential was stepped to -0.60 V until the current reached a minimum. The roughened Ag film was rinsed under a stream of water and then immersed into a 1.0 mM KI solution for 2 sec. The iodide-modified silver film was rinsed under a stream of water to remove excess KI and was then dried

under a stream of nitrogen gas for transfer to the cryostat. Solutions were purged with high purity nitrogen gas (99.995%) for at least 20 min prior to experiments.

Temperature Control. To achieve low temperatures, the iodide-modified silver films were mounted in a closed cycle cryogenic system (APD Cryogenics) employing gaseous helium as refrigerant. The temperature was selectable between room temperature (ca. 295 K) and 8.2 K. Controlled heating was possible through a resistive-type heating element mounted on the copper cold finger. Temperatures were measured by a calibrated chromel-gold(iron 0.07%) thermocouple and provided ± 0.1 K precision.

Raman Spectroscopy. Raman scattering and surface-enhanced Raman scattering were excited using a tunable dye laser (Coherent CR-599). The dye Stilbene 420 (Exciton, Inc.) in pure ethylene glycol was optically pumped by an Argon laser (Coherent Innova 200) operating in multi-line UV (333-363 nm) mode. The excitation wavelengths were determined using a Spex 1877 Triplemate spectrograph calibrated with a low-pressure argon lamp, providing wavelength accuracy ± 0.02 nm. Laser power at the sample was typically 1 mW or less. Scattered light was collected by an $f/1.5$ fused silica lens in a 180° backscattering geometry and analyzed by a Spex Triplemate spectrograph equipped with a Princeton Instruments back-thinned CCD detector (LN 1100x330). Accumulation times varied between 60 s and 400 s. Spectra were calibrated using a low-pressure argon lamp; frequency accuracy was ± 1 cm^{-1} . All spectra are reported with a spectral resolution of 0.046 nm (e.g. 2.6 cm^{-1} resolution at 420 nm). The accurate measurement of band widths for sharp Raman features was limited by the 1.2 cm^{-1} /pixel resolution of the individual CCD detector elements.

All data processing including spectral curve fitting was performed using procedures in the program Spectra Solve (Lastek Pty. Ltd.). A simplex optimization method was employed in the curve fitting routine to determine best-fit parameters.

RESULTS AND DISCUSSION

A detailed excitation profile of the resonance emission (Raman and fluorescence) from iodide adsorbed on an electrochemically roughened Ag surface (further referred to as Ag surface) was obtained in the spectral range from 409 to 433 nm. The excitation wavelength was tuned in small steps (ca. 0.25 nm) resulting in a total of 77 spectra. As an internal standard, a transparent polystyrene plate of 0.8 mm thickness was sandwiched with the iodide-modified Ag film and placed in a copper holder in the cryostat. Both the progression and the polystyrene spectra were recorded simultaneously. All spectra were normalized to the 1002 cm^{-1} band of polystyrene, thereby removing the instrument dependence as well as the ν^4 dependence of the Raman intensity. Special precautions were taken to eliminate the dependence of the relative intensities of the progression bands and the polystyrene spectrum on the depth of focusing of the collection optics. No observable photobleaching of the signal was noted at the low laser powers employed by comparing the spectra taken at the beginning and after completion of the excitation series. The sample was maintained at 20 Kelvin during the measurements. A temperature dependence of the Raman spectrum of iodide on Ag was discussed in the previous study.⁶

Raman spectra of iodide adsorbed on the Ag surface obtained at different excitation wavelengths are shown in Figure 1 and Figure 2. These spectra comprise a

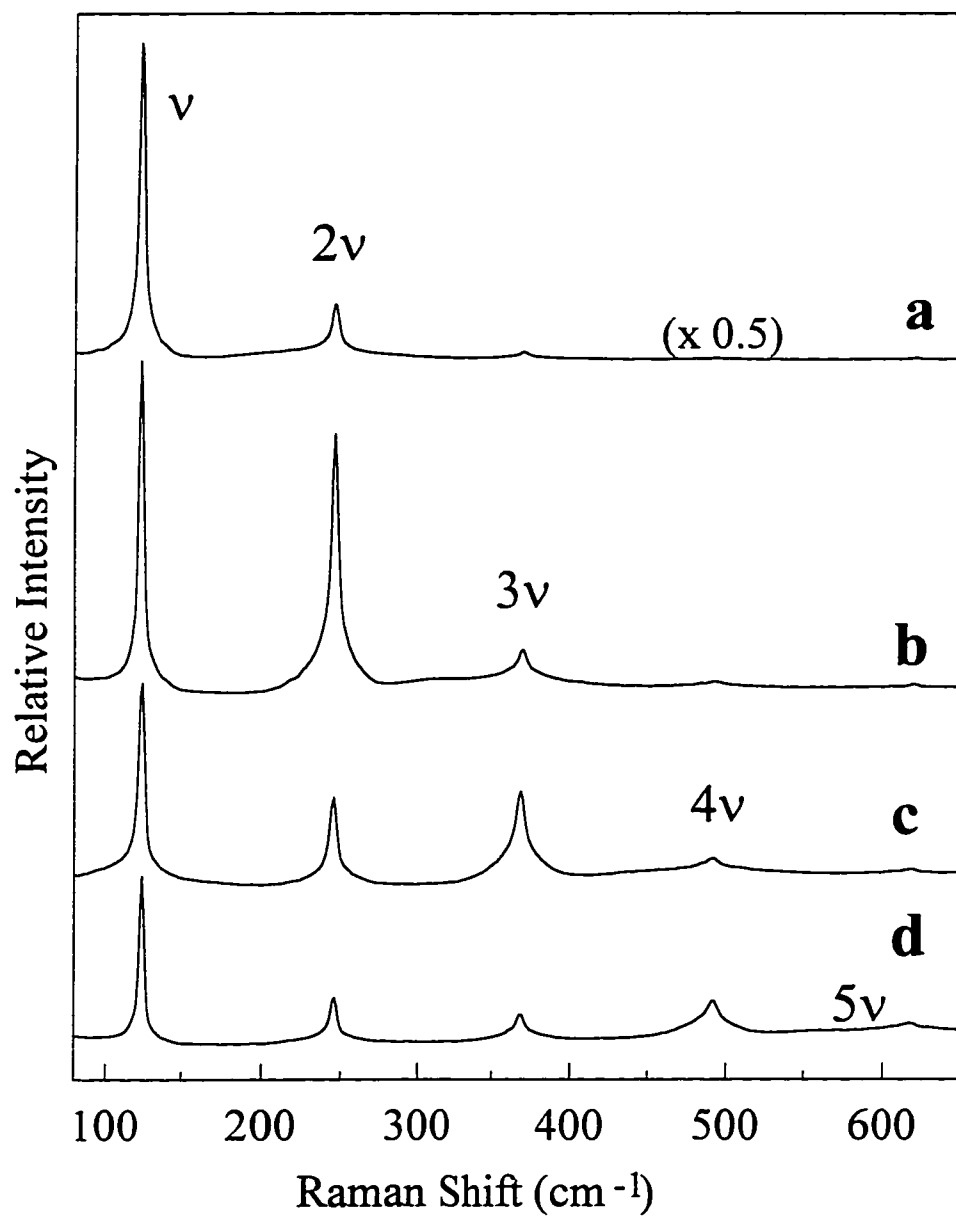


Figure 1. Resonance Raman spectra of iodide adsorbed on the Ag surface obtained at different excitation wavelengths: (a) 424.9 nm, (b) 423.0 nm, (c) 420.6 nm, and (d) 418.6 nm.

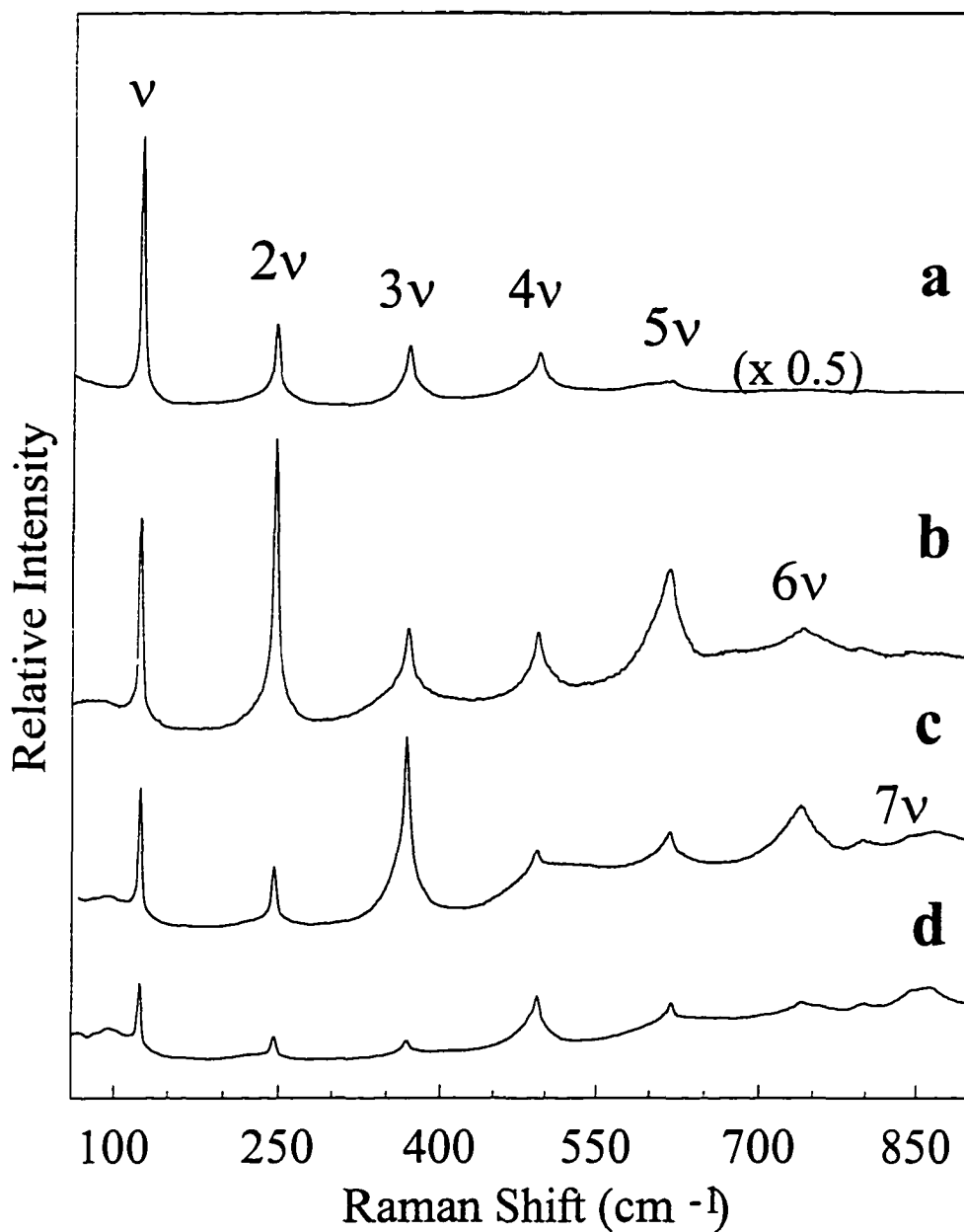


Figure 2. Resonance Raman spectra of iodide adsorbed on the Ag surface obtained at different excitation wavelengths: (a) 419.3 nm, (b) 416.6 nm, (c) 414.4 nm, and (d) 412.3 nm.

vibrational progression with a fundamental (ν) at 123 cm^{-1} , first overtone (2ν) at 246 cm^{-1} , second overtone (3ν) at 369 cm^{-1} , etc. Up to six overtones were observed depending on resonance excitation conditions. The regular spacing between overtones equal to $123 \pm 0.5\text{ cm}^{-1}$ suggests a high degree of harmonicity. Other bands were also present in the emission spectra and can be attributed to resonance and relaxed fluorescence.

It should be emphasized that the progression was observed on an electrochemically roughened Ag surface. Attempts to detect this spectrum on silver prior to electrochemical roughening or on silver chemically-etched by nitric acid were unsuccessful. In addition, the spectrum was extremely sensitive to the electrochemical roughening procedure. Based on these and previous experimental results, a model was developed in which iodide forms a complex with small Ag clusters formed during electrochemical roughening and associated with the metal surface.⁶ This Ag cluster-iodine complex exhibits a delocalized resonance transition in the blue spectral region. At low temperatures, under irradiation, a bond is formed between neighboring iodine adatoms producing a new I_2 species adsorbed on the Ag cluster. This model is depicted in Figure 3. Various diatomic and polyiodides are known to show vibrational progressions. Overtone progressions of $\nu(\text{I-I})$ have been reported in Raman spectra under resonance excitation for I_2 , I_2^+ , I_2^- , and I_3^- having fundamental frequencies at 212 , 238 , 114 , and 113 cm^{-1} , respectively.¹¹⁻¹⁴ The fact that the vibrational frequency of the new I_2 species (123 cm^{-1}) is close to that of I_2^- in solution (114 cm^{-1}) is consistent with the model of charge transfer from the metal to iodide. At temperatures higher than ca. 200K , the new I_2 species is dissociated to re-form a monoatomic iodide adsorbed on the silver surface.

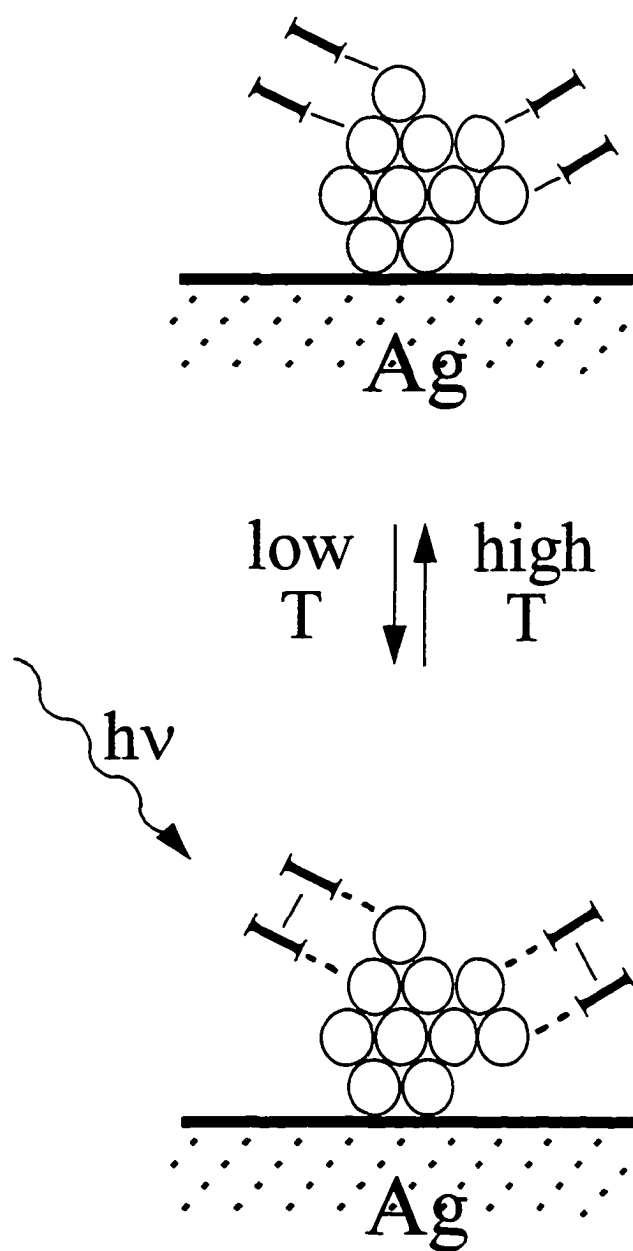


Figure 3. Model depicting the photoinduced formation at low temperatures of a new I_2 species adsorbed on a Ag cluster. The Ag cluster is produced during electrochemical roughening of the bulk metal.

For the same excitation wavelength, the relative intensities of the overtone bands as well as the overall intensity of the spectrum varied considerably at different spots on the silver surface (data not shown). However, the vibrational frequencies remained unchanged. This behavior can be explained as follows. The delocalized electronic transition in the Ag cluster - I complex can be strongly influenced by the size of the cluster, as long as the latter remains within the quantum limits. At the same time, the vibrational mode which reflects more the I - I interaction is expected to be insensitive to the cluster size. By changing the irradiated spot on the surface, the clusters with the different average size are excited, which is equivalent to probing with different excitation wavelengths. The intensity of the progression is known to be very sensitive to the excitation wavelength when tuned through the resonance transition, as discussed below.

Both the absolute intensity of the spectrum as well as the relative intensities of different bands varied with excitation wavelength. Only the fundamental band was observed with pre-resonance excitation at 435 nm. At 406 nm excitation, the overall weak spectrum also contained six overtones, the intensities of which did not change appreciably with excitation wavelength.⁶ The latter is characteristic of continuum resonance Raman scattering in which the incident frequency is above the excited state dissociation limit in a continuum region.¹⁵ When the incident frequency coincided with vibronic levels of the excited state, discrete resonance Raman occurred and the spectral intensity increased nearly 50 times relative to pre-resonance and continuum resonance conditions.

A three-dimensional contour plot of the resonance emission excitation profile is depicted in Figure 4. The intense features in the plot represent the progression-forming

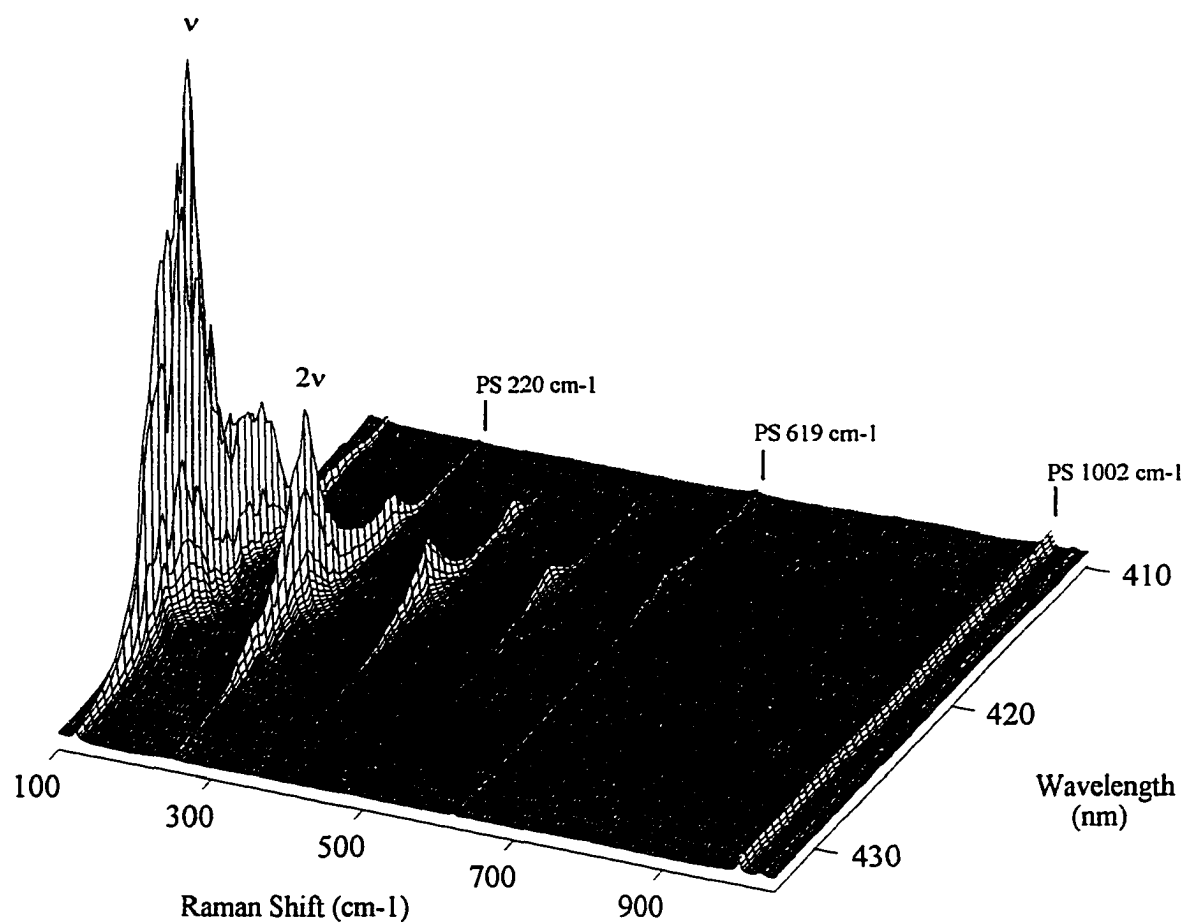


Figure 4. Three-dimensional contour plot of the resonance emission excitation profile from iodide adsorbed on the Ag surface. Bands labeled PS at 220, 619, and 1002 cm-1 are from the polystyrene internal standard to which all spectra were normalized.

vibration from iodide adsorbed on the Ag surface. Intensity-invariant bands resulting from normalization at 220, 619, 1002, and 1050 cm^{-1} are from polystyrene. The complex resonance character of the intensities of different overtones can be clearly seen. As the incident frequency was tuned to higher energies through the excited state, each band of the progression successively underwent resonance enhancement. In other words, the maximum enhancement for the fundamental and each overtone peaked at different wavelengths. Note that the excitation profile of each band exhibited two distinct maxima. (The spectra obtained with excitation wavelengths corresponding to the first and second maxima are shown in Figure 1 and Figure 2, respectively.) Additional weak emission features which appear in the contour plot as “ridges” between the Raman peaks represent resonance and relaxed fluorescence. The fluorescence bands appear to move across the plot occurring at different Stokes shifts, but maintaining their absolute frequency; on the contrary, the Raman bands remain at the same Stokes shift and follow the excitation wavelength.

Two-dimensional excitation profiles composed from the 77 experimental points for the first four bands in the progression are presented in Figure 5. The curves for (a), (b), (c), and (d) represent the fundamental band and the first, second, and third overtone bands, respectively. Each point on the curves corresponds to the normalized total intensity at the peak position after subtraction of the background. Intensities were used rather than integrated areas due to the different contributions from resonance Raman and resonance and relaxed fluorescence which varied with excitation frequency. These variations resulted in a complex bandshape making integration of the peak areas ambiguous.

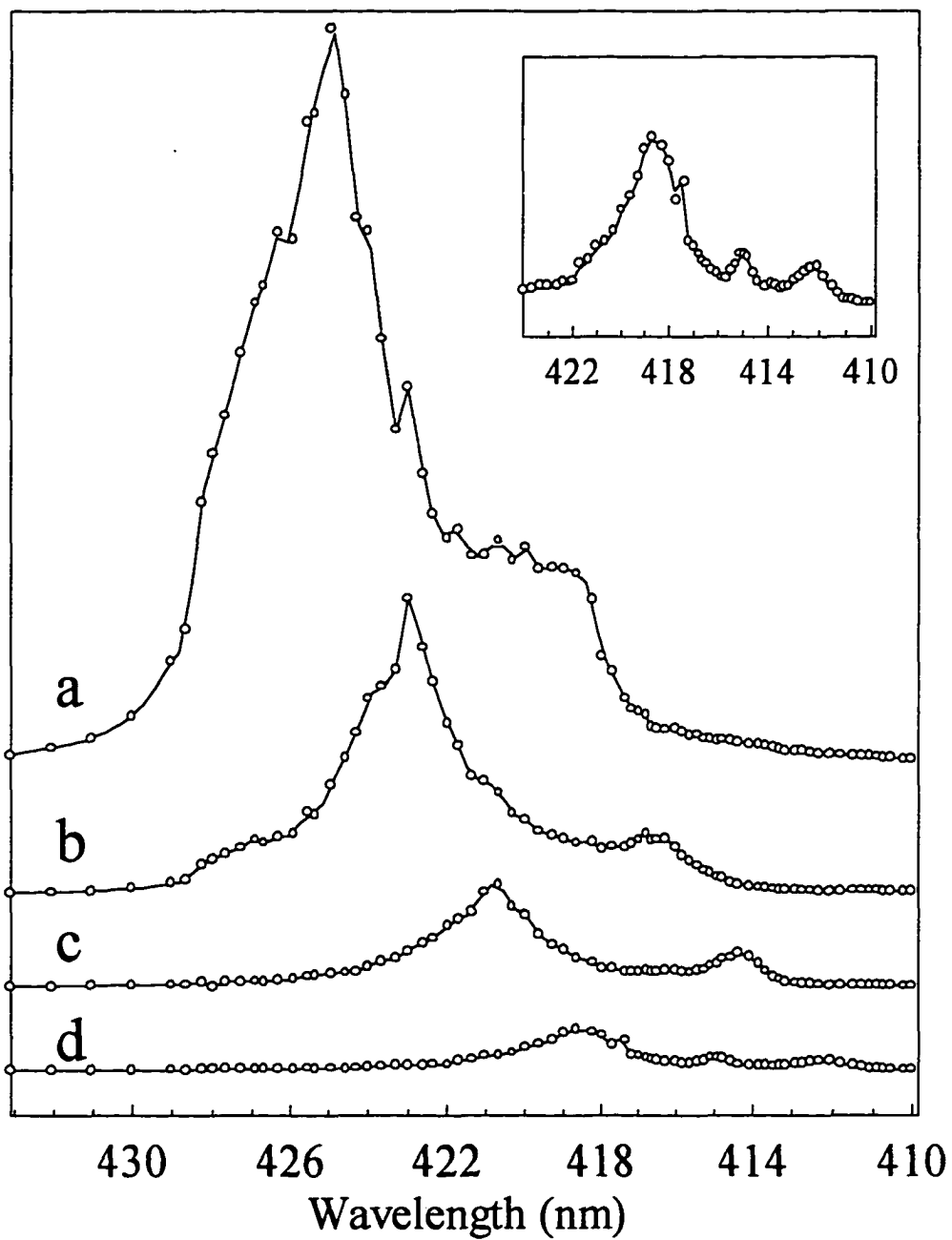


Figure 5. Excitation profiles composed from the 77 experimental points for the following bands in the Raman progression: (a) fundamental, (b) first overtone, (c) second overtone, (d) third overtone. Insert: Enlarged view of the curve in (d).

Because the width of the Raman bands is expected to be independent of the excitation wavelength, the use of peak intensities is equally illustrative of the Raman excitation profile as the use of integrated areas would be.

Only two resonances in the excitation profile for each band are apparent from Figure 5. The shifts between the first and second resonances for four bands in the Raman spectrum are summarized in Table I. The two resonances and the shift between maxima of ca. 370 cm^{-1} , equivalent to three quanta of the fundamental vibration, suggests that a significant displacement exists for the potential minimum of the excited electronic state relative to that of the ground electronic state. According to the Franck-Condon principle, the vertical transition of the emission process is most probable to occur from the turning points along the excited state surface.¹⁶ A displacement of the potential minima relative to each other leads to two vertical transitions from the excited state to the ground state which have different energies, manifested in the excitation profile by two resonance maxima.

Table I. Shifts between the first and second resonances in the excitation profile for single bands in the Raman progression.

Band in the Progression	Shift between 1st and 2nd Resonances, Δcm^{-1}
1	(344) ^a
2	365
3	369
4	372

^a Reflects uncertainty in determining the position of the maximum (see text).

Table II. Shifts between resonances in the excitation profile for adjacent bands in the Raman progression.

Bands in the Progression		1st Resonance, Δcm^{-1}	2nd Resonance, Δcm^{-1}
2	1	102	(123) ^a
3	2	120	124
4	3	122	125

^a Reflects uncertainty in determining the position of the maximum (see text).

The single resonances for each successive band in the progression appeared blue-shifted from the previous ones. The shifts between resonances for adjacent bands, determined from Figure 5, are summarized in Table II. To a first approximation, the shift of ca. 123 cm^{-1} corresponds to the spacing between vibronic levels in the excited electronic state. The fact that the vibrational frequency in the ground and excited states are similar indicates little change in the shape of the excited state potential energy surface relative to that in the ground state. This result is highly unusual for a simple diatomic molecule, but is reasonably well explained by the model of I_2 adsorbed on a small Ag cluster. Because the second resonance for the fundamental band (Figure 5a) appeared to be overlapped with the first resonance, its position was assumed to be at 418.7 nm, consistent with the shifts between first and second resonances of the other bands in the progression. Uncertainty in the calculated values resulting from this assumption is noted in the Tables by parentheses.

In addition to the two resonances characteristic for the excitation profile for every band, another resonance at 415.0 nm was observed for the third overtone in the

progression (Figure 5d and Figure 5 Insert). The apparent increase in the intensity at the position of the third overtone in the Raman spectrum is not due to an increase in Raman scattering *per se* but rather is due to a broad fluorescence band which contributes to the overall intensity as it moves through the unchanged, sharp Raman peak at different excitation wavelengths. In constructing the excitation profiles, no discrimination was made between contributions from different processes such as resonance Raman and resonance and relaxed fluorescence to the overall intensity of the emission. Therefore, an additional peak appeared in the excitation profile for the third overtone. The nature of the fluorescence will be discussed below.

The strongest resonance in the excitation profile was observed for the fundamental band. As the vibrational quantum number of the overtones increased, the strength of the resonance decreased rapidly (Figure 5). Such behavior indicates that the electronic transition which causes the resonance enhancement of the Raman scattering is centered around the first vibronic level of the excited state.¹⁶ The resonances also exhibit significant broadening on the order of 5-6 nm (ca. 300 cm^{-1}) which is significantly larger than the spacing between vibronic levels of the excited state (ca. 123 cm^{-1}) and two orders of magnitude larger than the width of vibronic levels in the ground state (ca. $< 2.5\text{ cm}^{-1}$). This broadening represents the electronic inhomogeneity of the system due to interactions of the I_2 species with different sized Ag clusters, as described previously in detail.⁶

A remarkable feature of the Raman progression is the extremely narrow bandwidths of the fundamental and overtone bands. The measured bandwidths were typically less than 3 cm^{-1} , but the actual width of the Raman transition could not be

accurately determined because of instrument limitations. The instrument function was limited by pixel resolution of ca. 2.5 cm^{-1} . When a Raman band was overlapped with the instrument function, both widths coincided indicating that the width of the Raman transition is much narrower than 2.5 cm^{-1} , Figure 6a. The shape of the fundamental band was readily fit by the shape of the instrument function. Whereas, the first and second overtones were found to exhibit an additional broad pedestal. This fact led to spectral bandshape analysis using curve fitting routines. The result of the curve fitting to the fundamental and first two overtones is shown in Figure 6b. A nearly ideal fit of the fundamental band required only a single Lorentzian shape. However, all overtones in the progression required both a sharp Lorentzian and a much broader Gaussian component. Recognizing the ambiguity of the curve fitting routine, other combinations of sharp and broad components were also considered. Sharp and broad Lorentzians as well as a sharp Gaussian and a broad Lorentzian resulted in an excellent fit to the observed bandshape. Less satisfactory fits were obtained with two Gaussian components. Regardless of the line shape of the components, two components were always required to reconstruct the shape of the observed Raman bands. This trend was consistent for Raman spectra obtained with different excitation wavelengths. In addition, the broad component appeared to be shifted $2\text{-}5 \text{ cm}^{-1}$ toward lower frequencies relative to the sharp feature. Both of the components tracked simultaneously with the excitation wavelength across the entire resonance profile. Even though both bands are attributed to Raman scattering, the phenomena causing their appearance are unclear.

Further analysis of the shape of the bands in the overtone progression revealed contributions from different emission processes. The presence of two weak bands which

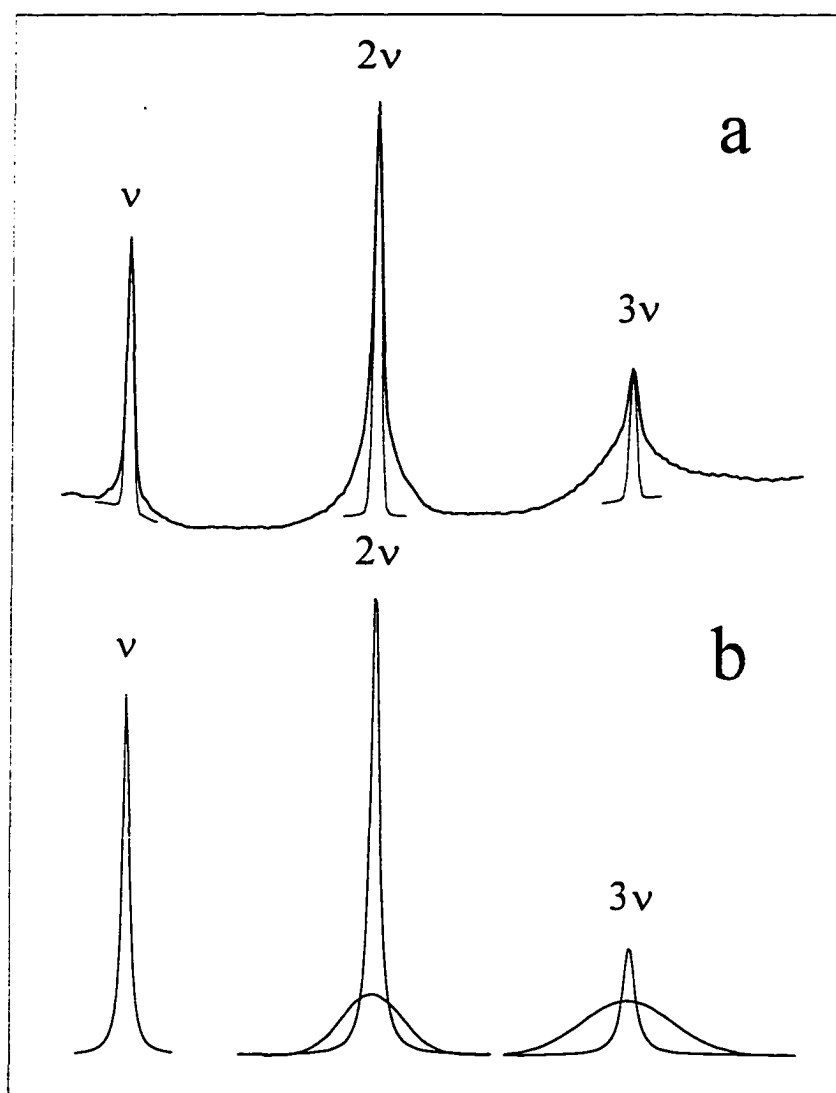


Figure 6. Bandshape analysis of the fundamental, first overtone, and second overtone bands of the Raman progression: (a) comparison of the Raman bands with the experimental instrument function and (b) calculated narrow Lorentzian and broad Gaussian components from fitted curves for the Raman bands. Excitation wavelength was 416.6 nm.

behave like relaxed fluorescence (a transition from the lowest vibronic level of the excited state) is depicted in Figure 7. Independent from the excitation wavelength, these bands maintain their position at ca. 430.0 nm and 428.7 nm and remain nearly constant in intensity. On the contrary, the intensity of resonance (unrelaxed) fluorescence which results from the transition between higher vibronic levels of the excited state and the ground state is expected to be enhanced as the excitation frequency coincides with the particular vibronic level of the excited state.^{5,16} An example of resonance fluorescence which was observed in the spectra of iodide adsorbed on the Ag surface is shown in Figure 8. The frames designated (a), (b) and (c) contain the original emission spectra obtained at different excitation wavelengths for which resonance fluorescence appears shifted to both sides of and under the Raman peak and corresponding fitted curves. As can be clearly seen in Figure 8b, the peak of the resonance fluorescence gains intensity when coincident with the Raman transition.

CONCLUSIONS

A detailed excitation profile of iodide adsorbed on an electrochemically-roughened silver surface revealed a series of resonance emission bands characteristic of resonance Raman scattering and resonance and relaxed fluorescence. A vibrational progression including a fundamental band and up to six overtones, previously assigned to the $\nu(\text{I-I})$ stretch of an I_2 species adsorbed on small Ag clusters, was observed at the temperature 20 K when excited between 409 nm and 433 nm. Low temperatures were previously found to

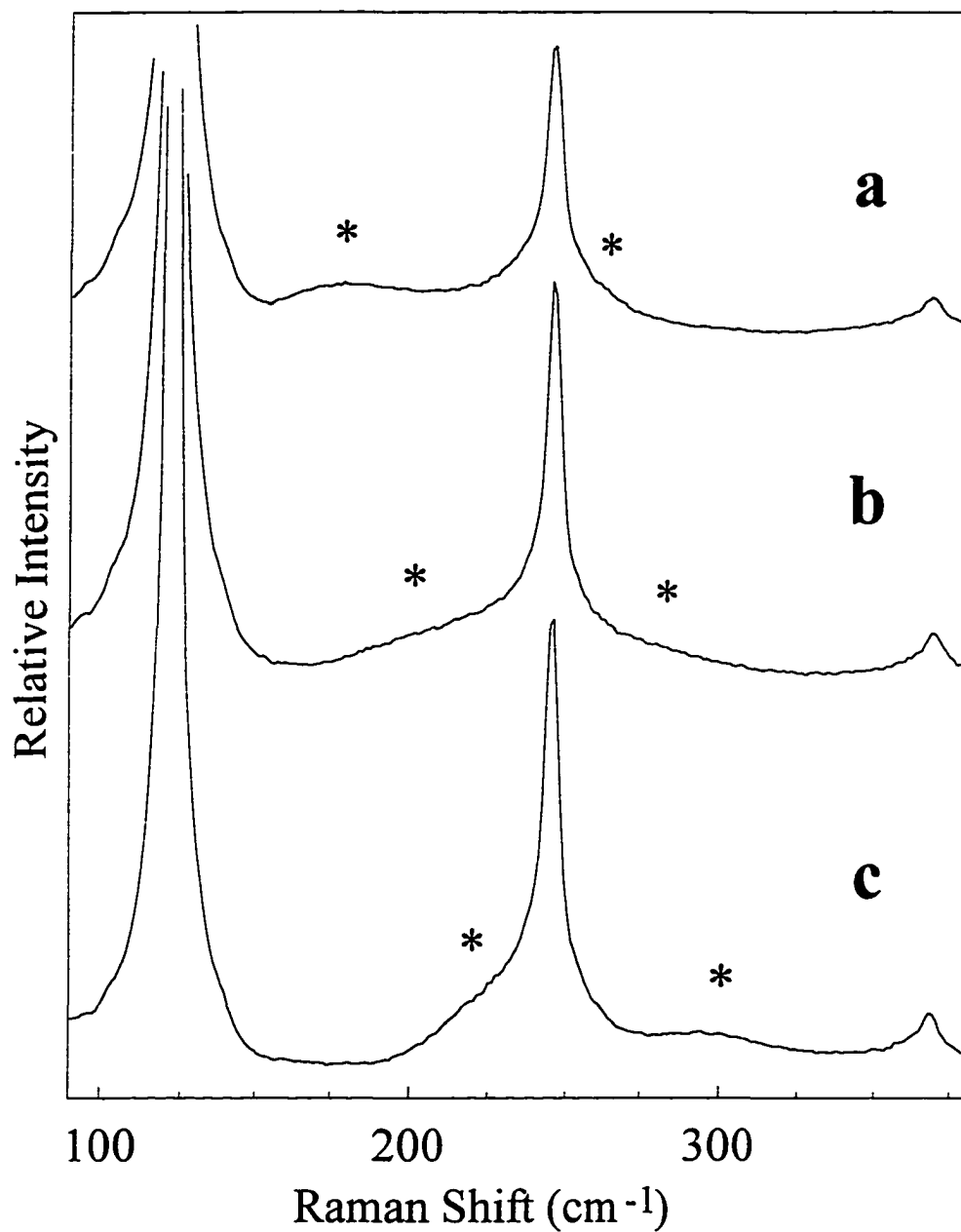


Figure 7. Excitation wavelength dependence of the resonance Raman and resonance fluorescence components of the emission spectrum from iodide adsorbed on the Ag surface: (a) 425.3 nm, (b) 424.9 nm, (c) 424.5 nm. Two fluorescence features are noted with an asterisk (*).

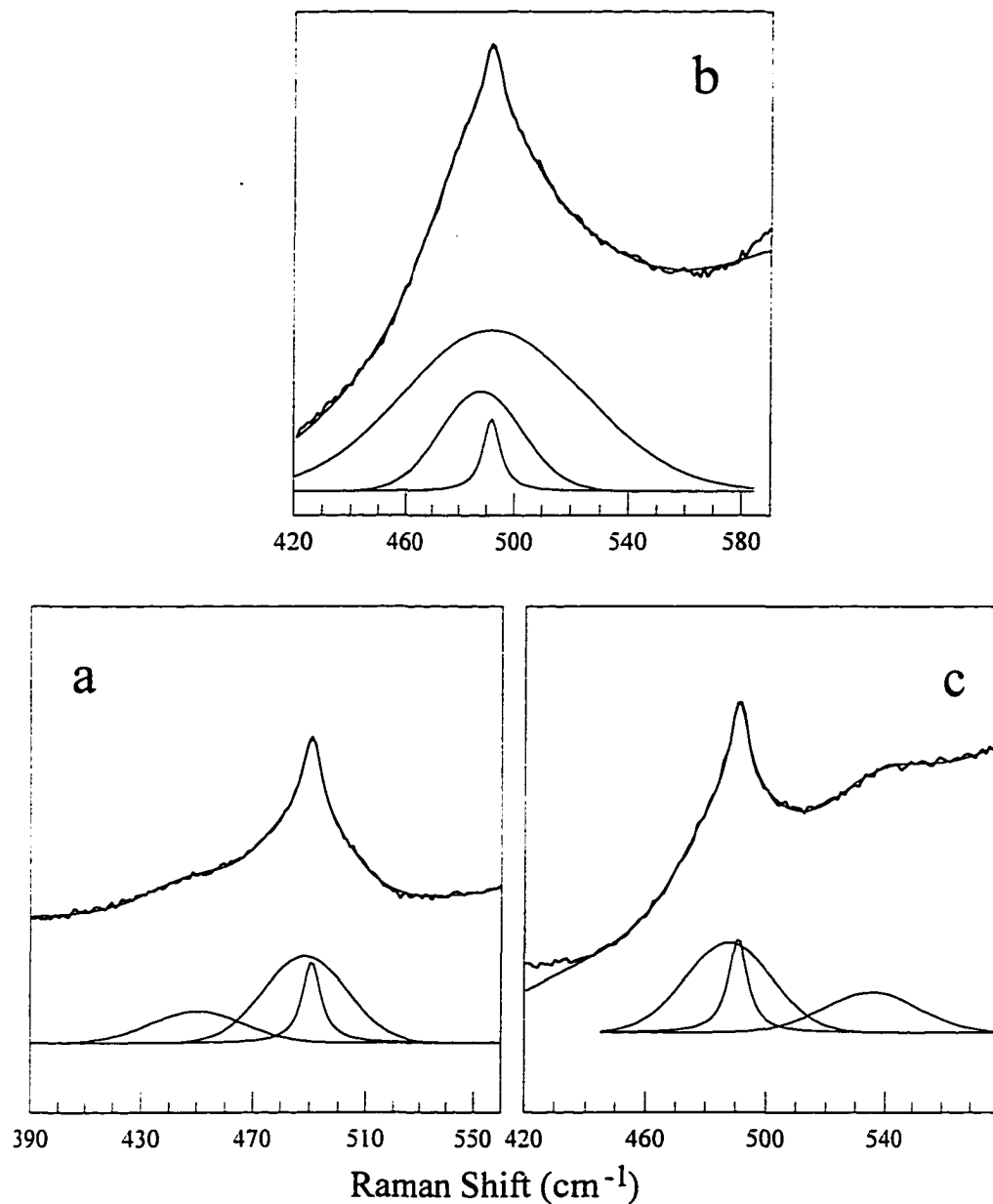


Figure 8. Resonance fluorescence observed in the emission spectra from iodide adsorbed on the Ag surface. The excitation wavelengths are (a) 415.6 nm, (b) 414.9 nm, and (c) 414.1 nm. In each frame, the fourth overtone in the Raman progression is overlapped with the calculated, convolved best-fit curve. Below the data and convolved best-fit curve are the three components required for fitting: a narrow Lorentzian (resonance Raman), a broad Gaussian (resonance Raman), and a broad Gaussian (resonance fluorescence).

stabilize this species which dissociates at higher temperatures to re-form monoatomic iodide adsorbed on the silver surface.

From the Raman excitation profile, a picture of the electronic structure of the surface-adsorbed I_2 species was developed. Vibronic spacing in both the ground and excited electronic states was ca. 123 cm^{-1} , not typical behavior for simple diatomic molecules but consistent with the model of an I_2 -silver complex. Significant displacement of the potential energy surfaces along the nuclear coordinate was suggested by the ca. 370 cm^{-1} spacing (three quanta) of the two resonance maxima for each band in the Raman progression.

Bandshape analysis of the progression revealed several remarkable features. The instrument-limited bandwidth of the fundamental was measured to be 2.5 cm^{-1} . The bandshape of the fundamental was readily fit by a single, sharp Lorentzian. Whereas, curve fitting of the overtones consistently required both a sharp and a broad feature to reconstruct the bandshape. Although both features behave like a Raman transition, the phenomena causing their appearance are unclear. Additional emission features including relaxed and resonance fluorescence were also observed. The intensity of the resonance fluorescence was shown to be significantly enhanced when the excitation frequency was tuned into a vibronic level of the excited state.

ACKNOWLEDGMENTS

The authors wish to thank Gerald J. Small and Mark Gordon (Iowa State University) for the many stimulating discussions. M.S.S also acknowledges Art Camire (Coherent Inc.)

for the generous advance of laser optics. Research at the Ames Laboratory was supported by the Division of Chemical Sciences, Office of Basic Energy Sciences, U.S. Department of Energy. Ames Laboratory is operated for the U.S. Department of Energy by Iowa State University under contract No. W-7405-Eng-82.

REFERENCES

- (1) Ziegler, L. D. *Acc. Chem. Res.* **1994**, *27*, 1.
- (2) Lee, D.; Albrecht, A. C. In *Advances in Infrared and Raman Spectroscopy*, Clark, R. J. H. and Hester, R. E., Eds.; Wiley: Heyden, 1985; Vol. 12, pp 179.
- (3) Mukamel, S. *Principles of Nonlinear Optical Spectroscopy*, Oxford University Press: New York, 1995; pp Chapter 9.
- (4) Holzer, W.; Murphy, W. F.; Bernstein, H. J. *J. Chem. Phys.* **1970**, *52*, 399.
- (5) Hochstrasser, R. M.; Nyi, C. A. *J. Chem. Phys.* **1979**, *70*, 1112.
- (6) Sibbald, M. S.; Chumanov, G.; Cotton, T. M. *J. Phys. Chem.* **1997**, to be submitted.
- (7) Sibbald, M. S.; Chumanov, G.; Cotton, T. M. *J. Phys. Chem.* **1996**, *100*, 4672.
- (8) Brandt, E. S.; Cotton, T. M. In *Investigations of Surfaces and Interfaces-Part B*, 2nd ed.; Rossiter, B. W. and Baetzold, R. C., Eds.; Physical Methods of Chemistry Series; Wiley: New York, 1993, pp 633.
- (9) Albrecht, A. C. *J. Chem. Phys.* **1961**, *34*, 1476.
- (10) Clark, R. J. H.; Dines, T. J. *Angew. Chem. Int. Ed. Engl.* **1986**, *25*, 131.
- (11) Mortensen, O. S. *J. Molec. Spectrosc.* **1971**, *39*, 48.
- (12) Gillespie, R. J.; Morton, M. J. *J. Molec. Spectrosc.* **1969**, *30*, 178.
- (13) Tripathi, G. N. R.; Schuler, R. H.; Fessenden, R. W. *Chem. Phys. Lett.* **1985**, *113*, 563.
- (14) Kiefer, W.; Bernstein, H. J. *Chem. Phys. Lett.* **1972**, *16*, 5.

- (15) Rousseau, D. L.; Williams, P. F. *J. Chem. Phys.* **1976**, *64*, 3519.
- (16) Herzberg, G. *Molecular Spectra and Molecular Structure I. Spectra of Diatomic Molecules*, 2nd ed.; Van Nostrand-Reinhold: New York, 1950.

CHAPTER 6. GENERAL CONCLUSIONS

The surfaces of various silver nanostructures were chemically-modified by the adsorption of ionic and molecular species, including iodide, bromide, and cytochrome *c*. Raman scattering, surface-enhanced Raman scattering, and UV-Vis absorption spectroscopies were particularly useful for studying the adsorption states and reactivities of these surface-modifiers. In Chapter 2, the crystal shape and structure of chemically-prepared Ag nanostructures were analyzed using both imaging and diffraction modes of a transmission electron microscope. Unmodified (“clean”) silver surfaces were studied in order to evaluate only the bulk silver phase. Individual crystals of about 100 nm mean diameter had highly regular polyhedral shapes (e.g. trigonal, pentagonal, etc.) and a lattice constant of ca. 4.05 Å, consistent with the expected value for a face-centered cubic phase of silver. Convergent beam electron diffraction studies revealed that the crystals were formed from either a single Ag phase or a multiply-twinned Ag phase.

The adsorption of iodide and bromide ions to the surfaces of silver nanostructures of 20 nm mean diameter was studied in Chapter 3. Adsorption of the modifier on the surface of Ag colloids was confirmed from surface-enhanced Raman spectra, where a characteristic halide-silver metal stretching vibration was observed, and from absorption spectra, where monolayer coverage of the halide was followed by the disappearance of a charge-transfer-to-solvent band of the free iodide in solution. Extinction spectra of the iodide-modified colloids also revealed that adsorption causes noticeable aggregation of the particles in solution, manifested by a shift to lower energy and damping of the surface plasmon resonance band; whereas by using colloidal metal films in which the particles

were isolated by covalent attachment to a thiol-derivatized substrate, the iodide-modifier caused only damping with no apparent change in the plasmon frequency.

Addition of the electroactive protein cytochrome *c* to a halide-modified Ag colloid resulted in the reduction of the protein. It was concluded that upon adsorption of the halides to the Ag surface, charge was donated to the particle as a whole which could be stored or donated to suitable electron acceptors. In Chapter 4, competitive binding of iodide ions between cytochrome *c* and the silver metal was observed, prompting the use of an uncharged, redox active indophenol dye molecule to obtain better quantitative results of the reduction efficiency. Two distinct processes were identified: reduction at iodide-coverages up to one monolayer on the Ag surfaces and reduction in the presence of excess iodide in solution. In the former, adsorption results in partial charge transfer from iodide to the silver metal, forming a unique iodide-Ag surface complex which is different than molecular AgI. Only around 5% of the electron accepting molecules became reduced. While in the latter, free iodide in solution reacts with the Ag metal in a 1:1 stoichiometry to form molecular AgI, confirmed by the appearance of a characteristic 425 nm emission band.

When the iodide-Ag surface complex was cooled to temperatures less than 150 K, a very strong progression with a fundamental band at 123 cm^{-1} and up to six overtones was observed in the Raman scattering with 413.1 nm excitation. The fundamental frequency did not coincide with those known for polyiodides (I_2 , I_2^- , I_3^- , etc.), diatomic AgI, or crystalline forms of AgI. A detailed excitation profile, presented in Chapter 5, was performed in the wavelength range 409-433 nm which revealed a series of resonance

emission bands characteristic of resonance Raman scattering and resonance and relaxed fluorescence. The conclusion was made that photoinduced formation occurred of a new I_2 species adsorbed on small Ag clusters.

The new I_2 species adsorbed on silver surfaces might be an ideal system for theoretical modeling of resonance emission processes for the following reasons. It is a simple case of a diatomic species exhibiting only one totally symmetric mode in which only diagonal components of the transition polarizability are non-zero. This diatomic molecule has only one resonant excited state (*A*-term scattering). It exists at low temperatures at which all molecules are in the lowest vibrational level of the ground state and interactions with the bath are expected to be minimal.

Recommendations for Future Work

Based on the present studies, there are two areas of research that deserve additional attention. First, chemically-prepared nanostructures of silver composed of a single crystalline phase should be isolated from those formed from multiple-twins. Research would then focus on determining the effects of grain boundaries on the optical properties of the particle as a whole. Second, the adsorption of bromide ions and other monolayer-forming species on silver surfaces should be monitored at low temperatures using Raman spectroscopy. With the appropriate excitation wavelength, perhaps a general class of new species (e.g. a Br_2 -like surface-adsorbed diatomic) could be discovered in the resonance emission spectra.

ACKNOWLEDGMENTS

First and foremost I would like to thank Professor Therese Cotton for providing me with the opportunity to develop further as a scientist under her tutelage. Professor Cotton is an exceptional person whom I wish all the best in life.

My sincere thanks to Dr. George Chumanov, a collaborator and friend, whose enthusiasm for science always inspired me to think deeply about the research.

Thanks also to the many present and past members of the Cotton Group with whom it has been a pleasure working. To those who have made the greatest contributions, Jeanne Wynn, Al Avila, Brian Gregory, Brian Cooper, and Kostia Sokolov, I am forever grateful. (P.S. Three years and counting for the “Normal Modes” winning the annual Departmental volleyball tournament... keep the record going!)

I would particularly like to thank Dr. Sergei Savikhin for his timely development and continued modification of the Spectra Solve for Windows program.

And thanks to my closest friends who have helped keep me “sane” throughout my graduate studies: my wife and best friend JeNell Sibbald, Don Gutzman, Heather Lybarger, Kim Sheard, Peter Marsch, and Mike Gekas. Finally, I wish to thank my parents William and Billie Vollmers and my brother Christopher and sister-in-law Donna Vollmers for their continued support.